Bioconversion of Crude Glycerol to Dihydroxyacetone using Immobilized *Gluconobacter oxydans*: Process Design, Optimization and Intensification

A
Thesis
Submitted in
Partial Fulfillment of the
Requirements for the Degree of

DOCTOR OF PHILOSOPHY

By

Pritam Kumar Dikshit

DEPARTMENT OF CHEMICAL ENGINEERING
Indian Institute of Technology Guwahati
Guwahati – 781 039, Assam, India
November 2017

Dedicated

To

Lord Lakshmi Varah

and

My Parents

कर्मण्येवाधिकारस्ते मा फलेषु कदाचन ।
मा कर्मफलहेतुर्भूर्मा ते सङ्गोऽस्त्वकर्मणि ॥

INDIAN INSTITUTE OF TECHNOLOGY GUWAHATI

DEPARTMENT OF CHEMICAL ENGINERING

STATEMENT

I do hereby declare that the content embodied in this thesis entitled "**Bioconversion of Crude Glycerol to Dihydroxyacetone using Immobilized *Gluconobacter oxydans*: Process Design, Optimization and Intensification**" is the result of investigations carried out by me in the Department of Chemical Engineering, Indian Institute of Technology Guwahati, Guwahati, India, under the guidance of Prof. Vijayanand S. Moholkar.

In keeping with the general practice of reporting scientific observations, due acknowledgements have been made wherever the work described is based on the findings of other investigators.

Date:

Pritam Kumar Dikshit

(Roll No.: 126107033)

CERTIFICATE

It is certified that the work contained in the thesis entitled "**BIOCONVERSION OF CRUDE GLYCEROL TO DIHYDROXYACETONE USING IMMOBILIZED *Gluconobacter oxydans*: PROCESS DESIGN, OPTIMIZATION AND INTENSIFICATION**", by **Pritam Kumar Dikshit** (Roll No. 126107033), has been carried out under my supervision and that this work has not been submitted elsewhere for degree.

Date:

Prof. Vijayanand S. Moholkar
Department of Chemical Engineering
Indian Institute of Technology Guwahati
Guwahati – 781039, Assam, India

ACKNOWLEDGEMENTS

I take utmost pleasure to express my gratitude to all who made this thesis possible. I owe my deepest gratitude to each one of them who stand by me constantly and dynamically during my research work to make this possible.

The first and foremost appreciation goes to my supervisor ***Prof. Vijayanand S. Moholkar*** for his valuable suggestions, encouragement, and constant support throughout my research work. I sincerely thank him for spending his valuable time for discussion by which I have gained immense skill and knowledge in terms of research and enlightening me the first glance of research. I could not have imagined having a better advisor and mentor for my Ph.D. study.

I would also like to express my sincere gratitude to all my doctoral committee members, ***Prof. Kaustubha Mohanty***, ***Prof. Kannan Pakshirajan***, and ***Dr. Pankaj Tiwari*** for their insightful advices, suggestions, and encouragement throughout the research that has led to the successful completion of my thesis.

My sincerely thanks go to the faculty and staff members of Department of Chemical Engineering and Center for Energy for their kind help and support. I am thankful to Department of Chemical Engineering, Center for Energy and Central Instruments Facilities (CIF) for providing facilities to carry out my research work. I am also thankful to the Indian Institute of Technology Guwahati for providing me with the infrastructure and facilities for advanced research.

I am thankful to *Dr. Susant Kumar Padhi* and *Abantika Pratap* for all the love and support.

I am immensely thankful to my seniors *Dr. Swati Khanna*, *Dr. Shuchi Singh*, *Dr. Sankar*

Chakma, Dr. Jaykumar B. Bhasarkar and research group members, *Arup, Maneesh, Shyamali, Ritesh, Amit, Neha, Kuldeep, Philip, Dr. Binota, Sushobhan*.

My PhD endeavor would not have been successful without the endless love, trust, support and blessing of these members of my family: Grandparents (*Pitambar Dikshit, Saraswati Dikshit, Sadashiba Mishra, Sarojini Mishra*); Uncles (*Dr. Bhupal Prasad Mishra, Mr. Aurobinda Mishra*), and Aunts (*Mrs. Gayatri Mishra, Mrs. Sachi Mishra, Mrs. Krushnapriya Hota, Mrs. Suravi Mishra, Mrs. Sandhyarani Rath*). I thank my sister, *Dr. Swagatika* and brother, *Dr. Puspak* for always standing by me and loving me selflessly. At last but not the least, I am highly indebted to my parents, *Mr. Prasanna Kumar Dikshit* and *Mrs. Geeta Mishra* for all their sacrifices they have made for my better future, to have faith in me, and giving me freedom to take my own decision. My Ph.D. endeavor could not be completed without them. This is for you "*Bapa*" and "*Bou*".

LIST OF ABBREVIATIONS

ADH	Alcohol dehydrogenase
CCD	Central composite design
CD	Circular dichroism
CDW	Cell dry weight
DHA	Dihydroxyacetone
DHAP	Dihydroxyacetone phosphate
DO	Dissolved oxygen
FAD	Flavin adenine dinucleotide
G. oxydans	*Gluconobacter oxydans*
GHG	Green House Gas
MRS medium	De Man, Rogosa and Sharpe medium
NAD (P)	Nicotinamide adenine dinucleotide phosphate
PQQ	Pyroloquinine quinone
PU foam	Polyurethane foam
PVA	Polyvinyl alcohol
SEM	Scanning electron microscope

TABLE OF CONTENTS

LIST OF TABLES

LIST OF FIGURES

CHAPTER 1

INTRODUCTION
AND
LITERATURE REVIEW

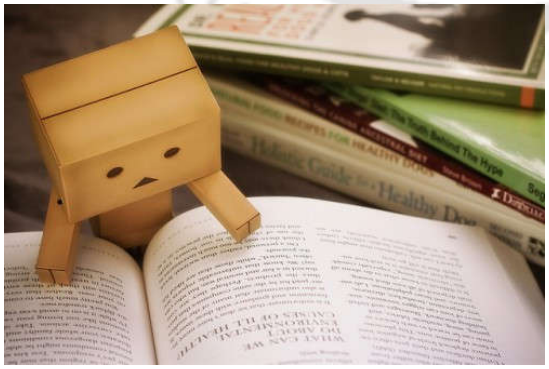

CHAPTER 1

INTRODUCTION AND LITERATURE REVIEW

1.1 INTRODUCTION

Due to large depletion in global reserves of fossil fuels and increasing greenhouse gas emission (GHGs), the issues of energy security and climate change risk have become a major concern for many countries in recent years. As a remedy to both of these issues, Governments of developing nations like India have undertaken major initiatives to promote research and development in the field of renewable energy. The consumption of petroleum products in India during 2015–2016 was 184.674 million metric tons, while the production of crude oil was 36.95 million metric tons (Indian Petroleum and Natural Gas Statistics, 2015–16). The consumption of petroleum products in India shows a growth of 11.57%, while the crude oil production shows a decrease of 1.36% during the year 2015–26, as compared to the year 2014–15. Crude oil production and import in India for a period of 6 years, from 2010 to 2016 are shown in Table 1.1. At the same time the international crude oil price has fluctuated from 26.65 (US $/bbl) in 2002–03 to 111.89 (US $/bbl) in 2011–12 and 46.17 (US $/bbl) at present, as per the annual report of Ministry of Petroleum and Natural Gas, India (Indian Petroleum and Natural Gas Statistics, 2015–16).

Marked increase in vehicular ownership in India (especially in urban areas) has led to enormous rise in GHG emissions through vehicular exhaust. India currently ranks among

top 5 contributors of CO_2 emission, with an emission of 2.45 billion tonnes in 2015 (Netherland Environmental Agency, 2016). The total global CO_2 emission in 1970 was ~16 Gton, which has increased to 36.25 Gton in 2015 (Olivier et al, 2015). The global oil production and consumption data for a period of 10 years, starting from 2005 to 2015 is shown in Table 1.2.

Table 1.1. Crude oil production and import in India in the years 2009–16 (Indian Petroleum and Natural Gas Statistics, 2015–16)

Year	Crude oil production (MMT)	Growth in crude oil production (%)	Import of crude oil (MMT)	Growth in import of crude oil (%)
2009–10	33.690	0.54	159.259	19.95
2010–11	37.684	11.85	163.595	2.72
2011–12	38.090	1.08	171.729	4.97
2012–13	37.862	–1.60	184.795	7.61
2013–14	37.788	–0.19	189.238	2.40
2014–15	37.461	–0.87	189.435	0.10
2015–16(P)	36.950	–1.36	202.851	7.08

MMT – Million Metric Tons; P – Provisional

As immediate solution to the problems related to energy security and environmental protection, Government has made a mandate of use of blends of conventional fuels with alternate renewable liquid fuels such as ethanol, butanol, and biodiesel. Bio–fuels are considered as sustainable source of fuel in terms of limiting GHG emission and improving air quality (Delfort et al., 2008). The production of biofuels by various countries as reported by Renewables 2016 is given in Table 1.3. The world biofuel production increased from around 20 billion tonnes in 2005 to 75 billion tonnes by the end of 2015 (BP Statistical Reviews, 2016). In this period the biofuels production in India increased from 114 million tonnes oil equivalent to 362 million tonnes, sharing 0.5% of total global biofuels production.

Table 1.2. Global oil **production** and **consumption** data from the year 2005 to 2015 (BP Statistical Review of World Energy June 2016)

	2005	2006	2007	2008	2009	2010	2011	2012	2013	2014	2015
Total North America	637.8	637.8	632.8	612.2	622.0	638.8	659.4	720.2	785.0	869.5	910.3
	1129.1	1119.7	1123.1	1068.2	1016.7	1040.3	1030.2	1012.6	1025.3	1026.6	1036.3
Total South & Central America	374.4	380.7	372.6	378.1	374.6	375.8	379.1	376.2	376.1	390.0	396.0
	248.6	257.0	267.9	281.1	279.3	294.6	305.6	312.9	322.9	329.8	322.7
Total Europe & Eurasia	849.0	852.4	863.8	855.0	861.4	859.3	844.4	833.3	833.0	834.7	846.7
	965.3	976.8	960.8	959.5	915.4	911.3	904.3	882.7	864.7	858.6	862.2
Total Middle East	1227.4	1236.9	1214.0	1266.4	1176.0	1220.7	1327.9	1345.1	1324.6	1340.3	1412.4
	301.5	308.4	319.0	343.4	358.6	368.3	375.6	390.3	402.0	417.1	425.7
Total Africa	466.4	475.1	486.1	486.6	468.6	481.8	406.3	444.0	413.9	397.5	398.0
	138.9	138.8	145.0	153.2	156.3	164.5	160.3	168.9	173.3	177.2	183.0
Total Asia Pacific	382.8	380.9	381.8	388.5	384.4	402.7	395.3	400.4	394.0	396.6	398.6
	1150.6	1176.5	1216.6	1212.7	1222.4	1300.9	1345.5	1401.2	1421.8	1442.2	1501.4
Total World	3937.8	3963.9	3951.2	3986.8	3887.0	3979.1	4012.4	4119.2	4126.6	4228.7	4361.9
	3933.9	3977.2	4032.3	4018.1	3948.7	4079.9	4121.6	4168.6	4209.9	4251.6	4331.3

Highlighted in red – Oil: Production in million tonnes; Highlighted in blue – Oil: Consumption in million tonnes

Table 1.3. Global biofuels production, top 16 countries and EU–28, 2015 as published in Renewables 2016 Global status Report

Country	Ethanol (in billion liters)	Biodiesel (in billion liters)
United States	56.1	4.8
Brazil	28.2	4.1
Germany	0.9	2.8
Netherlands	0.4	1.5
France	0.9	2.4
China	2.8	0.4
Argentina	0.8	2.1
Thailand	1.2	1.2
Singapore	~0	1.0
Canada	1.7	0.3
Indonesia	0.1	1.7
Spain	0.5	0.6
Colombia	0.5	0.6
Belgium	0.6	0.4
India	**0.7**	**0.1**
Malaysia	~0	0.7
EU–28	**4.1**	**11.5**
World	**98.3**	**30.1**

Among these, biodiesel has gained major popularity due to distinct advantages. This liquid fuel is produced from natural lipids such as vegetable oil or animal fat using industrial processes of esterification or transesterification. As biodiesel is produced from renewable feedstock, it is essentially a "carbon neutral" fuel that does not contribute to net carbon emission to the environment. It is biodegradable and non–toxic (Quispe et al., 2013). Its thermal and rheological properties are very similar to the petroleum–derived diesel. Table 1.4 lists the physical properties of alternate renewable liquid transportation fuels such as alcoholic biofuels and biodiesel (Ranjan and Moholkar, 2012).

Table 1.4. Comparative properties of different alternate liquid fuels

Fuel	Gasoline	Butanol	Ethanol	Methanol	Biodiesel
Energy density ($MJ \cdot L^{-1}$)	32	29.2	19.6	16	31–33
Air:fuel ratio	14.6	11.2	9.0	6.5	12.5
Heat of vaporization (MJ/kg)	0.36	0.43	0.92	1.2	–
Research octane number	91–99	96	129	136	–
Motor octane number	81–89	78	102	104	–
Cetane number	–	–	54	–	48–65

These distinct features of biodiesel have made it a potential renewable alternative to fossil fuel, which can help in reducing GHGs emission and environmental pollution (Vidosh et al., 2011). Government of India has a strong mandate of implementing 5% blends of biodiesel by year 2020. In order to attract investment in biodiesel industry and promote production of biodiesel, Government of India has implemented numerous policies, schemes and incentives (Biswas et al., 2010). One of these schemes is to offer a Minimum Support Price (MSP) for procurement of biodiesel by the petroleum industry. The net MSP for biodiesel in India is Rs. 16.59/liter, which is still much higher than the production cost. It has been reported that from 75 to 95% of the end price of biodiesel is influenced by the cost of the raw material, i.e. the oil seeds (Yuste and Dorado, 2006). In the Indian context, the typical oil content of non–edible oil seeds such as Jatropha or Karanja or Neem is not more than 30% w/w. Therefore, the net oil yield from a hectare of plantation (that would yield approx. 4 to 5 tons of seeds) is merely 1.2 to 1.5 tons. The typical cost of the seeds is about Rs. 20 per kg. Moreover, sufficient availability of the seeds throughout year is also not guaranteed. These factors make ex–works price of biodiesel is almost at par with the petro–diesel (Tran et al., 2011), and hence, the economy of biodiesel production is not at all attractive. The production cost of biodiesel in India from jatropha is given in Table 1.5. The biodiesel industry needs to look for alternative source of revenue in order to make the business economically feasible.

Table 1.5. Production cost per liter of biodiesel from jatropha (adopted from Mandal, 2005)

Items	Cost (Rs.)	Remarks
Cost of seed (Rs./kg Oil)	16.4	Seed Rs. 5/kg, oil yield 33%, 3.28 kg seed – >41 kg oil
Cost of collection & oil extraction	2.48	Losses 5%, 1.05 kg –>41 kg oil, cost @ Rs. 2.36/kg
Transesterification cost	6.67	For 300 tonnes/day plant
Cost of biodiesel per kg	25.55	
Less byproduct (oil cake)	–2.23	2.23 kg cake @ Rs. 1/kg
Less byproduct (glycerol)	–3.8	0.095 kg @ Rs. 40/kg
Net cost of biodiesel per kg	19.52	As per Planning Commission
Net cost of biodiesel per litre	16.59	Specific gravity of oil – 0.85
Sale price of biodiesel to oil companies per litre (excluding excise/sales tax)	20	Profits @ 12% (Rs. 2/L), transport @ Rs. 0.41/L and interest/miscl. @ Rs. 1/L
Cost of petrodiesel per litre	18	Excluding excise/sales tax (based on $50/ barrel crude)

A possible means of earning higher revenue are sale of the oilseed cake after extraction of oil as animal feed or proper utilization of the co–product, glycerol. Glycerol is a highly versatile chemical that finds numerous applications as antifreeze agent in liquid fuel, liquid base in cosmetics, pharmaceuticals, or even as food preservative. However, the glycerol originating from biodiesel industry is not much useful for these applications, due to the contaminations by alkali and alcohol in it. Hansen et al. (2009) studied the chemical compositions of 11 varieties of crude glycerol collected from 7 Australian biodiesel producers and indicated that the glycerol content varies in the range of 38 to 96%, with more than 14% methanol and 29% ash. An effective means of utilization of the crude glycerol is to convert it into value–added products through either catalytic or biochemical route (Pagliaro et al., 2007). It is estimated that by year 2020 the global production of biodiesel would reach 32 billion liters (~ 8.2 billion gallons). This would concurrently produce approx. 2.6 million tons (5.9 billion gallons) of crude glycerol (Renewables, 2016). During transesterification reaction in biodiesel industry (in which vegetable oil reacts with

methanol in presence of an alkali like NaOH or KOH as catalyst), 1 mole of triglyceride produces 3 moles of methyl esters (i.e., biodiesel) and 1 mole of glycerol. In other words, 1 kg of crude glycerol is produced per 9 kg of biodiesel with a ratio of 10:1.

The major conventional applications of glycerol are such as additives in food, tobacco, pharmaceutical industry, while the other applications include as a feedstock for the production of value–added product such as biofuels, bioplastics, and various other chemicals. The traditional uses of glycerin are shown in Fig. 1.1. Main uses of purified glycerin are in cosmetics and food products which accounts for 65% of total consumption.

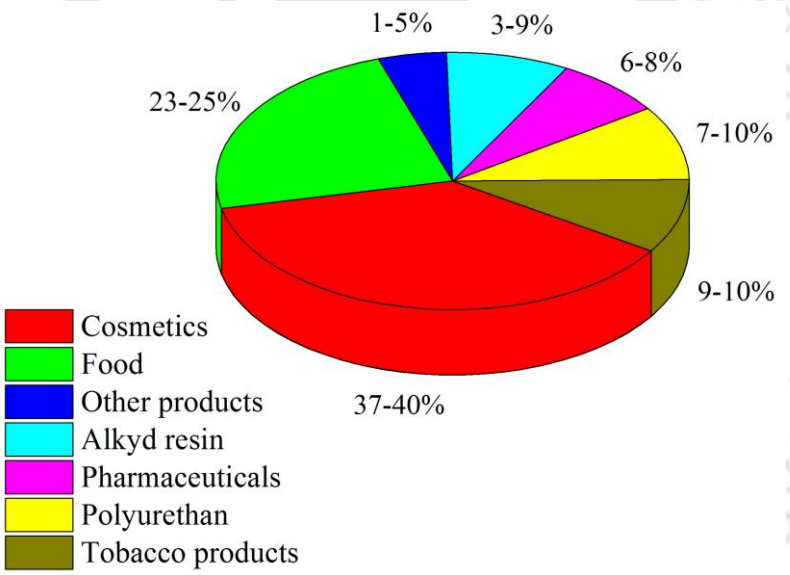

Figure 1.1. Traditional glycerol uses with average worldwide values (Stelmachowski, 2011)

Conventionally, glycerol is an excellent carbon source for fermentation. Many microbial species are able to grow on glycerol as carbon source and convert it into numerous value–added products (Khanna et al., 2012). A comprehensive review on production of various value–added products from glycerol as feedstock (mainly 1,3–

propanediol, dihydroxyacetone, butanol, citric acid, succinic acid etc.) can be found in Khanna et al. (2012).

1.2 CONVERSION OF GLYCEROL TO HIGHER VALUE PRODUCTS

Conversion of enormous quantities of crude glycerol generated as co–product of biodiesel into value–added products is a potential way of enhancing the economics of the biodiesel industry. Two different techniques, e.g. catalytic conversion (inorganic synthesis) and bioconversion (or microbial fermentation) has been examined for valorization of crude glycerol. A brief description of these two routes along with suitable examples is given below.

1.2.1 Catalytic conversion

Numerous review papers report the production of several value–added products through catalytic conversion route (Bagheri et al., 2015; Pagliaro et al., 2007; Zhou et al., 2013). Glycerol can be converted to value–added products through several catalytic routes, such as selective oxidation, selective hydrogenolysis, catalytic dehydration, pyrolysis & gasification, selective glycerol transesterification & esterification, selective etherification & carboxylation (Fan et al., 2010). The principal products derived from chemical (or catalytic) transformation of glycerol and relevant reaction schemes are shown in Table 1.6 and Fig. 1.2, respectively.

1.2.2 Bioconversion (or microbial fermentation)

An alternate route for production of value–added chemicals from crude glycerol is bioconversion or microbial fermentation. In comparison to the catalytic conversion route, the bioconversion route has two distinct merits, e.g. operation at ambient conditions, and high selectivity of products.

Table 1.6. Summary of reaction processes and valued–added products from catalytic conversion of glycerol

Reaction processes	Principal products
Oxidation	Dihydroxyacetone; glyceraldehyde; acids such as glyceric acid, mesoxalic acid, tarconic acid, hydroxypyruvic acid and oxalic acid
Dehydration	Acroline
Acetylation	Acetins (mono–, di– and triesters of glycerol)
Esterification	Glycerol carbonate; glycerol ester (mono, di, and tri)
Gasification	H_2 or syngas
Reduction	Ethyleneglycol; 1,2–propileneglycol, 1,3–propileneglycol; lactic acid; acetol; propanol
Etherification	Polyglycerols (e.g.: glycerol tertiary butyl ether, methyl tertiary butyl ether, 1,3–ditertbutyl glycerol, 1,2–ditertbutyl glycerol and 1,2,3–tri–tertbutyl glycerol)
Ammoxidation	Acrylonitrile; acrolein
Acetalization	Isomeric six–(1,3–dioxane) and five membered (1,3–dioxolane) cyclic products

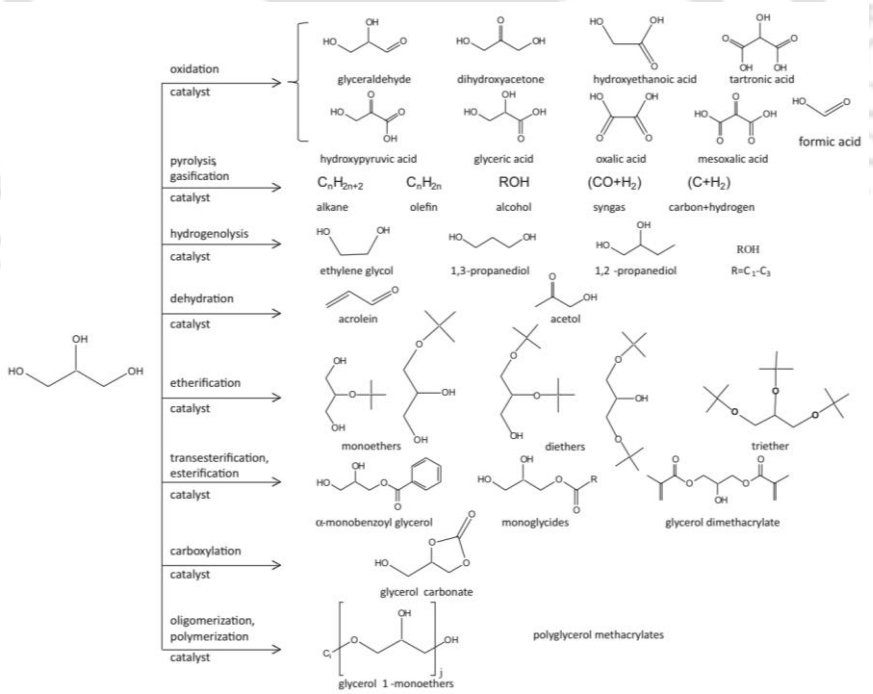

Figure 1.2. Catalytic conversion of glycerol to higher value products (adopted from Aresta and Dibenedetto, 2014)

Certain microbial strains can utilize glycerol as a main carbon source for their growth and maintenance. Apart from growth, glycerol is utilized by the cells for production of various enzymes, proteins, amino acids, vitamins, etc. The glycerol metabolism by the microbial cells has two distinct pathways: oxidative and reductive (Yazdani and Gonzalez, 2007). Several microbial species belonging to genus of *Escherichia*, *Klebsiella*, *Enterobacter*, *Gluconobacter*, *Clostridium*, *Candida*, and *Aspergillus* have been reported as capable of metabolizing glycerol as a sole source of carbon, via either aerobic or anaerobic route (Solomos et al., 1995). The generalized metabolic pathway of glycerol conversion by micro–organisms is shown in Fig. 1.3. Table 1.7 gives a summary of products and the respective micro–organisms used for biochemical conversion of glycerol.

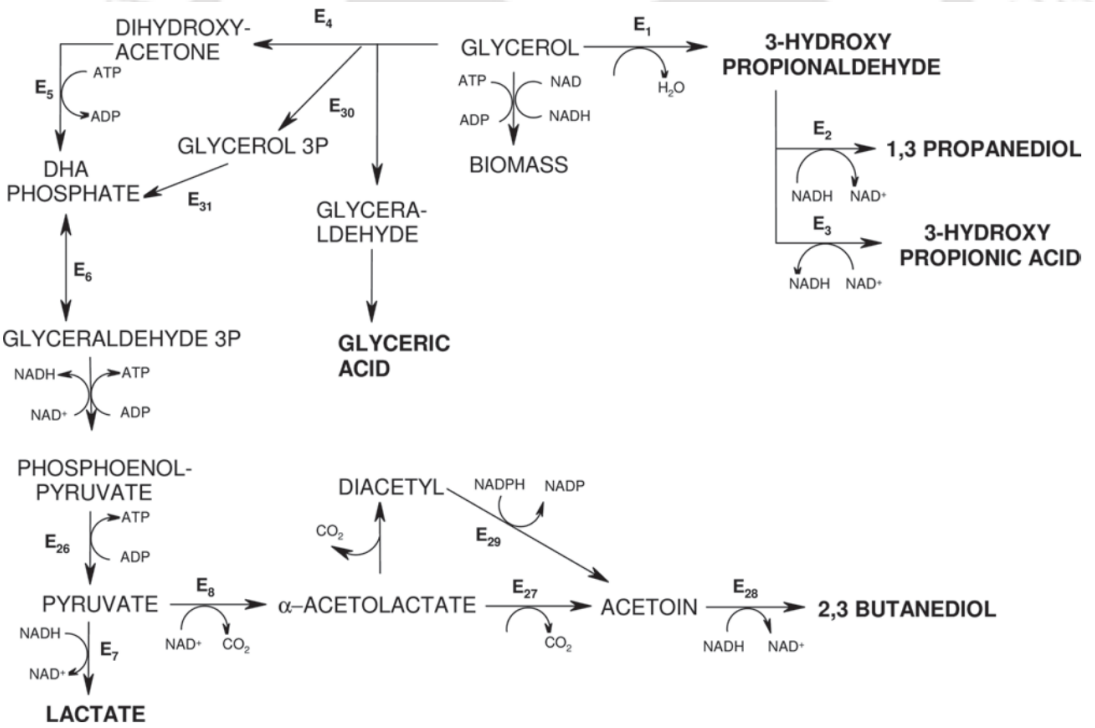

Figure 1.3. Metabolic pathway of glycerol bioconversion: Oxidative and reductive wings of glycerol assimilation (E_1–Glycerol dehydratase; E_2–1,3 PDO dehydrogenase; E_3–Aldehyde dehydrogenase; E_4–Glycerol dehydrogenase type 1; E_5–Dihydroxy acetone kinase; E_6–Triose phosphate isomerase; E_7–Lactate dehydrogenase; E_8–Pyruvate decarboxylase; E_{26}–Pyruvate kinase; E_{27}– α–Acetolactate decarboxylase; E_{28}–Acetoin reductase; E_{29}–Diacetyl reductase; E_{31}–Glycerol 3–phosphate dehydrogenase) (adopted from Khanna et al., 2012).

Table 1.7. List of micro–organisms capable of utilizing glycerol and the final product of the metabolism

Final product	Micro–organisms
1,3–Propanediol	*Klebsiella, Clostridia, Citrobacter, Enterobacter, Lactobacillus*
Butanol	*Clostridium pasteurianum, Clostridium acetobutylicum*
Dihydroxyacetone	*Gluconobacter oxydans, Acetobacter xylinum*
Citric acid	*Aspergillus niger, Yarrowia lipolytica, Candida oleophila*
Glyceric acid	*Gluconobacter, Acetobacter, Gluconacetobacter*
3–Hydroxypropionaldehyde	*Lactobacillus, Enterobacter, Desulphovibrio, Methanospirillum*
Biosurfactants	*Pseudomonas, Candida, Rhodococcus*
Propionic acid	*Propionibacteria*
Polyhydroxyalkanoates	*Ralstonia eutropha, Pseudomonas, Cupriavidus necator*
Extracellular polysaccharides	*Pseudomonas oleovorans*
Succinic acid	*Anaerobiospirillum succiniproducens, Escherichia coli, Actinobacillus succinogenes*
Erythritol	*Y. lipolytica*
Mannitol	*Y. lipolytica, Candida magnoliae, Candida azyma*
Ethanol	*Enterobacter aerogenes, E. coli*
Lactic acid	*Lactobacilli, Pediococcus pentosaceus*
Methane	*Methanobacterium sp., Methanosarcina sp.*
Hydrogen	*Clostridia, E.coli, Enterobacter*
Oxalic acid	*Aspergillus sp.,*
2,3–Butanediol	*Klebsiella oxytoca, Klebsiella pneumoniae*
3–Hydroxypropionic acid	*Lactobacillus sp.*, recombinant *E. coli*

1.3 PRODUCTION OF DIHYDROXYACETONE FROM GLYCEROL

Among value–added chemicals resulting from crude glycerol conversion (both chemical and biochemical routes), dihydroxyacetone (DHA) has special importance. Its commercial value is 25,000 $/ton, which is 100× that of crude glycerol (1,000 USD/ton).

It is mainly used as artificial tanning agent for protection of skin from UV rays. Additionally, it also finds application in pharmaceuticals as intermediate compound for drug production, and medicine (treatment of vitiligo, antidote to cyanide–induced intoxications, components of hemorrhage arresting biomaterials) (Cummings, 2004; Gatgens et al., 2007; Henderson et al., 2010). DHA also acts as precursor for synthesis of various chemicals, such as methotrexate, lactic acid, surfactants, 1,2–propylene glycol etc. and pharmaceutical products (Hekmat et al., 2003). DHA is used in food industry as an artificial sweetener in products for diabetic patients, and as a dietary supplement for sports person (Nabe et al., 1979; Stanko et al., 1993). Greater details on catalytic and microbial production of DHA from glycerol are given in following sections.

1.3.1 Catalytic conversion of glycerol to DHA

1,3–dihydroxyacetone is produced from glycerol by oxidation reaction in presence of catalyst. Published literature also reports catalytic production of DHA from formaldehyde. The formaldehyde route to DHA is based on condensation reaction called "formoin reaction". Josep Castells and co–workers first described this reaction in 1980, according to which condensation of formaldehyde in the presence of conjugate bases of thiazolium ions (thiazolium ylides) yields a complex mixture of branched and unbranched aldehydes and ketones (Castells et al., 1980). A process based on this method obtained DHA yield of 82% of initial glycerol concentration. The problem associated with this method is difficulty in purifying DHA, which also adds to the cost.

The production of DHA from glycerol via chemical means can be done either catalytically or electrocatalytically. A review on catalytic conversion of glycerol to different fuels and value–added chemical can be found in Zhou et al. (2013). The authors reviewed production of fine chemicals, e.g. hydrogen, propanediols, dihydroxy–acetone,

glyceric acid, by adopting various modes of reactions that include steam reforming, aqueous–phase reforming, hydrogenolysis, oxidation etc. The production of DHA from glycerol in the presence of catalyst was carried out under mild operating conditions, usually at a temperature lower than 373 K and atmospheric pressure. A summary of other literature on catalytic oxidation of glycerol to DHA is presented in Table 1.8. Many studies summarized in Table 1.8 report formation of several valuable side products, along with DHA, during glycerol oxidation: glyceric acid, tartronic acid, glycolic acid, and mesoxalic acid (Awbrey, 2010; Katryniok et al., 2011). Typical catalysts that have been employed as reported by previous authors are supported mono– and bimetallic systems. The catalytic oxidation of glycerol was commonly conducted in acidic or alkaline media in presence of oxygen as oxidant in a liquid–phase batch reactor or in a continuous flow gas–phase reactor (Demirel et al., 2007; Pollington et al., 2009; Worz et al., 2010). With small particle size and suitable support, Au is an excellent catalyst for glycerol oxidation. For instance, use of multi–walled carbon nanotubes supported Au nanoparticles resulted in oxidation of glycerol preferentially in its secondary alcohol function, thereby leading to DHA formation. In contrast, conventional activated carbon supported Au catalysts showed more selectivity toward glyceric acid, with lesser selectivity towards DHA (Rodrigues et al., 2011). In addition, many studies reported that carbon–supported bimetallic catalysts, such as Bi–Pt/C, Au–Pt/C, and Pd–Ag/C, have better performance than single metal catalysts. Demirel et al. (2007) used bimetallic Au–Pt/C which showed DHA selectivity of 36%, as compared to selectivity of 10% obtained with Au/C catalyst. Use of Pt–Bi/C bimetallic catalyst also lead to higher DHA selectivity of 48% than single metal Pt/C catalyst that showed selectivity of 17% (Hu et al., 2010c). In another study by Hirasawa et al. (2013), higher DHA selectivity (81.9%) and activity was detected for Pd–Ag/C bimetallic catalyst than single metal Pd/C catalyst. For SiO_2 support (instead of carbon), the selectivity increased

to 91.6%. The DHA selectivity was proportional to Ag concentration in the catalyst mixture.

In addition to noble metal–based catalysts, organometallic compounds were also found to be able to catalyze the oxidation of glycerol to DHA. However, in these cases, H_2O_2 or tert–butyl hydroperoxide was used as the oxidant. Kirillova et al. (2010) used a system consisting of aqua–soluble tetra copper(II) triethanol aminate complex $[O\subset Cu_4\{N(CH_2CH_2O)_3\}_4(BOH)_4][BF_4]_2$, H_2O_2, H_2O, acetonitrile and glycerol under a mild reaction condition. Selectivity of 93% to DHA at a 7.5% conversion of glycerol was achieved. Using H_2O_2 as the oxidant, Shulpin et al. (2010) tested two manganese–containing catalysts, soluble catalyst $[LMn(\mu–O)_3MnL](PF_6)_2$ and heterogenized catalyst $[LMn(\mu–O)_3MnL]_2[SiW_{12}O_{40}]$ (L is 1,4,7–trimethyl–1,4,7–triazacyclononane) for oxidation of glycerol. Both catalysts were found to be effective. The oxidation of 0.5 M glycerol catalyzed by 1 M $[LMn(\mu–O)_3MnL](PF_6)_2$ with 0.3 M H_2O_2 in 30 min led to 12.5% yield of DHA. Moreover, these catalysts were also able to be heterogenized with conversion to solid phase $[LMn(\mu–O)_3MnL]_2[SiW_{12}O_{40}]$, thereby making them reusable.

Although catalytic route of DHA oxidation has merit of faster kinetics, it has several limitations, especially from viewpoint of large scale implementation. These limitations include: (1) high costs – both capital and operating – of the process, (2) use of expensive catalysts, (3) harsh operating conditions with extensive effluent treatment and gaseous emissions, and (4) limited product selectivity and difficulty in purification of DHA.

The biochemical route of glycerol oxidation overcomes most of these limitations. However, this route has its own limitation of slow kinetics (Hekmat et al., 2003).

Table 1.8. Summary of literature on catalytic route of oxidation of glycerol to dihydroxyacetone

Catalysts	Reaction volume/ Glycerol concentration	Oxidant	Reactor and reaction conditions	Glycerol conversion (%)	DHA yield/Selectivity	Salient features of the study	References
Pt–Bi/C	175 mL, 1 M	0.2 MPa O_2	A high pressure Parr reactor; temp. – 80 °C; 30 psig; pH – 2.1	80	Y_{DHA} – 48%	• Highest glycerol conversion obtained with catalytic composition of 3% Pt and 0.6% Bi. • Effect of temperature, oxygen pressure and reaction pH were optimized.	Hu et al., 2010c
Au–Pt/C	150 mL, 1.5 M	0.1 MPa O2 (300mL min^{-1})	A 300 mL semi–batch glass reactor; temp. – 60 °C; stirring – 500 rpm; pH – 12	50	S_{DHA} – 36%	• Carbon support influence the catalytic activity with its pore texture.	Demirel et al., 2007
Au/MW CNT	195 mL, 0.3 M	0.3 MPa O_2	Temp. – 60 °C; stirring – 1000 rpm; NaOH/Gly molar ratio = 2	93	S_{DHA} – 60%	• High DHA selectivity observed because of the peculiar porous characteristics of the support.	Rodrigues et al., 2011
Au/C	195 mL, 0.3 M	0.3 MPa O_2	Temp. – 60 °C; stirring – 1000 rpm; NaOH/gly molar ratio = 2	72	S_{DHA} – 18%	• Selectivity is less in this case because of the confined structure of the Au/C catalyst.	Rodrigues et al., 2011
Pt/C	50 mL, (1.09 M)	150 mL/min O_2	A 100 mL glass reactor; catalyst – 0.5 g; temp.– 60 °C; time – 6 h	50	S_{DHA} – 17%	• Different sized Pt catalyst for glycerol oxidation was verified. • Small sized Pt catalyst (<6 nm) had stable glycerol conversion. • Apart from DHA, other major products detected are glyceric acid, glycolic acid, hydroxypyruvic acid.	Liang et al., 2009

Table 1.8 (*continued…*)

Pt–Cu/C	50 mL, (1.09 M)	150 mL/min O_2	A 100 mL glass reactor; catalyst – 0.5 g; temp. – 60 °C; time – 6 h	47.8	S_{DHA} – 16.3%	• Another major product is glyceric acid with selectivity – 62.2%. • Highest DHA selectivity was observed for 1Pt–Cu/C catalysis (1 wt% Pt). • Bimetallic Pt–Cu/C was more active than monometallic Pt/C towards selective oxidation of glycerol to glyceric acid	Liang et al., 2011a
Pt/MWNT and Pt/AC	50 mL , (1.09 M)	150 mL/min O_2	A 100 mL three neck flask; catalyst – 0.5 g; temp. – 60 °C; time – 6 h	70.1 (Pt/MWNT); 46.7 (Pt/AC)	S_{DHA} – 2.8% (Pt/MWNT) S_{DHA} – 3.9% (Pt/AC)	• Pt/MWNTs catalyst was more active than Pt/AC for glycerol oxidation. • The highest DHA selectivity was observed in case of Pt/AC catalyst. • The other major product than DHA is glyceric acid with higher selectivity.	Gao et al., 2009
Pt/S–pretreated MWNTs	50 mL, (1.09 M)	150 mL/min O_2	A 100 mL three–neck flask; catalyst – 0.5 g; temp. – 60 °C; time – 6 h; NaOH/Gly molar ratio = 2	92.6	S_{DHA} – 23.5%	• Without addition of base (NaOH), the highest DHA selectivity was 13.3 with glycerol conversion of 90.4%.	Liang et al., 2011b
Bi–Au–Pt/AC	10 mL, 0.3 M	0.3 MPa O_2	A 30 mL glass reactor; temp. – 80 °C; Gly/metal = 500 (mol/mol)	30	S_{DHA} – 65%	• Addition of Bi favors the production of dihydroxyacetone as main product instead of glyceric acid. • DHA selectivity of 63% was observed for 80% glycerol conversion.	Villa et al., 2015

Table 1.8 (*continued…*)

Pt–Bi/C	50 mL, (1.09 M)	150 mL/min O_2	A reactor; temp. – 60 °C; time – 6 h; catalyst – 0.5 g	91.5	S_{DHA} – 49%	• This higher conversion was achieved due to the presence of specially configured Pt–Bi nanoparticles with size of 3.8 nm on the active carbon support. • The catalyst was stable for five consecutive cycles with a decrease in glycerol conversion from 91.5 to 84.85%.	Liang et al., 2011c
Pd–Ag/C	20 mL Gly (0.54 M)	0.3 MPa O_2	A 190 mL stainless steel autoclave; catalyst – 0.05 g; temp. – 80°C; stirring – 500 rpm; time – 4 h	9.5	S_{DHA} – 81.9%	• Pd catalyst with higher Ag tends to be more selective for DHA formation. • The selectivity of the catalyst increased up to 91.6% when supported with SiO_2. • Effect of organic additives (carboxylic acids or ketones) over glycerol oxidation was also screened.	Hirasawa et al., 2013
$[O\subset Cu_4\{N(CH_2CH_2O)_3\}_4(BOH)_4[BF_4]_2$	2.5 mmol gly (5 M gly soln.)	5.0 mmol H_2O_2 (35% in H_2O)	A thermostated round–bottom flasks or Pyrex cylindrical vessels; temp. – 25 °C; time – 30 h; acetonitrile was added to reach 5.0 mL of the reaction mixture	7.5	S_{DHA} – 93%	• The DHA selectivity increases with decrease in H_2O_2 concentration from 5 to 0.5 mmol. • The glycerol conversion percentage decreases from 18% to 7.5% with decrease H_2O_2 concentration.	Kirillova et al., 2010
Cu(II) sulfonato–salen complex	0.54 M (100 mL 3% H_2O_2)	3% H_2O_2	A flask; temp. – 60 °C; time – 4 h; pH – 7	40.3	S_{DHA} – 52.9%	• This catalyst was favorable for activation of H_2O_2, promoting the oxidation of glycerol to DHA. • Effect of reaction time, temperature, pH value and reusability of the catalyst were conducted.	Jing et al., 2015

Gly – Glycerol; MWCNT – Multi walled carbon nanotubes; NCNT – N doped carbon nanotubes

1.3.2 Microbial conversion of glycerol to DHA

In 1898, Bertrand first reported the microbial production of DHA using glycerol as substrate. A year later the microbial strain used for this study was identified as *Bacillus xylinum*. Till now, several different microbial species have been identified as potential candidates for DHA production from various substrates. Most of the strains reported in previous literature belong to the genus of *Bacillus*, *Gluconobacter*, *Acetobacter*, *Candida*, *Klebsiella*, *Escherichia* etc. Recently, Liu et al. (2008) have reported the production of DHA from glycerol using a new species, *Pichia membranifaciens* isolated from soil sample. Many studies have also reported the use of genetically modified strains of *Escherichia*, *Gluconobacter*, *Acetobacter* etc. for the production of DHA. Among all microbial species, *Gluconobacter* strains are the most extensively used micro–organism (in laboratory as well as industrial scale) for production of DHA from glycerol. A review by Gupta et al. (2001) reports commercial application and importance of *Gluconobacter oxydans* cells from past few decades. Apart from glycerol, it also has an ability to utilize other carbon substrates like D–sorbitol, D–fructose, D–glucose etc. through oxidative metabolism for the synthesis of compounds like Vitamin C, D–gluconic acid, ketogluconic acid, xylitol, vinegar etc. (Macauley et al., 2001). *Gluconobacter oxydans*, formerly known as *Acetobacter suboxydans* is a gram negative bacteria in the family of *Acetobacteraceae* (Gupta et al., 2001). DHA is produced via incomplete oxidation of glycerol by membrane–bound glycerol dehydrogenase enzyme.

1.3.2.1 Structure and activity of glycerol dehydrogenase

Acetic acid bacteria are characterized by their ability to carry out incomplete oxidation of alcohols, sugars and other related compounds. Oxidation of sugars, alcohols and related compounds takes place through two alternate metabolic pathways with

involvement of two different enzymes (De Ley et al. 1984; Matsushita et al. 1994). These enzymes can be classified as (1) $NAD(P)^+$ dependent enzymes, which are located in the cytoplasm, and (2) $NAD(P)^+$ independent enzymes which are membrane bound. In case of $NAD(P)^+$ dependent enzyme system, the substrate molecules need to enter inside the cytoplasm for oxidation. The substrates are oxidized by $NAD(P)^+$–dependent enzymes, and the resulting intermediates are phosphorylated, and further metabolized via the pentose phosphate pathway (Deppenmeieret al., 2002). Whereas for $NAD(P)^+$ independent system, the reactions are carried out inside the periplasmic space by the membrane bound enzymes. The membrane–bound dehydrogenases are further classified into two types, viz. (a) quinoproteins that contains pyrroloquinoline quinone (PQQ), and (b) flavoproteins that have and covalently–bound flavin adenine dinucleotide (FAD) as prosthetic groups, respectively. The oxidation reactions are catalyzed by membrane bound dehydrogenases, which are located in the cytoplasmic membrane and coupled to the respiratory chain. The active sites of the enzymes are oriented towards the periplasm, so the substrate molecules have only to cross the outer membrane; and the transport into the cytoplasm is not necessary. After oxidation, the reactions products are easily released into the medium via porines present in the outer membrane of the Gram–negative bacteria.

Oxidation of glycerol to DHA by the membrane bound PQQ dependent glycerol dehydrogenase in *G. oxydans* is well known. The graphical representation of this phenomenon is shown in Fig. 1.4A and B. The exact physiology (or bio–mechanism) of DHA formation during glycerol metabolism was explained by Claret et al. (1992). *G. oxydans* lacks glycolytic and carboxylic acid pathways, hence the pathway involving membrane bound glycerol dehydrogenase is indispensable for its energy requirements. On the other hand, cytoplasmic pathway begins with phosphorylation of glycerol followed by dehydrogenation to DHAP. This pathway allows for bacterial growth. DHAP produced is

catabolized by pentose phosphate pathway. The pathway for DHA production is shown in Fig. 1.4A.

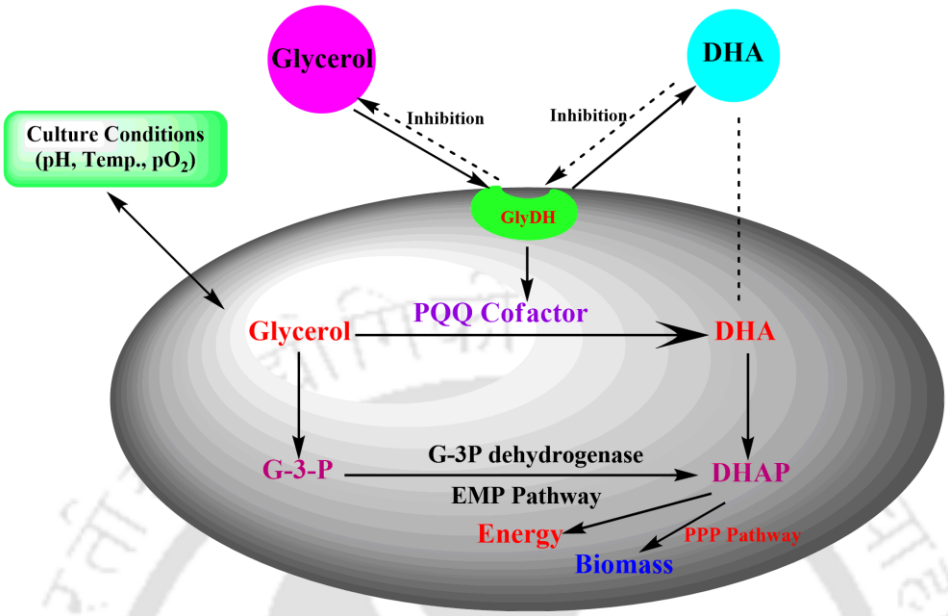

(A)

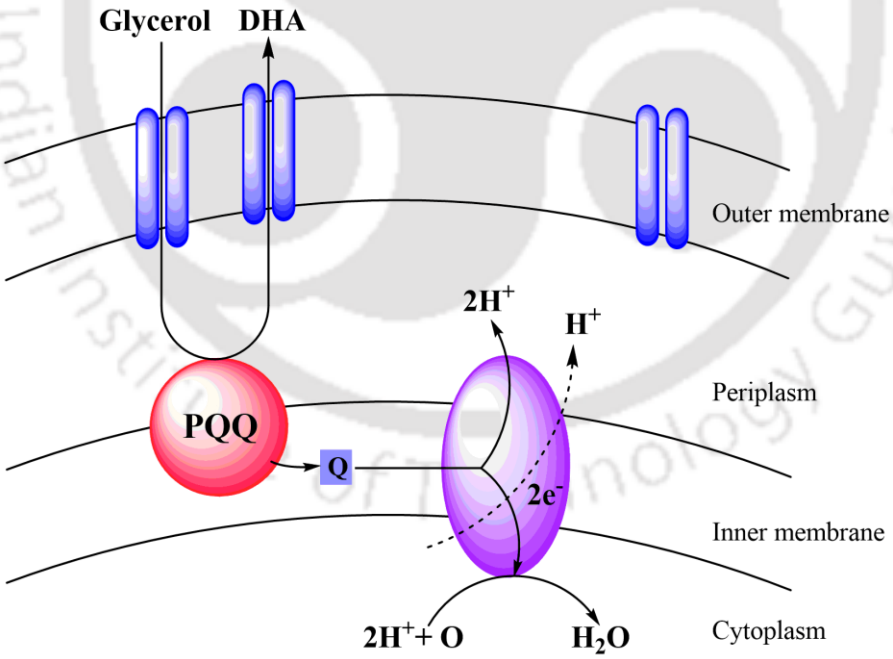

(B)

Figure 1.4. Microbial conversion of glycerol to DHA by *G. oxydans*. (A) Reaction pathway; (B) Mechanism inside cells

1.3.2.2 Production of DHA by free cells

Several literature has been published on DHA production from glycerol oxidation using free cells of numerous microbial species. The microbial strains employed in previous studies include *G. oxydans*, *G. frateurii*, *Pichia membranifaciens* and genetically modified strains of *E. coli*, *G. oxydans* etc. A summary of previous literature is presented in Table 1.9.

1.3.2.3 Production of DHA by immobilized cells

The kinetics as well as yield of biochemical processes is influenced by the density or population of the microbial cells in the fermentation mixture. Immobilization of these cells to a suitable support greatly controls the cell density in the fermentation mixture and also makes product separation process easier. By definition, immobilization is the physical confinement or localization of intact cells to a certain defined region of space with preservation of their desired catalytic activity. Confinement of cells mobility to surfaces facilitates easy separation of cells in fermentation mixture after completion of fermentation, and may permit their repeated use (the biocatalyst) eliminating the washout in continuous reactor. An added advantage of the immobilization is that it provides protection to the cells from shear forces. Previous authors have reported production of DHA from glycerol using immobilized cells of various microbial species, and the summary of the previous literature is given in Table 1.10. Most of the previous studies have used calcium alginate beads as a support matrix for glycerol conversion to DHA (Adlercreutz et al., 1985; Lidia and Stanisław, 2012; Stasiak–Rozanska et al., 2010; Tramper et al., 1983).

Table 1.9. Summary of literature on production of dihydroxyacetone from glycerol using free cells

Micro–organisms	Initial glycerol concentration (g/L)	Final DHA concentration (g/L)	Glycerol conversion (%)	Fermentation conditions	Salient features of the study	Reference
Gluconobacter oxydans NH10	160	139.2 (7.5 L stirred tank reactor)	87.9%	pH – 5.0; temp – 30 °C; aeration – 1.0 vvm; time – 52 h	Two stage agitation speed strategy was employed. Firstly 800 rpm (0 – 21 h) for increasing the cell growth, followed by 600 rpm (after 21 h) for DHA production. Batch fermentation carried out in a 7.5 L stirred tank reactor.	You et al., 2013
Pichia membranifaciens ZJB –0009	40	12.88 (shake flask) 13.57 (15 L bioreactor)	32.2% (shake flask) 33.93% (bioreactor)*	pH – 6.74; temp – 29.6 °C; time – 48.8 h For bioreactor – aeration rate – 0.8 vvm; agitation – 300 rpm	Box–Behnken factorial design was used to optimize 3 parameters, viz. pH (4 to 6), Temperature (15 °C to 45 °C) and fermentation time (24 to 48 h).	Liu et al., 2008
Gluconobacter frateurii	100 (crude glycerol from biodiesel synthesis)	73.1 (shake flask, batch process) 80.2 (7 L stirred bioreactor, batch mode)	89.5% (shake flask) Approx. 90% (bioreactor)	For shake flask: pH – 6.0; temp – 30°C; agitation – 220 rpm; time – 48 h For bioreactor studies: pH – 5.5; temp – 30 °C; aeration – 1.5 vvm; agitation – 350 rpm	Fed batch fermentation carried out with initial glycerol conc. of 20 g/L and substrate added periodically to maintain glycerol conc. within 5–15 g/L. At the end of fed–batch process the DHA concentration and yield were 125.8% and 90.5%, respectively. Effect of nitrogen source, initial glycerol conc., chloride salts (NaCl and KCl) was assessed.	Liu et al., 2013

Table 1.9 (*continued*…)

UV mutant of *G. oxydans* ZJB–605	Initial – 20 g/L, feeding 0.5 – 0.7 g/min (fed batch)	209. 6	90.1	15 L fermenter; temp – 30 °C; pH – 6.0 (for first 6 h); 5.0 (till the end); DO – 20% (24 h); 30% (60 h); 40 % (till the end)	This mutant strain exhibits high productivity and can tolerate high DHA concentrations. DO shift controlled strategy found to be more effective for DHA production.	Hu and Zheng, 2011
Gluconobacter oxydans (alcohol dehydrogenase – deficient mutant)	40, 100, and 140	26.3 (for glycerol conc. – 40 g/L, shake flask), 96 (for glycerol conc. – 100 g/L, 5 L fermenter) and 134 (for glycerol conc. – 140 g/L, 5 L fermenter)	66% (for initial glycerol conc. – 40 g/L) 96% (for initial glycerol conc. – 100 g/L and 140 g/L)	For shake flask: pH – 6.0; temp – 30°C; agitation – 250 rpm; time – 24 h For fermenter: pH – 6.0; temp – 30 °C; agitation – 900 rpm; time – 8 h (for glycerol conc. – 100 g/L); time – 14 h (for glycerol conc. – 140 g/L)	*E. coli* strain was used for host plasmid construction. 2.4–fold increase in activity observed in batch fermentation for initial glycerol conc. of 100 g/L	Li et al., 2010a
Gluconobacter oxydans GM51	100	86.38 (shake flask)	91.5% (bioreactor)	Shake flask: pH – 6.0; temp. – 30 °C; time – 42 h For fermenter: aeration – 6 vvm; agitation – 500 rpm; pH – 6.0; time – 40 h	He–Ne laser irradiation technology was employed for construction of mutant strains. Activity of the enzyme glycerol dehydrogenase, in mutant strain gives high DHA yield (75.17% higher yield than wild strain for initial glycerol conc. of 100 g/L). Experiments in fermenter revealed shortening of culture time by 16 h, with a yield of 91.5% in a 7 L bioreactor.	Ma et al., 2010

Table 1.9 (*continued*…)

Resting cells of *Gluconobacter oxydans* ZJB09113	— (fed–batch operation)	156.3	89.8%	2 L airlift bioreactor; temp – 30 °C; airflow rate – 1.5 vvm; pH – 5.0; resting cells – 10 g/L; time – 72 h	pH, yeast extract conc., carbon source conc. optimized using Box–Behnken experimental design method. Effects of pH, aeration rate and cell content on DHA production were investigated.	Hu et al., 2011
Mutant strain *Gluconobacter oxydans* ZJB09112	— (feeding glycerol)	175.9	—	15 L fermenter; temp – 30 °C; pH 6.0 (for 20 h) and 5.0 (till end); 30% air saturation	For batch fermentation 30% DO concentration was optimal for DHA production. DO–stat feeding fermentation using a pH control strategy for DHA production was employed.	Hu et al., 2010a
Gluconobacter oxydans ZJB09112	92.5 (Initial 2.5 g L^{-1} then 18 g/L feeding per interval)	161.9	88.7	500 mL bubble column reactor; temp – 30 °C; pH – 5.0; gas flow rate – 1.5 vvm; time – 68h	Effect of carbon and nitrogen source, initial pH, gas flow rate of DHA production was investigated. Different initial conc. of glycerol feeding strategy was employed to reduce substrate inhibition.	Hu et al., 2010b

Table 1.10. Summary of literature on production of DHA from glycerol using immobilized cells

Micro–organism and immobilized support	Initial glycerol concentration (g/L)	Final DHA concentration (g/L)	Glycerol conversion (%)	Fermentation conditions	Salient features of the study	Reference
Gluconobacter oxydans ATCC 621; calcium alginate	30 g/L	24.6	87	Shake flask; pH 5; temp – 28 °C; time – 3 days	The DHA concentration for free cell was 25.8 g/L. Calcium alginate limit oxygen and substrate diffusion to the interior leading to lower DHA concentration. The efficiency of reused cells was 44, 84 and 94 %, respectively for three consecutive cycles.	Lidia and Stanisław, 2012
Gluconobacter oxydans; polypropylene Ralu–rings	Glycerol feeding with repeated–fed–batch process	82	87	2 L bubble–column reactor; time – 430 h	The carrier matrix proved to be biocompatible, durable, mechanically stable, and chemically inert. A higher space–time yield approx. 76% was observed compared to a similar process which was performed without an optimized fermentation medium.	Hekmat et al., 2007
Gluconobacter oxydans DSM 2003, polyvinyl alcohol	59.86 g/L	57.3	95.8	1.5 L fermenter; aeration – 1.5 vvm; agitation – 200 rpm; temp – 30 °C; pH – 6.0	Effect of pH, temperature, storage stability was performed. The immobilized cells were active for a period of 14 days and lost 10% of its activity. After regeneration, the biocatalyst could recover 90% of its initial activity.	Wei et al., 2007

Table 1.10 (*continued…*)

Micro–organism and immobilized support	Initial glycerol concentration (g/L)	Final DHA concentration (g/L)	Glycerol conversion (%)	Fermentation conditions	Salient features of the study	Reference
Gluconobacter xylinus, calcium alginate	100	10.9	–	Shake flask; pH – 5.0; temp. – 28 °C; agitation – 200 rpm; time – 36 h	The pH doesn't have any significant effect over the DHA production irrespective of the glycerol concentration. Increasing biotransformation time (over 36 h) resulted in decrease in DHA concentration due to phosphorylation of produced DHA.	Stasiak–Rozanska et al., 2010
Gluconobacter oxydans, hydrophili–zed Ralu–rings	Feeding glycerol, 10–30 g/L	60	–	Combined bioreactor system (stirred tank and packed trickle–bed column); pH – 4.5; temp. – 30°C	Cleaning, sterilization, and inoculation procedures reduced significantly. The productivity of the process reached by 75% to about 2.8 kg m^{-3} h^{-1}, within 17 days.	Hekmat et al., 2003

Wei et al. (2007) have reported the use of polyvinyl alcohol (PVA) as support matrix for immobilization. PVA is prepared by cross–linking with boric acid, with the addition of small amount of calcium alginate and provides a better support in terms of cost and toxicity tolerance. The immobilized cells retained activity over a period of 14 days, with loss of ~ 10% activity. More recent studies on DHA production by immobilized cells reported by Hekmat et al. (2003, 2007) used polypropylene Ralu–rings as immobilization support. This macro–porous support proved to be thermally and mechanically stable, biocompatible and chemically inert, and allowed better oxygen permeation. Due to macroporous structure of the support, the microbial cells could penetrate into deeper layer of this support, which resulted in rise in cell density.

1.3.3 Techniques for intensification of DHA production: conventional approach

Previous research in intensification of glycerol fermentation for DHA production has adopted several techniques: improvement of oxygen supply to microbial cells, use of genetically modified microbial strains, optimization of media components and process parameters, efficient reactor design, and better fermentation protocols etc. Each of these techniques has its merits and limitations, as discussed below.

1.3.3.1 Effect of dissolved oxygen concentration

As reported in the literature, oxygen partial pressure in the fermentation medium has significant effect on cell growth as well as DHA production. The cell growth and DHA production increases with increase in dissolved oxygen (DO) concentration (Li et al., 2010b; Ohrem and Voss, 1996; Svitel and Sturdik, 1994). DO concentration is known to be an important parameter for many industrial bioprocesses and can be controlled by regulating the agitation speed, flow rate of sparge gas and partial pressure of oxygen in the

sparge gas through the fermentation medium. Flickinger and Perlman (1977) reported DO concentration to be the vital parameter in glycerol metabolism, and no DHA formation was observed under oxygen–limited fermentation conditions. The DHA production increases with supply of oxygen enriched air into the medium. You et al. (2013) reported final DHA concentration of 139. 2 g/L with productivity of 2.72 $g \cdot L^{-1} \cdot h^{-1}$ by adopting two–stage agitation speed strategy. In the first stage, high specific cell growth rate was achieved by controlling the agitation speed at 800 rpm for 21 h. In the second stage, the agitation speed was reduced to 600 rpm to achieve high DHA production. The microbial species used in fermentation was *G. oxydans* NH–10. The average DHA concentration and productivity achieved with 2–stage strategy was 10.3% and 10.1% higher than that obtained for constant agitation speed of 600 rpm in both stages, respectively. Hu and Zheng (2011) reported a higher DHA concentration and productivity using mutant strain of *G. oxydans* as compared to wild type strain, with fed–batch fermentation in a 15 L bioreactor. They have adopted two protocols for controlling the DO concentration in the fermentation mixture by varying the O_2 content of sparge air through fermentation medium: (1) In the first approach, air with O_2 content of 20 mol% was sparged through fermentation mixture for 24 h. Thereafter, O_2 content in sparge air was raised to 30% till the end of fermentation. (2) In second approach, air with 20 mol% O_2 was sparged for first 24 h. Next, O_2 content was raised to 30% for 60 h, and finally O_2 content was adjusted to 40 mol% until the end of the fermentation. Higher DHA concentration (209 g/L) and productivity (2.91 $g \cdot L^{-1} \cdot h^{-1}$) was observed in the second protocol, while the DHA concentration and productivity in first protocol were 197.0 g/L and 2.74 $g \cdot L^{-1} \cdot h^{-1}$, respectively. Hu et al. (2010a) reported that very high O_2 content in sparge gas adversely affects cell growth as well as DHA production, as it leads to very high dissolved O_2 concentration. They found that increasing O_2 content of sparge gas from 30 to 50 mol% increased the *G. oxydans* ZJB09112 cell concentration

from 2.05 to 2.57 g/L, with concurrent reduction in final DHA concentration in fermentation broth from 8.4 to 7.2 g/L, respectively. A probable cause leading to this effect is rapid consumption of glycerol by high cell mass for maintenance and growth, and less utilization of glycerol for DHA production. This essentially means that DO in the medium needs to be at an optimal concentration for high DHA yield. Too low concentration of DO hampers cell growth, while too high concentration leads to excessive cell growth, and both of these consequences result in reduction of DHA yield (Imlay and Linn, 1988).

For immobilized cells, oxygen transfer in liquid phase to the cells is a mass–transfer limiting process. High agitation rate and sparge gas flow rate may cause physical damage to immobilization support. In view of this, Hoist et al. (1982, 1985) used H_2O_2 for improving O_2 supply to microbial cells in immobilized systems. Hydrogen peroxide is decomposed to oxygen and water *in–situ*, and oxygen generated in the medium is utilized for glycerol oxidation to DHA. Hoist et al. (1982) used *G. oxydans* cells immobilized in calcium–alginate beads and H_2O_2 was supplied after 40 h of fermentation. 20 fold increase in DHA productivity was observed as compared to sparge gas technique even with pure O_2. DHA productivity increased with H_2O_2 concentration up to 1.5 mM (Hoist et al., 1985). Very high concentration of H_2O_2 in the fermentation mixture could lead to deactivation of *G. oxydans* cells.

1.3.3.2 Use of genetically modified strains

Use of genetically engineered or mutant strains is potential alternative for enhancing DHA production, as compared to natural strains. Genetically engineered strains also have distinct merits such as higher resistance towards product/substrate inhibition, ability to grow/utilize cheap substrates, and overproduction of the key enzyme (glycerol dehydrogenase), which lead to improvement in DHA production.

As stated earlier, high concentration of glycerol and DHA inhibit the cell growth causing irreversible damage to cells, and adversely affecting DHA production (Claret et al., 1992). Gatgens et al. (2007) reported enhancement in DHA production by overexpression of *sldAB* gene, which encodes membrane–bound glycerol dehydrogenase. The recombinant *G. oxydans* MF1 showed higher DHA yield of 350 mM, as compared to natural (control) strain which yielded 200–280 mM DHA for glycerol input of 550 mM. Li et al. (2010a) adopted same approach and overexpressed the glycerol dehydrogenase gene by interrupting the membrane–bound alcohol dehydrogenase (ADH) gene in *G. oxydans* M5AM mutant strain. The DHA productivity increased to 2.4 fold, yielding 96 g/L DHA from 100 g/L of glycerol in a batch fermentation using resting cells as catalyst. For repeated batch experiments, 385 g DHA was achieved from fermentation of 400 g glycerol in 34 h with an average productivity of 2.2 g/g CDW/h. Recent study by Habe et al. (2010) reported improved growth of *G. oxydans* in high glycerol concentration by disruption of membrane–bound alcohol dehydrogenase (ADH). The authors reported that the Δ*adhA* deficient *G. oxydans* cells in log–phase could grow in high initial glycerol concentration of 220 g/L to produce 125 g/L DHA during 3–day of fermentation period. The resting Δ*adhA* deficient cells converted 230 g/L glycerol to 139.7 g/L DHA, which was much higher than wild strain. In addition to this, low–power laser irradiation technology and UV irradiation technology were used as mutagens for producing mutants for industrial application (Hu and Zheng, 2011; Ma et al., 2010). Hu and Zheng (2011) used an ultraviolet lamp (15 W, 253 nm) for mutagenesis, and among several mutants the *G. oxydans* ZJB11001 produced the highest DHA concentration of 209.6 g/L in 72 h of fed–batch fermentation using the DO–shift strategy. The mutant *G. oxydans* GM51 produced under the He–Ne laser irradiation technology (21 mW, 21 min) showed an increase in DHA yield of 77.6%, as compared to the wild type strain (Ma et al., 2010). Other than *G. oxydans* cells, *E. coli* was engineered

for DHA production by co–expressing *gldA* (glycerol dehydrogenase) and *nox* (NADH oxidase) gene (Yang et al., 2013).

1.3.3.3 Fermentation protocols and bioreactor design

Fed–batch fermentation is one of the most acknowledged methods to overcome the substrate (i.e., glycerol) inhibition in DHA production that has been reported by numerous authors (Hekmat et al., 2007; Hu et al., 2010a, b; Liu et al., 2013). Apart from this typical process, Bauer et al. (2005) implemented a novel semi–continuous, two–stage repeated–fed–batch process to overcome the inhibition effect of DHA on *G. oxydans* metabolism. The experiments were conducted in two stages; in the first stage, culture were grown under non–product inhibited condition in a laboratory–scale bubble column reactor, and then transferred to a stirred tank reactor for DHA formation in the second stage. The activity of *G. oxydans* cells was not affected by product inhibition till DHA concentration of 80 g/L. At higher DHA concentrations, some product inhibition effect was observed, but due to robust membrane–bound glycerol dehydrogenase of *G. oxydans*, product formation was active for a prolonged period of time. The final DHA concentration reached was 220 kg/m^3. DHA production using different reactor configurations was reported by Hu et al. (2011b) and Hekmat et al. (2003). Hu et al. (2011b) used 2 L custom–built airlift bioreactor with internal loop, which had several merits such as high fluid circulation, mass and heat transfer, low shear stress, low energy consumption and low operating and maintenance costs. Hekmat et al. (2003) designed a combination of conventional aerated stirred tank reactor and a column packed with hydrophilized Ralu–rings for immobilization of micro–organisms. The total volume of reactor was 110 L with working volume of 32 L. The fermentation broth was continuously circulated from the stirred tank into the top of the packed column with immobilized cells.

1.3.4 Substrate and product inhibition study

The glycerol metabolism by *G. oxydans* (or oxidation of glycerol by glycerol dehydrogenase) is limited by both substrate and product inhibition. In order to study the substrate inhibition effect (at high substrate concentration), Claret et al. (1992) recorded specific microbial growth and product formation rate for different initial glycerol concentrations (viz. 31, 51, 76, 95, and 129 g/L) in fermentation mixture. The experimental data was fitted to substrate inhibition models, and exponential model found to fit best for substrate inhibition effect on product formation. A maximal specific growth rate of 0.53 h^{-1} and specific product formation rate of 11.7 h^{-1} was obtained with substrate inhibition constants (K_{IS}) of 93.6 g/L and 76.7 g/L, respectively. This study, however, reported the inhibitory effect of substrate alone, without accounting for the simultaneous product inhibition effect induced by the accumulated DHA. The previous literature also reported inhibitory effect of DHA over cell growth. According to Nabe et al. (1979), the stability of glycerol dehydrogenase, the key enzyme responsible for glycerol oxidation could be altered by contact of *G. oxydans* cells to high DHA concentration. The inhibitory effect of initial DHA concentration in the fermentation medium has also been studied by Bories et al. (1991), Claret et al. (1993) and Ohrem and Voβ (1995). Claret et al. (1993) determined the specific parameters such as growth rate, substrate consumption rate and product formation rate by varying the initial DHA concentration in the range of 0–100 g/L and with a fixed glycerol concentration of 50 g/L. After fitting the experimental data to various models which includes linear, inverse and exponential, authors found exponential model as best fit. The initial DHA inhibitory threshold concentration for bacterial cell growth and production formation was found to be 87 and 96 g/L, respectively. This results also concluded that bacterial growth was more sensitive to high DHA concentration in fermentation medium. The results of Stasiak–Rozanska et al. (2014) corroborated this conclusion that mitotic

activity of *G. oxydans* was inhibited at low concentration of DHA (20–30 g/L) and no cell division occurred at DHA concentration of 70 g/L. These results essentially emphasize the role of substrate and product inhibition in glycerol metabolism by *G. oxydans*, and also justify a detailed study of these phenomena.

1.4 BASIC CONCEPT OF ULTRASOUND AND ITS APPLICATION IN FERMENTATION PROCESS

Ultrasound essentially refers to longitudinal acoustic waves beyond upper limit of human hearing range, i.e., 16 Hz – 20 kHz. The frequency range of ultrasound extends from 20 kHz to 20 MHz. Being a longitudinal wave, ultrasound passes through a compressible medium, such as air and water, in the form of alternate compression and rarefaction cycles. Propagation of ultrasound waves in the medium generates periodic variation in bulk pressure as well as density of the medium. Passage of ultrasound wave in the medium sets fluid elements in the medium in oscillatory motion around a mean position (Shah et al. 1999). Ultrasound wave is characterized by physical properties of frequency, velocity and pressure amplitude. During the propagation through medium, the pressure amplitude of the ultrasound wave is attenuated or dampened by various physical mechanisms. These mechanisms include thermal loss, frictional loss and scattering due to bubbles.

Frictional loss is a manifestation of finite viscosity of the medium. During oscillatory motion of the fluid elements of the medium, some of the momentum of the fluid elements is dissipated in the medium, which results in their unidirectional (and not truly oscillatory) motion. Thermal loss is attributed to heat conduction between adjacent regions of compression and rarefaction that results in loss of compression work. For propagation of ultrasound wave through liquid, bubbles present in the medium scatter the ultrasound waves causing severe attenuation. Presence of gas bubbles in the liquid also alters the

compressibility of the medium, as a result of which the speed of sound in the medium reduces. The properties of the sound wave in gaseous medium are strongly influenced by the static pressure in the medium. For sound wave propagation in liquids, the static pressure in the medium does not affect much, as the liquid properties are relatively insensitive to static pressures (at least for moderate levels of pressure).

1.4.1 Cavitation bubble dynamics

Cavitation can be defined as nucleation, growth, oscillation and transient collapse of gas/vapor bubbles driven by variation in bulk pressure in the medium. The cause leading to variation in bulk pressure could be propagation of an acoustic wave or variation in flow geometry (in case of flow cavitation like hydrodynamic cavitation), or in general, energy dissipation in the system. The efficiency of any physical/chemical/biological process depends on the method of introducing energy into the system. Cavitation has proven to be an efficient tool of introducing energy into the system for intensification of large number of physical/chemical/biological processes. Ultrasound makes available energies on extremely small time and spatial scales that are not available from any other source.

Using the criterion of nature of energy dissipation in the system, cavitation can be categorized as: Acoustic cavitation – which is generated due to pressure variation generated due to passage of an acoustic wave and Hydrodynamic cavitation – which results due to pressure variation in the liquid flow due to change in the flow geometry. Hypothetically, the phenomenon of cavitation refers to creation of voids in the liquid medium by pulling adjacent molecules apart by overcoming the Laplace pressure ($2\sigma/R$). As $R \rightarrow 0$, Laplace pressure $\rightarrow \infty$. Thus, theoretically, extremely high acoustic pressure amplitudes (exceeding ~100 MPa) would be required for generation of cavitation. However, in actual practice, cavitation occurs at very low pressure amplitudes (~ 1 bar). This result is attributed to

phenomenon of nucleation that drastically lowers the intermolecular forces. Nucleation in the liquid medium is induced by solid particles suspended or tiny free–floating bubbles present in the liquid. Another source of nuclei for occurrence of cavitation are gas pockets trapped in the crevices of the solid boundaries in the liquid medium. These gas pockets can grow in response to reduction in bulk pressure in the rarefaction cycle of acoustic wave.

1.4.2 Radial motion of cavitation bubbles

The periodic variation of bulk pressure in the medium induces volume oscillations of cavitation bubbles. The amplitude of these oscillations is directly proportional to pressure amplitude of the acoustic wave. For relatively low acoustic pressure amplitudes (typically < 1 bar), the volume oscillations of the bubble are small and in phase with the acoustic wave. These oscillations are driven mainly by the pressure forces. As the acoustic pressure amplitude increases (and typically crosses the static pressure in the medium), the radial motion of the bubbles becomes increasingly non–linear with large volumetric oscillations, in which radius of the cavitation bubbles increases several times its initial value. This explosive growth is ensued by transient collapse and few after–bounces. In this case, the volume oscillations (or radial motion) of the bubble are dominated by inertial forces (Flynn 1975).

1.4.3 Modeling of the sonochemical and sonophysical effects

As noted in previous section, for large pressure amplitudes of the ultrasound wave (typically higher than the static pressure in the medium), the bubble undergoes an explosive growth to several times its original size in the rarefaction half cycle of ultrasound. This expansion is accompanied by large evaporation of water at the bubble interface. The vapor

molecules diffuse towards the core of the bubble after evaporation into the bubble. The vapor transport in the bubble is a crucial aspect of the cavitation bubble dynamics.

The general treatment of the vapor transport and entrapment in the cavitation bubble was given by Storey and Szeri (2000) showed that in the compression phase of radial bubble motion, counter diffusion of the vapor molecules occurs with condensation at the bubble wall. The rate of transport of vapor molecules is proportional to the difference between partial pressure of liquid in the bubble and the saturation (or vapor) pressure at the bubble interface. However, in the final moments of transient collapse of the bubble, the air/water or bubble interface recedes at extremely fast rate, or bubble wall velocity becomes extremely high. At this stage, vapor molecules have insufficient time to diffuse to the bubble wall. Moreover, not all vapor molecules that approach the bubble interface stick to it, giving rise to non–equilibrium phase change. The principal result of the study of Storey and Szeri (2000) was that water vapor transport in the bubble is a two–step process, i.e. diffusion to the bubble wall and condensation at the wall. Thus, it is influenced by two time scales, *viz*. time scale of diffusion (t_{diff}) and time scale of condensation (t_{cond}) (Eames 1997) and their magnitudes relative to the time scale of bubble dynamics, t_{osc}. In the initial phase of bubble collapse, $t_{osc} >> t_{diff}$, t_{cond}, due to which the phase change at the bubble interface is in equilibrium and the concentration of vapor molecules at the bubble interface is essentially same as that in the bubble core. As the bubble wall acceleration increases during collapse, the time scales of bubbles dynamics and vapor diffusion becomes equal. At this stage, the rate of reduction of vapor molecules in the central region of the bubble is less than that at the bubble wall. With further acceleration of the bubble wall in final stages of bubble collapse, $t_{osc} << t_{diff}$ condition is reached and the vapor molecules have insufficient time to diffuse to the bubble wall, which results in a fixed and uneven distribution of vapor

molecules in the bubble. At this condition, the bubble composition is "freezed" and the vapor present inside the bubble is essentially "trapped" in the bubble.

The entrapped vapor and gas molecules in the bubble are subjected to extreme conditions generated during transient collapse, due to which they undergo thermal dissociation to several chemical species – some of which are radical species. The bubble may get fragmented at the point of minimum radius or maximum compression. At this moment, the chemical species formed in the bubble get released into the medium where they induce the sonochemical effect such as induction of a stubborn reaction or acceleration of the kinetics of a reaction etc.

1.4.4 Physical effects of ultrasound and cavitation on reaction system

Ultrasound and cavitation render several physical effects on a reaction system. The main manifestation of all of these results is generation of intense micro–convection and micro–mixing in the reaction system. A brief description of all physical effects of ultrasound and cavitation is given below (Leighton 1994; Mason and Lorimer 2002; Shah et al. 1999; Young 1989).

Micro–streaming: This is essentially small amplitude oscillatory motion of fluid elements around a mean position, which is induced by propagation of ultrasound wave. For a typical ultrasound wave with pressure amplitude of 120 kPa in water (ρ = 1000 kg/m^3, C = 1500 m/s), the micro–streaming velocity = 0.08 m/s.

Acoustic streaming: During propagation of ultrasound wave, the momentum of the wave is absorbed by the medium due to finite viscosity. This results in setting up of low velocity unidirectional currents of the fluid known as acoustic streaming (Kolb and Nyborg 1956; Nyborg 1958).

Microturbulence: The oscillatory motion of fluid induced due to volume oscillations of the bubble is called microturbulence. This phenomenon is explained as follows: in the expansion phase of radial motion of the cavitation bubble, the liquid is displaced away from bubble interface. During the collapse phase the liquid is pulled towards the bubble as it fills the vacuum created in the liquid with size reduction of bubble. The mean velocity of microturbulence depends on the amplitude of bubble oscillation.

Acoustic (or shock) waves: During the compression phase of radial motion, as the bubble contracts void space is created in the liquid and the fluid element spherically converge (or essentially "gush") in this void space and work is done on the bubble. For a cavitation bubble containing non–condensable gas such as air, the adiabatic compression results in rapid rise of pressure inside the bubble. At the point of minimum radius (or maximum compression), the bubble wall comes to a sudden halt. At this instance, the fluid elements converging towards the bubble are reflected back from the interface. This reflection creates a high pressure shock wave that propagates through the medium. The pressure exerted by the non–condensable gas inside the bubble causes re–bounce of the bubble.

Microjets: During radial motion driven by ultrasound wave, the cavitation bubble maintains spherical geometry as long as the motion of liquid in its vicinity is symmetric and uniform and thus there are no pressure gradients. If the bubble is located close to a phase boundary, either solid–liquid, gas–liquid or liquid–liquid, the motion of liquid in its vicinity is hindered, resulting in development of pressure gradient around it. This non–uniformity of pressure results in the loss of spherical geometry of the bubble. During the asymmetric radial motion, the portion of bubble exposed to higher pressure collapses faster than rest of the bubble, which gives rise to the formation of a high speed liquid jet directed towards the boundary. The velocity of these microjets has been estimated in the range of 120–150 m/s, and they can cause severe damage at the point of impact (leading to effects like particle

size reduction, microbial cell disruption, degradation of polymer chains etc.). The case of metal surfaces, these microjets can cause erosion of the surface.

1.5 OBJECTIVES, APPROACH AND SCOPE OF THE PRESENT THESIS

As noted in previous sections, effective utilization of crude glycerol produced as a co–product of biodiesel industry, is of urgent need of the hour. Conversion of this crude glycerol to high value–added product is an effective means of generating revenue for the biodiesel industry to make it economically attractive. Glycerol, with its three carbon atoms, is an excellent fermentation substrate. Many micro–organisms can utilize glycerol as sole carbon and energy source. The prominent value–added products from glycerol fermentation are 1,3–propanediol, dihydroxyacetone, butanol, biohydrogen, ethanol, succinic acid etc.

This study was aimed at development, optimization and intensification of a biochemical process for producing DHA from biodiesel–derived crude glycerol. The micro–organism used for in study is *Gluconobacter oxydans* (natural isolate), which is widely used strain for DHA production. In addition to fermentation with free cells of *G. oxydans*, this study also involved use of immobilized cells of *G. oxydans*, as immobilized microbial cultures are highly suited for large–scale operations. Commercial polyurethane foam (PU foam) was selected as immobilization (or support) matrix due to its highly porous structure with large surface area. This thesis essentially presents a step–by–step approach for development, optimization, and intensification of the bioprocess for fermentation of glycerol to DHA by free and immobilized cells of *G. oxydans*.

The objectives of the present thesis are listed below:

1. Optimization of medium components for DHA production by immobilized *G. oxydans* cells

2. Optimization of process parameters for DHA production by *G. oxydans* cells

3. Kinetic analysis of substrate inhibition effect over DHA production by free and immobilized *G. oxydans* cells

4. Analysis of product inhibition kinetics by free and immobilized *G. oxydans* cells

5. Batch and repeated-batch fermentation using free, immobilized, and resting cells of *G. oxydans*

6. Sonication-induced intensification of glycerol fermentation for DHA production

The thesis comprises of 7 chapters (including the present one) that address different facets of glycerol fermentation. The brief content of each chapter is outlined below:

- Chapter 1 presents the general introduction to the subject of glycerol conversion to dihydroxyacetone using chemical oxidation and microbial fermentation route. A brief review of literature in various aspects of DHA production using free and immobilized cells, and techniques for enhancement of DHA yield has been presented followed by description of aim, approach and scope of the thesis.
- Chapter 2 presents kinetic analysis of DHA production from crude glycerol. The effect of substrate inhibition has been studied by fitting different inhibition models to the experimental data. This study was further extended by fitting modified Haldane kinetic model to the experimental data of immobilized cells.
- Chapter 3 deals with the statistical optimization of medium components for DHA production by immobilized cells of *G. oxydans*. The statistical experimental designs comprising six essential medium components were applied in two steps. Three essential medium components were selected by Plackett–Burman design, which were further optimized using Central Composite Design (CCD).
- Chapter 4 describes the optimization three different process parameters (pH, temperature, initial glycerol conc.) by response surface methodology (RSM). This

study was further extended for studying the effect of product inhibition on growth and DHA production of free and immobilized cells.

- Chapter 5 presents the fermentation studies using free and immobilized cells under conditions of both optimized fermentation medium (results of chapter 3) and fermentation parameters (results of chapter 4). In addition to glycerol fermentation in batch mode, the fermentation experiments in this chapter also employ repeated–batch mode with pulse feeding of glycerol. Fermentation was carried out with different combinations of pulse feeding of glycerol, while maintaining the net substrate concentration in the broth below minimum inhibitory level.
- Chapter 6 addresses the important facet of intensification of glycerol fermentation with free and immobilized *G. oxydans* cells using sonication (or ultrasound irradiation). This study has also tried to gain insight into the biomechanics of the enhancement in glycerol fermentation induced by sonication. The structural changes of the key enzyme glycerol dehydrogenase were analyzed using Circular Dichroism (CD) analysis after partial purification of the enzyme. The CD analysis of intracellular proteins obtained from native and ultrasound–treated microbial cells has revealed conformational changes in secondary structure of enzyme induced by sonication.
- Chapter 7 represents the summary of the results and overall conclusion of the thesis. Some suggestions have been made to carry this work forward to an advance level.

REFERENCES

Adlercreutz, P., Holst, O., Mattiasson, B., 1985. Characterization of *Gluconobacter oxydans* immobilized in calcium alginate. Appl. Microbiol. Biotechnol. 22:1–7.

Aresta, M., Dibenedetto, A., 2014. Catalysis for the valorization of low–value C–streams. J. Braz. Chem. Soc. 25, 2215–2228.

Awbrey, S.S., 2010. Systems and Methods for Processing Glycerol. US Patent 2011140032A1.

Bagheri, S., Julkapli, N.M., Yehye, W.A., 2015. Catalytic conversion of biodiesel derived raw glycerol to value added products. Renew. Sust. Energ. Rev. 41, 113–127.

Bauer, R., Katsikis, N., Varga, S., Hekmat, D., 2005. Study of the inhibitory effect of the product dihydroxyacetone on *Gluconobacter oxydans* in a semi–continuous two–stage repeated–fed–batch process. Bioprocess Biosyst. Eng. 28(1), 37–43.

Biswas, P.K., Pohit, S., Kumar, R., 2010. Biodiesel from jatropha: can India meet the 20% blending target? Energ. Policy 38(3), 1477–1484.

Bories, A., Claret, C., Soucaille, P., 1991. Kinetic study and optimisation of the production of dihydroxyacetone from glycerol using *Gluconobacter oxydans*. Process Biochem. 26, 143–248.

BP Statistical Review of World Energy June 2016. bp.com/statisticalreview.

Castells, J., Geijo, F., Calahorra, F.L., 1980. The "Formoin Reaction": a promising entry to carbohydrates from formaldehyde. Tetrahedron Lett. 27, 4517–4520.

Claret, C., Bories, A., Soucaille, P., 1992. Glycerol inhibition of growth and dihydroxyacetone production by *Gluconobacter oxydans*. Curr. Microbiol. 25, 149–155.

Claret, C., Bories, A., Soucaille, P., 1993. Inhibitory effect of dihydroxyacetone on *Gluconobacter oxydans*: Kinetic aspects and expression by mathematical equations. J. Ind. Microbiol. 11, 105–112.

Cummings, T.F., 2004. The treatment of cyanide poisoning. Occup. Med. 54, 82–85.

De Ley, J., Gillis, M., Swings, J., 1984. The genus *Gluconobacter*. In: Krieg NR, Holt JG (eds) Bergey's manual of systematic bacteriology, vol 1. Williams and Wilkins, Baltimore, pp 267–278.

Delfort, B., Durand, I., Hillion, G., Jaecker–Voirol, A., Montagne, X., 2008. Glycerin for new biodiesel formulation. Oil Gas Sci. Technol. 63, 395–404.

Demirel, S.; Lehnert, K.; Lucas, M., Claus, P., 2007. Use of renewables for the production of chemicals: Glycerol oxidation over carbon supported gold catalysts. Appl. Catal., B–Environ. 70(1–4), 637–643.

Deppenmeier, U., Hoffmeister, M., Prust, C., 2002. Biochemistry and biotechnological applications of *Gluconobacter strains*. Appl. Microbiol. Biotechnol. 60, 233–242.

Eames, I.W., Marr, N.J., Sabir, H. 1997. The evaporation coefficient of water: A review. Int. J. Heat Mass Tran. 40, 2963–2973.

Fan, X., Burton, R., Zhou, Y., 2010. Glycerol (Byproduct of Biodiesel production) as source for fuels and chemicals–min review. The Open Fuel. Energ. Sci. J. 3, 17–22.

Flickinger, C., Perlman, D., 1977. Application of oxygen–enriched aeration in the conversion of glycerol to dihydroxyacetone by *Gluconobacter oxydans* IFO 3293. Appl. Environ. Microbiol. 33, 706–712.

Flynn, H.G., 1975. Cavitation dynamics I. A mathematical formulation. J. Acoust. Soc. Am. 57, 1379–1396.

Gao, J., Liang, D., Chen, P., Hou, Z., Zheng, X., 2009. Oxidation of glycerol with oxygen in a base–free aqueous solution over Pt/AC and Pt/MWNTs catalysts. Catal. Lett. 130(1–2), 185–191.

Gatgens, C., Degner, U., Bringer–Meyer, S., Herrmann, U., 2007. Biotransformation of glycerol to dihydroxyacetone by recombinant *Gluconobacter oxydans* DSM 2343. Appl. Microbiol. Biotechnol. 76, 553–559.

Gupta, A., Singh, V.K., Qazi, G.N., Kumar, A., 2001. *Gluconobacter oxydans*: Its biotechnological applications. J. Mol. Microbiol. Biotechnol. 3, 445–456.

Habe, H., Fukuoka, T., Morita, T., Kitamoto, D., Yakushi, T., Matsushita, K., Sakaki, K., 2010. Disruption of the membrane–bound alcohol dehydrogenase–encoding gene

improved glycerol use and dihydroxyacetone productivity in *Gluconobacter oxydans*. Biosci. Biotechnol. Biochem. 74, 1391–1395.

Hansen, C.F., Hernandez, A., Mullan, B.P., Moore, K., Trezona–Murray, M., King, R.H., Pluske, J.R., 2009. A chemical analysis of samples of crude glycerol from the production of biodiesel in Australia, and the effects of feeding crude glycerol to growing–finishing pigs on performance, plasma metabolites and meat quality at slaughter. Anim. Prod. Sci. 49, 154–161.

Hekmat, D., Bauer, R., Fricke, J., 2003. Optimization of the microbial synthesis of dihydroxyacetone from glycerol with *Gluconobacter oxydans*. Bioprocess Biosyst. Eng. 26, 109–116.

Hekmat, D., Bauer, R., Neff, V., 2007. Optimization of the microbial synthesis of dihydroxyacetone in a semi–continuous repeated–fed–batch process by in situ immobilization of *Gluconobacter oxydans*. Process Biochem. 42, 71–76.

Henderson, P.W., Kadouch, D., Singh, S.P., Zawaneh, P.N., Weiser, J., Yazdi, S., Weinstein, A., Krotscheck, U., Wechsler, B., Putnam, D., Spector, J.A.J., 2010. A rapidly resorbable hemostatic biomaterial based on dihydroxyacetone. Biomed. Mater. Res. A. 93, 776–782.

Hirasawa, S., Watanabe, H., Kizuka, T., Nakagawa, Y., Tomishige, K., 2013. Performance, structure and mechanism of Pd–Ag alloy catalyst for selective oxidation of glycerol to dihydroxyacetone. J. Catal. 300, 205–216.

Hoist, O., Enfors, S., Mattiasson, B., 1982. Oxygenation of immobilized cells using hydrogen–peroxide; A model study of *Gluconobacter oxydans* converting glycerol to dihydroxyacetone. European J. Appl. Microbiol. Biotechnol. 14, 64–68.

Hoist, O., Lundback, H., Mattiasson, B., 1985. Hydrogen peroxide as an oxygen source for immobilized *Gluconobacter oxydans* converting glycerol to dihydroxyacetone. Appl. Microbiol. Biotechnol. 22, 383–388.

Hu, W.B., Knight, D., Lowry, B., Varma, A., 2010c. Selective oxidation of glycerol to dihydroxyacetone over Pt–Bi/C catalyst: Optimization of catalyst and reaction conditions. Ind. Eng. Chem. Res. 49(21), 10876–10882.

Hu, Z.–C., Liu, Z.–Q., Zheng, Y.–G., Shen, Y.–C., 2010b. Production of 1,3–dihydroxyacetone from glycerol by *Gluconobacter oxydans* ZJB09112. J. Microbiol. Biotechnol. 20, 340–345.

Hu, Z.–C., Zheng, Y.–G., 2011. Enhancement of 1,3–dihydroxyacetone production by a UV–induced mutant of *Gluconobacter oxydans* with DO control strategy. Appl. Biochem. Biotechnol. 165, 1152–1160.

Hu, Z.–C., Zheng, Y.–G., Shen, Y.–C., 2010a. Dissolved–oxygen–stat fed–batch fermentation of 1,3–dihydroxyacetone from glycerol by *Gluconobacter oxydans* ZJB09112. Biotechnol. Bioprocess Eng. 15, 651–656.

Hu, Z.–C., Zheng, Y.–G., Shen, Y.–C., 2011b. Use of glycerol for producing 1,3–dihydroxyacetone by *Gluconobacter oxydans* in an airlift bioreactor. Bioresour. Technol. 102, 7177–7182.

Imlay, J. A., Linn, S., 1988. DNA damage and oxygen radical toxicity. Science 240, 1302–1309.

Indian Petroleum and Natural Gas Statistics. Ministry of Petroleum and Natural Gas, Government of India, 2015–16.

Jing, L.U.O., LI, H.G., Ning, Z.H.A.O., Feng, W.A.N.G., XIAO, F.K., 2015. Selective oxidation of glycerol to dihydroxyacetone over layer double hydroxide intercalated with sulfonato–salen metal complexes. J. Fuel Chem. Technol. 43(6), 677–683.

Katryniok, B., Kimura, H., Skrzynska, E., Girardon, J.–S., Fongarland, P., Capron, M., Ducoulombier, R., Mimura, N., Paul, S., Dumeignil, F., 2011. Selective catalytic oxidation of glycerol: Perspectives for high value chemicals. Green Chem. 13(8), 1960–1979.

Khanna, S., Goyal, A., Moholkar, V.S., 2012. Microbial conversion of glycerol: Present status and future prospects. Crit. Rev. Biotechnol. 32, 235–262.

Kirillova, M.V., Kirillov, A.M., Mandelli, D., Carvalho, W.A., Pombeiro, A.J., Shul'pin, G.B., 2010. Mild homogeneous oxidation of alkanes and alcohols including glycerol with tert–butyl hydroperoxide catalyzed by a tetracopper (II) complex. J. Catal. 272(1), 9–17.

Kolb, J., Nyborg, W.L., 1956. Small scale acoustic streaming in liquids. J. Acoust. Soc. Am. 28, 1237–1242.

Leighton, T.G., 1994. The acoustic bubble. Academic Press, San Diego.

Li, M.H., Wu, J., Lin, J. P., Wei, D. Z., 2010b. Expression of Vitreoscilla hemoglobin enhances cell growth and dihydroxyacetone production in *Gluconobacter oxydans*. Curr. Microbiol. 61, 370–375.

Li, M.H., Wu, J., Liu, X., Lin, J.P., Wei, D.Z., Chen, H., 2010a. Enhanced production of dihydroxyacetone from glycerol by overexpression of glycerol dehydrogenase in an alcohol dehydrogenase–deficient mutant of *Gluconobacter oxydans*. Bioresour. Technol. 101, 8294–8299.

Liang, D., Gao, J., Sun, H., Chen, P., Hou, Z., Zheng, X., 2011b. Selective oxidation of glycerol with oxygen in a base–free aqueous solution over MWNTs supported Pt catalysts. Appl. Catal. B–Environ. 106(3), 423–432.

Liang, D., Gao, J., Wang, J., Chen, P., Hou, Z., Zheng, X., 2009. Selective oxidation of glycerol in a base–free aqueous solution over different sized Pt catalysts. Catal. Commun. 10(12), 1586–1590.

Liang, D., Gao, J., Wang, J., Chen, P., Wei, Y., Hou, Z., 2011a. Bimetallic Pt—Cu catalysts for glycerol oxidation with oxygen in a base–free aqueous solution. Catal. Commun. 12(12), 1059–1062.

Liang, D., Shiyu, C.U.I., Jing, G.A.O., Junhua, W.A.N.G., Ping, C.H.E.N., Zhaoyin, H.O.U., 2011c. Glycerol oxidation with oxygen over bimetallic Pt–Bi catalysts under atmospheric pressure. Chinese J. Catal. 32(11), 1831–1837.

Lidia, S.–R., Stanislaw, B., 2012. Production of dihydroxyacetone from an aqueous solution of glycerol in the reaction catalyzed by an immobilized cell preparation of acetic acid bacteria *Gluconobacter oxydans* ATCC 621. Eur. Food Res. Technol. 235, 1125–1132.

Liu, Y.–P., Sun, Y., Tan, C., Li, H., Zheng, X.–J., Jin, K.–Q., Wang, G., 2013. Efficient production of dihydroxyacetone from biodiesel–derived crude glycerol by newly isolated *Gluconobacter frateurii*. Bioresour. Technol. 142, 384–389.

Liu, Z., Hu, Z., Zheng, Y., Shen, Y., 2008. Optimization of cultivation conditions for the production of 1, 3–dihydroxyacetone by *Pichia membranifaciens* using response surface methodology. Biochem. Eng. J. 38(3), 285–291.

Ma, L., Lu, W., Xia, Z., Wen, J., 2010. Enhancement of dihydroxyacetone production by a mutant of *Gluconobacter oxydans*. Biochem. Eng. J. 49, 61–67.

Macauley, S., McNeil, B., Harvey, L.M., 2001. The genus *Gluconobacter* and its applications in biotechnology. Crit. Rev. Biotechnol. 21, 1–25.

Mandal, R., 2005. Energy—alternate solutions for India's needs: biodiesel. Planning Commission, Government of India.

Mason, T.J., Lorimer, J.P., 2002. Applied sonochemistry: The uses of power ultrasound in chemistry and processing. Wiley–VCH, Coventry.

Matsushita, K., Toyama, H., Adachi, O., 1994. Respiratory chains and bioenergetics of acetic acid bacteria. Adv. Microb. Physiol. 36, 247–301.

Nabe, K., Izuo, N., Yamada, S., Chibata, I., 1979. Conversion of glycerol to dihydroxyacetone by immobilized whole cells of *Acetobacter xylinum*. Appl. Environ. Microbiol. 38, 1056–1060.

Netherlands Environmental Assessment Agency. EDGARv4.3.2, European Commission, Joint Research Centre (JRC)/PBL. Emission Database for Global Atmospheric Research (EDGAR), release version 4.3.2. http://edgar.jrc.ec.europe.eu, 2016.

Nyborg, W.L., 1958. Acoustic streaming near a boundary. J. Acoust. Soc. Am. 30, 329–339.

Ohrem, H.L., Voβ, H., 1995. Inhibitory effects of dihydroxyacetone *Gluconobacter* cultures. Biotechnol. Lett. 17, 981–984.

Ohrem, H.L., Voβ, H., 1996. Process model of the oxidation of glycerol with *Gluconobacter oxydans*. Proc. Biochem. 31, 295–301.

Olivier, J.G.J., Janssens–Maenhout, G., Muntean, M., Peters, J.A.H.W., Trends in global CO_2 emissions: 2015 Report. PBL Netherlands Environmental Assessment Agency, The Hague; European Commission, Joint Research Centre (JRC), Institute for Environment and Sustainability (IES). JRC98184, PBL1803.

Pagliaro, M., Ciriminna, R., Kimura, H., Rossi, M., Della Pina, C., 2007. From glycerol to value-added products. Angew. Chem. Int. Ed. 46(24), 4434–4440.

Pollington, S.D., Enache, D.I., Landon, P., Meenakshisundaram, S., Dimitratos, N., Wagland, A., Hutchings, G.J., Stitt, E.H., 2009. Enhanced selective glycerol oxidation in multiphase structured reactors. Catal. Today 145(1–2), 169–175.

Quispe, C.A.G., Coronado, C.J.R., Carvalho Jr, J.A., 2013. Glycerol: Production, consumption, prices, characterization and new trends in combustion. Renew. Sust. Energ. Rev. 27, 475–493.

Ranjan, A., Moholkar, V.S., 2012. Biobutanol: science, engineering, and economics. Int. J. Energy Res. 36, 277–323.

Renewables, 2016. Global Status Report, Renewable Energy Indicators, 2015. United Nations Environment Program, Paris, France, p. 272.

Rodrigues, E.G., Pereira, M.F.R., Delgado, J.J., Chen, X., Orfao, J.J.M., 2011. Enhancement of the selectivity to dihydroxyacetone in glycerol oxidation using gold nanoparticles supported on carbon nanotubes. Catal. Commun. 16(1), 64–69.

Shah, Y.T., Pandit, A.B. Moholkar, V.S., 1999. Cavitation reaction engineering. Plenum Press, New York.

Shulpin, G.B., Kozlov, Y.N., Shulpina, L.S., Strelkova, T.V., Mandelli, D., 2010. Oxidation of reactive alcohols with hydrogen peroxide catalyzed by manganese complexes. Catal. Lett. 138(3–4), 193–204.

Solomos, B., Zeng, A.P., Biebl, H., Schlieker, H., Posten, C., Deckwer, W.D., 1995. Comparison of the energetic efficiencies of hydrogen and oxochemicals formation in *Klebsiella pneumonia* and *Clostridium butylicum* during anaerobic growth on glycerol, J. Biotechnol. 39, 107–117.

Stanko, R.T., Diven, W.F., Robertson, R.J., Spina, R.J., Galbreath, R.W., Reilly, J.J., Goss, F.L., 1993. Amino acid arterial concentration and muscle exchange during submaximal arm and leg exercise: The effect of dihydroxyacetone and pyruvate. J. Sports Sci. 11, 17–23.

Stasiak–Rozanska, L., Błażejak, S., Gientka, I., 2014. Effect of glycerol and dihydroxyacetone concentrations in the culture medium on the growth of acetic acid bacteria *Gluconobacter oxydans* ATCC 621. Eur. Food Res. Technol. 239(453), 2238–2244.

Stasiak–Rozanska, L., Błażejak, S., Ratz, A., 2010. Investigations into the optimizations of parameters of glycerol biotransformation to dihydroxyacetone with the use of immobilized cells of *Gluconobacter xylinus*. Pol. J. Food Nutr. Sci. 60(3), 273–280.

Stelmachowski, M., 2011. Utilization of glycerol, a by–product of the transesterification process of vegetable oils: a review. Ecol. Chem. Eng. 18, 9–30.

Storey, B.D., Szeri, A.J., 2000. Water vapor, sonoluminescence and sonochemistry. P. Roy. Soc. London A, 456, 1685–1709.

Svitel, J., Sturdik, E., 1994. Product yield and by–product formation in glycerol conversion to dihydroxyacetone by *Gluconobacter oxydans*. J. Ferment. Bioeng. 78, 351–355.

Tramper, J., Luyben, K.C.A., Van den Tweel, W.J.J., 1983. Kinetic aspects of glucose oxidation by *Gluconobacter oxydans* cells immobilized in calcium alginate. European J. Appl. Microbiol. Biotechnol. 17(1), 13–18.

Tran, N., Illukpitiya, P., Yanagida, J.F., Ogoshi, R., 2011. Optimizing biofuel production: An economic analysis for selected biofuel feedstock production in Hawaii. Biomass Bioenerg. 35(5), 1756–1764.

Vidosh, M., Praksh, V., Alok, Ch., 2011. Impacts of bio–fuel use: a review. Int. J. Eng. Sci. Technol. 3, 3776–3782.

Villa, A., Campisi, S., Chan–Thaw, C.E., Motta, D., Wang, D., Prati, L., 2015. Bismuth modified Au–Pt bimetallic catalysts for dihydroxyacetone production. Catal. Today 249, 103–108.

Wei, S., Song, Q., Wei, D., 2007. Epeated use of immobilized *Gluconobacter oxydans* cells for conversion of glycerol to dihydroxyacetone. Prep. Biochem. Biotechnol. 37, 67–76.

Worz, N., Brandner, A., Claus, P., 2010. Platinum–bismuth–catalyzed oxidation of glycerol: Kinetics and the origin of selective deactivation. J. Phys. Chem. C. 114(2), 1164–1172.

Yang, W., Zhou, Y., Zhao, Z.K., 2013. Production of dihydroxyacetone from glycerol by engineered *Escherichia coli* cells co–expressing gldA and nox genes 12, 4387–4392.

Yazdani, S.S., Gonzalez, R., 2007. Anaerobic fermentation of glycerol: a path to economic viability for the biofuels industry. Curr. Opin. Biotechnol. 18, 213–219.

You, Q., Xu, H., Yin, X., Zhu, H., Dai, X., 2013. Improvement of dihydroxyacetone production by *Gluconobacter oxydans* NH–10 using a two–stage agitation speed operation strategy. J. Food Agric. Environ. 11, 389–393.

Young, F.R., 1989. Cavitation. McGraw Hill, London.

Yuste, A.J., Dorado, M.P., 2006. A neural network approach to simulate biodiesel production from waste olive oil. Energ. Fuel. 20, 399–402.

Zhou, C.H., Zhao, H., Tong, D.S., Wu, L.M., Yu, W.H., 2013. Recent advances in catalytic conversion of glycerol. Catal. Rev. 55, 369–453.

CHAPTER 2

KINETIC ANALYSIS OF SUBSTRATE INHIBITION ON DIHYDROXYACETONE PRODUCTION

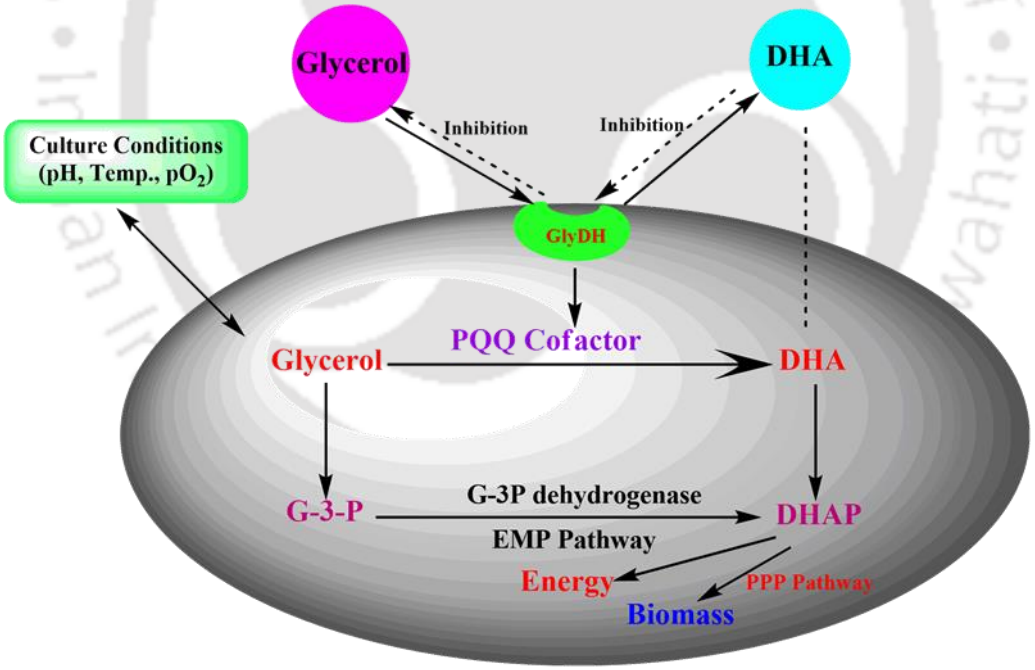

CHAPTER 2

KINETIC ANALYSIS OF SUBSTRATE INHIBITION ON DIHYDROXYACETONE PRODUCTION

2.1 INTRODUCTION

The high concentration of both substrate (i.e. glycerol) and product (i.e. DHA) can inhibit cell growth and DHA biosynthesis, leading to low DHA yield and productivity (Claret et al., 1992). Claret et al. (1993) also reported investigations into the inhibitory effect of initial dihydroxyacetone concentration on cell growth and DHA production using *G. oxydans* ATCC 621. In these investigations, the specific rate of cell growth and DHA production were fitted to various biokinetic models accounting for substrate inhibition to calculate the kinetic parameters, which depicted quantitative estimates of the inhibition effect. However, the substrate used by Claret et al. (1993) was pure glycerol (without any contaminations) with free *G. oxydans* cells. This study aimed at extending the kinetic analysis of bioconversion of crude glycerol to DHA using immobilized cells of *G. oxydans* with essentially same methodologies as adopted by Claret et al. (1993). The alkali, alcohol and salt contaminations in the glycerol could have significant effect on the biokinetics. It has also been reported that the proliferation of acetic acid bacteria was inhibited by stress induced by the initial glycerol concentration and/or increasing concentration of DHA

(Stasiak–Rozanska et al., 2014). However, the exact cellular mechanism and the concentration of glycerol/DHA responsible for this inhibition have not been identified yet (Hekmat et al., 2003), especially in the context of immobilized cells. The present investigation also attempted to address this issue. We used immobilized cells of *G. oxydans* in this study, as they resulted in better and more effective control over the cell density in the medium. For the analysis of the kinetic data, we have also drawn analogies of the present bioconversion system with other immobilized systems which also undergo substrate inhibition.

For immobilization of *G. oxydans*, we selected reticulated polyurethane foam as substrate based on our previous studies (Agarwal et al., 2016; Bhasarkar et al., 2015; Malani et al., 2013). Polyurethane foam has highly porous structure with large surface area, and cells can easily get immobilized over the surface as well as inside the pores, which results in high cell density in relatively small volume. The experimental data of reaction velocity versus initial substrate concentration has been fitted to kinetic models accounting for substrate inhibition. In order to get deeper insight into the effect of immobilization of the cells on DHA production, experiments have also been conducted under identical conditions using free cells of *G. oxydans* and the kinetic parameters for the free and immobilized cells have been compared.

2.2 MATERIALS AND METHODS

2.2.1 Materials

Microbial strains of *G. oxydans* MTCC 904 were procured from Microbial Type Culture Collection (MTCC), Chandigarh (India). DHA and pure glycerol were obtained from Merck, Germany. Reticulated polyurethane foam was purchased from local market. All other medium components and chemicals used in this study were procured from

HiMedia Pvt. Ltd., India unless mentioned.

Crude glycerol was synthesized through transesterification reaction conducted with soybean oil, methanol and alkali (NaOH) as catalyst. The parameters for transesterification reaction were as follows: oil = 60 mL, alcohol = 30 mL, alcohol to oil molar ratio = 12:1, catalyst = 0.54 g (1% w/v), temperature = 65°C, time = 1 h. After completion of the reaction, the reaction mixture was kept standing in separating funnel for 18–20 h. The mixture separates into two layers, viz. upper layer of biodiesel and lower layer of glycerol. Approximately, 27 mL of crude glycerol was produced from the transesterification reaction. The alkali and alcohol contaminations in crude glycerol were as follows: 0.85% (w/v) of sodium hydroxide (calculated by acid base titration), 0.26% (w/v) methanol (determined using gas chromatography).

2.2.2 Growth and maintenance of *G. oxydans* culture

The lyophilized cells were revived in MRS medium and kept on a rotary incubator shaker (Make: Lab Companion; Model: SI–300R) at 30ºC, 150 rpm for 24 h. The revived cells were grown on agar slant and kept at 4ºC. The cultures were sub–cultured every month. Composition of the MRS medium was as follows: 10.0 g Peptone, 10.0 g beef extract, 5.0 g yeast extract, 10.0 g glucose, 1 mL Tween–80, 2.0 g Na_2HPO_4, 5.0 g sodium acetate, 2.0 g triammonium citrate, 0.2 g $MgSO_4 \cdot 7H_2O$, and 0.2 g $MnSO_4 \cdot 4H_2O$ per liter of distilled water. pH of the medium was adjusted to 6.0 ± 0.2 with addition of 1 N NaOH/HCl. 15 g/L of agar was added in MRS medium to prepare the agar plates and slants.

2.2.3 Seed culture and fermentation medium compositions

The composition of seed culture medium was as follows: 5 g yeast extract, 3 g peptone, 3 g $K_2HPO_4 \cdot 3H_2O$, 2 g $(NH_4)_2SO_4$, 0.51 g $MgSO_4 \cdot 7H_2O$, and 10 g carbon source

per liter. The initial pH of the medium was adjusted to 6.0 ± 0.2. The composition of fermentation medium was decided on the basis of published literature as follows: yeast extract = 2.5 g/L, K_2HPO_4 = 0.1 g/L, KH_2PO_4 = 0.9 g/L, $(NH_4)_2SO_4$ = 2 g/L, $MgSO_4 \cdot 7H_2O$ = 1 g/L, and $CaCl_2$ = 1.5 g/L. Initial concentrations of pure and crude glycerol in fermentation medium were varied in the range of 10 to 150 g/L. The pH of the medium was adjusted to 5.0 ± 0.2 by 1 N NaOH/HCl. The medium was autoclaved at 121ºC, 15 psi for 20 min prior to inoculation.

2.2.4 Immobilization and cross–linking of cells on support

The commercial grade polyurethane foam was cut into cubical pieces of appropriate size (1 cm × 1 cm × 1 cm). These pieces were washed 3–4 times with d–H_2O and autoclaved prior to addition. The PU foam cubes were added to the broth at the onset of log phase of the culture, which was reached after 10 h of incubation (as per growth profile determined in preliminary experiment). The broth containing PU foam cubes was further incubated for 50 h at 30ºC and with shaking speed of 150 rpm. Next, polyurethane cubes with immobilized cells (immobilized supports) were separated from the medium and were added to phosphate buffer (50 mM, pH 6.0) with shaking for 10 min. Subsequently, the foam pieces were washed with phosphate buffer, followed by drying at room temperature for 12 h. The dried PU foam pieces were added to 0.1% gluteraldehyde solution for cross–linking of cells and incubated for 1 h, followed by washing with phosphate buffer and subsequently drying at room temperature for 24 h.

Preliminary confirmation of immobilization of the cells on PU foam was done by Lowry assay (Lowry et al., 1951). Four pieces of PU foam were added to 20 mL of 50 mM phosphate buffer of pH 6.0 in an Erlenmeyer flask. This system was sonicated at 20 kHz using a probe type ultrasound processor (Make – Sonics and Materials Inc., Model – VCX

500) for disruption of cells with release of cells proteins. In order to avoid temperature rise during sonication, the flask was kept in ice bath. An aliquot of 1 mL of this solution was used to conduct Lowry assay for determination of all cell proteins. A positive Lowry assay test confirms the presence of proteins in the solution, released from disruption of the cells immobilized on the surface of the support. Immobilization of microbial cells over PU foam was also confirmed from scanning electron microscope analysis (SEM, Make – Leo, Model – 1430vp). Fig. 2.1 shows SEM micrographs of native cells, original PU foam, and PU foam with immobilized *G. oxydans* cells on the surface.

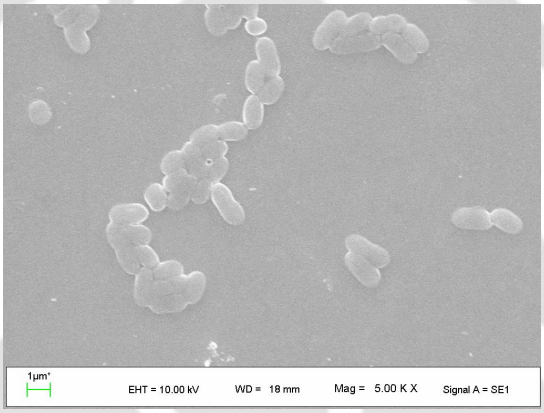

(A)

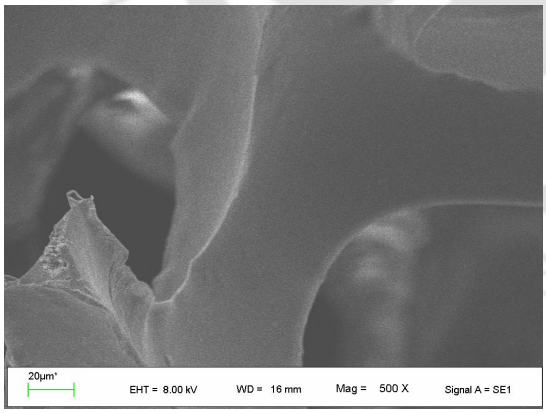

(B)

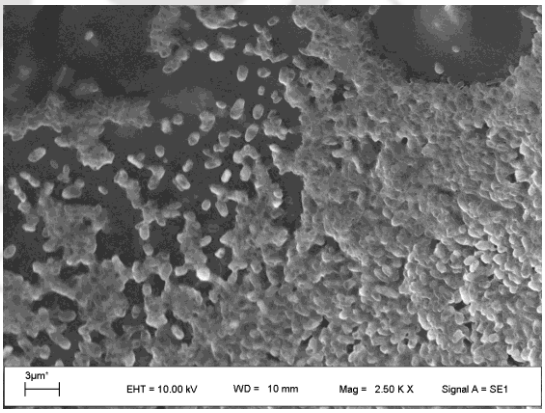

(C)

Figure 2.1. Scanning Electron Microscope micrographs of native and immobilized *G. oxydans* cells. (A) Native cells; (B) Original reticulated PU foam used as support for cell immobilization; (C) PU foam with immobilized and cross–linked *G. oxydans* cells;

2.2.5 Ascertaining equal number of cells in free and immobilized cultures

The cells of *G. oxydans* were grown at 30°C and 150 rpm in two flasks each containing 100 mL of seed culture medium (with composition mentioned earlier). One of these flasks was labeled as "control" and the other as "test". The cell density in the medium in both flasks was determined by recording absorbance at 660 nm using UV–Vis spectrophotometer. The absorbance in both flasks was determined as 0.223 ± 0.003 at onset of exponential phase, which corresponded to cell density of 0.083 ± 0.001 g/L. 8 PU foam cubes were added to the "test" flask at the onset of exponential phase. Both flasks were incubated again for 24 h, during which the cells in the "test" flask underwent immobilization on PU foam. After 24 h of incubation and immobilization, the non–immobilized cells present in supernatant of the "test" flask were determined by measuring absorbance and comparing with the "control" flask. The cell densities in the media of the "control" flask and "test" flask were 0.587 g/L and 0.482 g/L, respectively. The difference in these cell densities (0.105 g/L) gives the number of cells immobilized over the surface of 8 PU foam cubes added to "test" flask.

To ascertain uniform distribution of 0.105 g of total immobilized cells over 8 PU foam cubes, each cube was separately used for fermentation experiment. The glycerol concentration in each flask is kept at 10 g/L. The final DHA concentration was found to be 7.236 g/L with standard deviation of 0.029 g/L. Thus, the standard deviation was within 0.4% of the mean value. This result confirms that distribution of cells over PU foam support was nearly uniform, and that the numbers of cells added to reaction mixture in each experiment were practically constant.

2.2.6 Preliminary experiments

Prior to main experiments, the preliminary experiments were conducted for assessment of effect of certain experimental parameters as follows:

***Effect of carbon source*:** Effects of three different carbon sources in seed culture medium on DHA production were examined. Three different carbon sources, viz. (A) glycerol (B) sorbitol (C) mannitol, with a fixed concentration of 10 g/L were added separately to the seed culture medium. Rest of the composition of seed culture medium remained same as mentioned in section 2.3. 5% inoculum from seed culture medium at log phase was transferred to the fermentation broth containing pure glycerol (at concentration of 10 g/L) as substrate. Final DHA concentration and cell mass yield was determined after 48 h of fermentation.

***Selection of immobilization support and its reusability*:** The optimum amount of immobilized support for fermentation, i.e. number of PU foam pieces with immobilized cells added to fermentation broth, was determined by varying the number of cubes from 2 to 6. These experiments revealed optimum number of PU foam cubes during fermentation as 3. After completion of first fermentation experiment, the PU foam pieces were separated from the broth and washed twice with phosphate buffer (pH 6.0) to remove the medium components. These pieces were reused in the next fermentation experiment. This procedure was repeated for five successive fermentations. The duration of each fermentation experiment was 4 days with initial glycerol concentration of 20 g/L.

***Effect of nitrogen source on DHA formation*:** Effect of two different nitrogen sources in the fermentation broth, viz. yeast extract and ammonium sulfate, on the DHA yield was assessed. The concentration of each nitrogen source in fermentation broth was 2 g/L. Rest of the medium components remained same as mentioned in section 2.3. Glycerol concentration in the broth was 20 g/L.

2.2.7 Main experiments

***DHA production from crude/pure glycerol by free cells*:** Fermentation experiments with free cells of *G. oxydans* were carried out using different initial glycerol concentrations. Both pure and crude glycerol were used with 5% v/v inoculum added to fermentation broth in each experiment. The concentration of pure and crude glycerol was varied in the range of 10–150 g/L. The DHA concentration was monitored with fixed interval time.

***DHA production from crude/pure glycerol by immobilized cells*:** Glycerol fermentation using immobilized cells of *G. oxydans* has been carried out using varying glycerol concentration in the range of 10–150 g/L. DHA production profiles at different initial concentration of crude and pure glycerol concentration has been examined. As per the results of preliminary experiments, 3 cubes of PU foam with immobilized cells were added to fermentation broth.

2.2.8 Analytical methods

The growth of *G. oxydans* cells (in case of experiments with free cells) in fermentation broth was monitored by measuring absorbance at 660 nm with a UV–Vis spectrophotometer (Make: Perkin Elmer, Model: LAMBDA 35). The DHA in the aliquots withdrawn from the broth was quantified after centrifugation (10,000 rpm, 20 min) and proper dilution of the aliquot. DHA was assayed with diphenylamine reagent (Chen et al., 2008; Rocha–Martin et al., 2014) containing diphenylamine (0.6 g), sulfuric acid (6 mL) and acetic acid (54 mL). 0.5 mL of the aliquot of fermentation broth was mixed with 4.5 mL of diphenylamine reagent and incubated in closed tubes for 20 min in boiling water bath. The samples were cooled down to room temperature and absorbance was recorded at 615 nm immediately. The concentration of DHA in the sample was determined using the standard graph of concentration versus absorbance.

2.2.9 Preliminary kinetic analysis

Previous literature reports numerous models for describing the inhibitory effect of glycerol on DHA production. Some common kinetic models for specific production rate in case of substrate–inhibited systems are as follows (Basak et al., 2014):

Haldane model: $$V = \frac{V_{max}[S_o]}{K_S + [S_o] + \left(\frac{[S_o]^2}{K_I}\right)} \quad (2.1)$$

Yano model: $$V = \frac{V_{max}[S_o]}{K_S + [S_o] + \left(\frac{[S_o]^2}{K_I}\right)\left(1 + \frac{[S_o]}{K}\right)} \quad (2.2)$$

Aiba Model: $$V = \frac{V_{max}[S_o]}{K_S + [S_o]} \exp\left(-[S_o]/K_I\right) \quad (2.3)$$

These models involve three parameters, viz. V_{max} (maximum reaction velocity), K_S (substrate concentration at $V = V_{max}/2$) and K_I (inhibition constant). The experimental data of reaction velocity against initial substrate concentration was fitted to these models to obtain numerical values of the model parameters.

2.3. RESULTS AND DISCUSSION

2.3.1 *Preliminary experiments*

***Effect of carbon source in seed culture medium*:** The experimental results for the effect of carbon source in seed culture medium are depicted in Fig. 2.2. Among three carbon sources used, microbial culture grown in mannitol containing medium gave the maximum DHA concentration of 6.28 ± 0.32 g/L and a higher cell mass of 0.59 ± 0.31 g/L in 48 h of fermentation (Fig. 2.2).

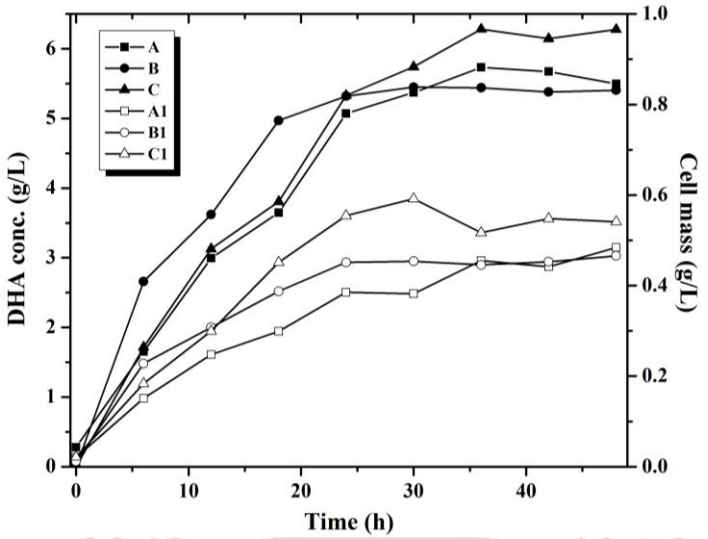

Figure 2.2. Time profiles of *G. oxydans* cell growth and DHA production for three different carbon sources in seed culture medium (at conc. 10 g/L). Legends: A, B, C – Time profiles of DHA concentration for glycerol, sorbitol, and mannitol, respectively. A1, B1, and C1 – cell mass profiles for glycerol, sorbitol, and mannitol, respectively. Glycerol conc. in fermentation medium = 10 g/L

On the other hand, the maximum DHA concentrations attained during glycerol fermentation with microbial cultures grown in glycerol and sorbitol containing seed culture medium were 5.73 and 5.44 g/L, respectively. An explanation for this effect can be given as follows: some polyols such as mannitol, sorbitol and glycerol have been reported to act as inducers of dehydrogenase activity in *G. oxydans* (Rollini and Manzoni, 2005; White and Claus, 1982), which improve the cell's ability of glycerol bioconversion to corresponding ketone. The enzyme in *G. oxydans* responsible for conversion of glycerol to DHA is glycerol dehydrogenase, which is a membrane–bound enzyme located at the outer surface of the cytoplasmic membrane. For low concentrations in growth medium, glycerol can induce this enzyme. However, glycerol dehydrogenase also suffers from substrate inhibition by glycerol. Therefore, it is likely that the enzyme may get partially inhibited during microbial growth itself before inoculation in the fermentation broth. This also makes

cells more prone to inhibition in fermentation broth, where glycerol is present at higher concentrations. However, such limitation does not occur for mannitol as substrate. In addition, mannitol is the optimal carbon source for the formation of the intra-cytoplasmic membrane of *G. oxydans* cells, which further assists in increasing the catalytic activity of glycerol dehydrogenase (Hu et al., 2010).

Amount of support selection and its reusability: The optimum amount of immobilized support in the fermentation medium was determined by varying the number of cubes of polyurethane foam added to medium. Results shown in Fig. 2.3A reveal that the highest DHA concentration was achieved for 3 cubes. Lesser cubes reduce the microbial cell population in the fermentation medium, whereas large numbers of cubes in the reaction mixture hinder the mixing process, and reduce intensity of convection. This restricts the effective transport of nutrients and substrate to the cells inside the PU foam. Reduced convection in the medium also restricts the induction of oxygen from the air to the medium that results in depletion of the dissolved oxygen in the medium. As a consequence, the DHA production drops sharply.

For the assessment of reusability of biocatalyst, the PU foam cubes with immobilized cells from the first fermentation experiment were used in four consecutive experiments. Fig. 2.3B depicts the results of this study. The DHA concentration attained in the first fermentation was 12.13 ± 0.53 g/L, which gradually reduced to 4.85 g/L at the end of fifth fermentation. The reduction in DHA concentration is attributed to reduction in the microbial cell density on PU foam due to detachment of the cells from the surface and/or decrease of activity of the dehydrogenase enzyme during long periods of cultivation (Loyarkat et al., 2015).

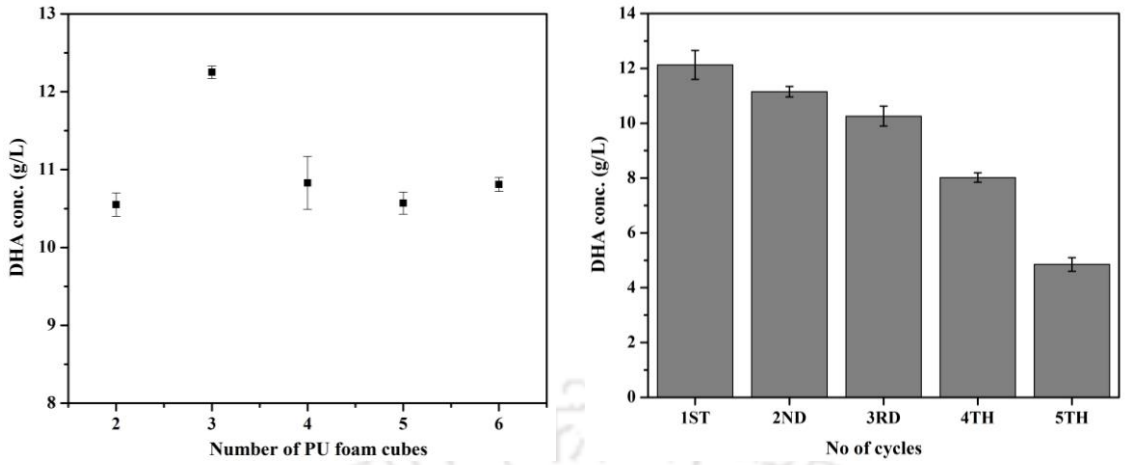

(A) (B)

Figure 2.3. (A) Optimization of amount of immobilized support (no. of cubes) for DHA production (B) Reusability of PU foam for the production of DHA from pure glycerol (initial concentration = 20 g/L)

Effect of nitrogen sources: Among the two sources of nitrogen, viz. yeast extract and ammonium sulfate, employed in glycerol fermentation, yeast extract was the most favorable nitrogen source for DHA production by both free and immobilized cells of *G. oxydans*. The maximum DHA concentrations of 11.09 ± 0.25 g/L and 11.85 ± 0.32 g/L were achieved for free and immobilized cells, respectively, using yeast extract as nitrogen source (Fig. 2.4). On the contrary, for ammonium sulphate, maximum DHA concentrations of 10.69 ± 0.31 and 9.98 ± 0.46 g/L were attained for free and immobilized cells, respectively. Thus, yeast extract was revealed to be more effective nitrogen source for DHA production by *G. oxydans* cells. The results obtained by Flickinger and Perlman (1977) and Underkofler and Fulmer (1937) also reported yeast extract to be a favorable nitrogen source for growth of *Gluconobacter* strains.

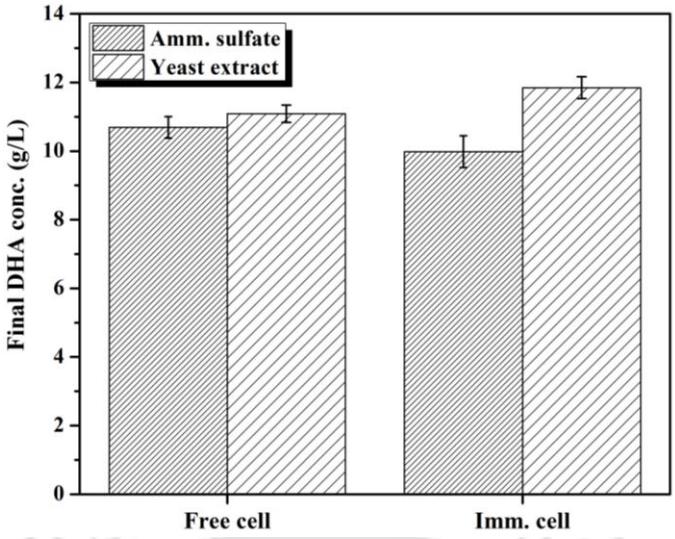

Figure 2.4. Effect of nitrogen source over DHA production by free and immobilized *G. oxydans* cells

2.3.2 Main experiments

Trends in DHA yield: The results of main experiments of glycerol fermentation are depicted in Fig. 2.5. The range of initial glycerol concentration for both pure and crude glycerol was 10 – 150 g/L. The maximum DHA concentrations attained during fermentation with free and immobilized cells, and the corresponding initial glycerol concentrations were as follows:

1. Free cells, pure glycerol: DHA = 14.66 g/L, Glycerol = 20 g/L.

2. Free cells, crude glycerol: DHA = 13.85 g/L, Glycerol = 20 g/L.

3. Immobilized cells, pure glycerol: DHA = 18.76 g/L, Glycerol = 30 g/L.

4. Immobilized cells, crude glycerol: DHA = 15.49 g/L, Glycerol = 30 g/L.

The DHA production (or final DHA concentration) in glycerol fermentation dropped after initial glycerol concentration of 20 g/L and 30 g/L for free and immobilized cells, respectively, which clearly represented substrate inhibition. Higher initial glycerol concentration corresponding to maximum DHA yield for immobilized cells indicates

greater resistance of immobilized cells towards substrate inhibition. As a consequence, the DHA yield for both pure and crude glycerol as substrate was higher for immobilized cells for lower concentration of glycerol. However, for higher initial concentrations such as 100 and 150 g/L this trend reverses, and higher DHA yield is seen for the free cells. For example, for initial glycerol (pure) concentration of 150 g/L, free cells give DHA yield of 12.11 g/L, while immobilized cells give yield of 11.7 g/L. For same initial concentration of crude glycerol, the DHA yields for free and immobilized cells are 10.44 and 8.81 g/L, respectively. These results also indicate that reduction in DHA yield for immobilized cells, as compared to free cells, is more marked for crude glycerol as substrate.

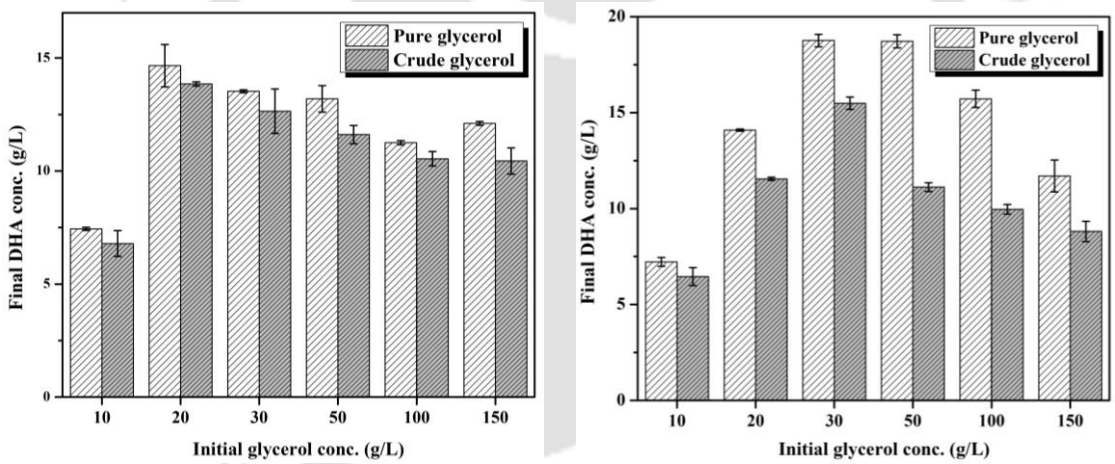

Figure 2.5. Results of DHA fermentation with pure and crude glycerol as substrate using free and immobilized *G. oxydans* cells: Trends with varying initial concentrations of the substrate. (A) Final DHA concentration for free cells; (B) Final DHA concentration for immobilized cells.

Trends in reaction velocities: Fig. 2.6 shows the trend of reaction velocities (determined experimentally) with initial glycerol concentration for both pure and crude versions of glycerol. Fig. 2.6A reveals that the reaction velocities for pure glycerol as substrate are almost similar for both free and immobilized cells till initial concentration of 20 g/L.

Maximum reaction velocity for free and immobilized cells is seen for initial glycerol concentration of 20 and 30 g/L, respectively. After this maximum, reaction velocities for both free and immobilized cells reduce with increasing initial glycerol concentration demonstrating substrate–inhibition behavior. For higher glycerol concentrations (50, 100 and 150 g/L), the reaction velocities for immobilized cells are significantly higher than free cells.

The trends in reaction velocities for free and immobilized cells reverse for crude glycerol as substrate (Fig. 2.6B). Till initial glycerol concentration of 30 g/L, immobilized cells have higher reaction velocity than free cells. Thereafter, reaction velocity shows a sharp drop for immobilized cells, while the velocity for the free cells reduces only marginally. Still, the highest initial glycerol concentration of 150 g/L, free cells have significantly higher reaction velocity.

We analyzed these results to greater depth in the next section using the biokinetics model.

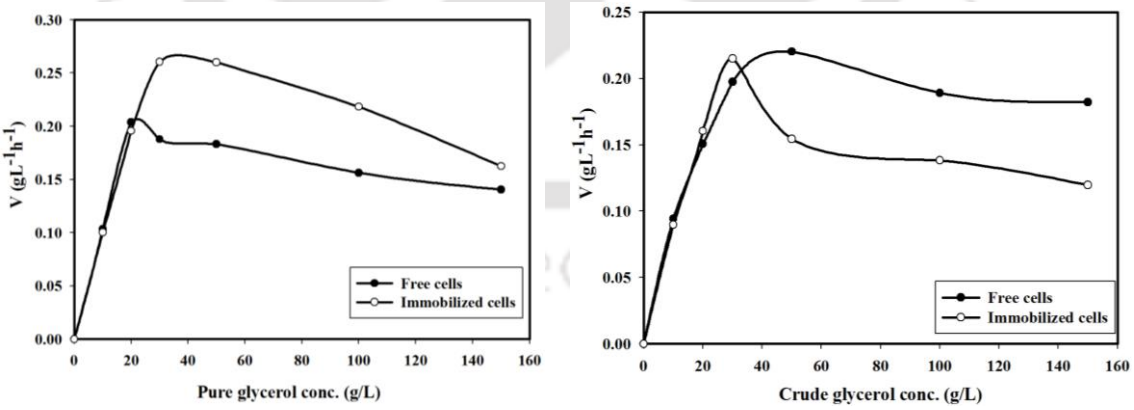

(A) (B)

Figure 2.6. Comparative evaluation of the reaction velocities of glycerol bioconversion for the free and immobilized cells for different substrates. (A) Pure glycerol (B) Crude glycerol

2.3.3 Biokinetic analysis

Fig. 2.7 shows the results of fitting of different kinetic models to reaction velocity versus initial substrate concentration. Table 2.1 lists the values of the model parameters for Haldane, Aiba and Yano models for pure and crude glycerol as substrate. The values of the root mean square error (RMSE) for each model are also listed in Table 2.1. Although the numerical values of the parameters are different for each model, the trends in the parameter values with system, viz. pure / crude glycerol for free / immobilized cells. These trends are as follows:

1. For free cells, V_{max} and K_S show marked increase, while K_I shows marginal increase for crude glycerol as substrate as compared to pure glycerol.

2. For immobilized cells, V_{max} and K_S show marked reduction, while K_I shows significant increase for crude glycerol as substrate as compared to pure glycerol.

It could be inferred from comparison of the RMSE values of different models that Haldane model shows the best fit with minimum RMSE. Hence, further analysis of the kinetics of glycerol bioconversion to DHA has been done using Haldane and modified Haldane kinetics model.

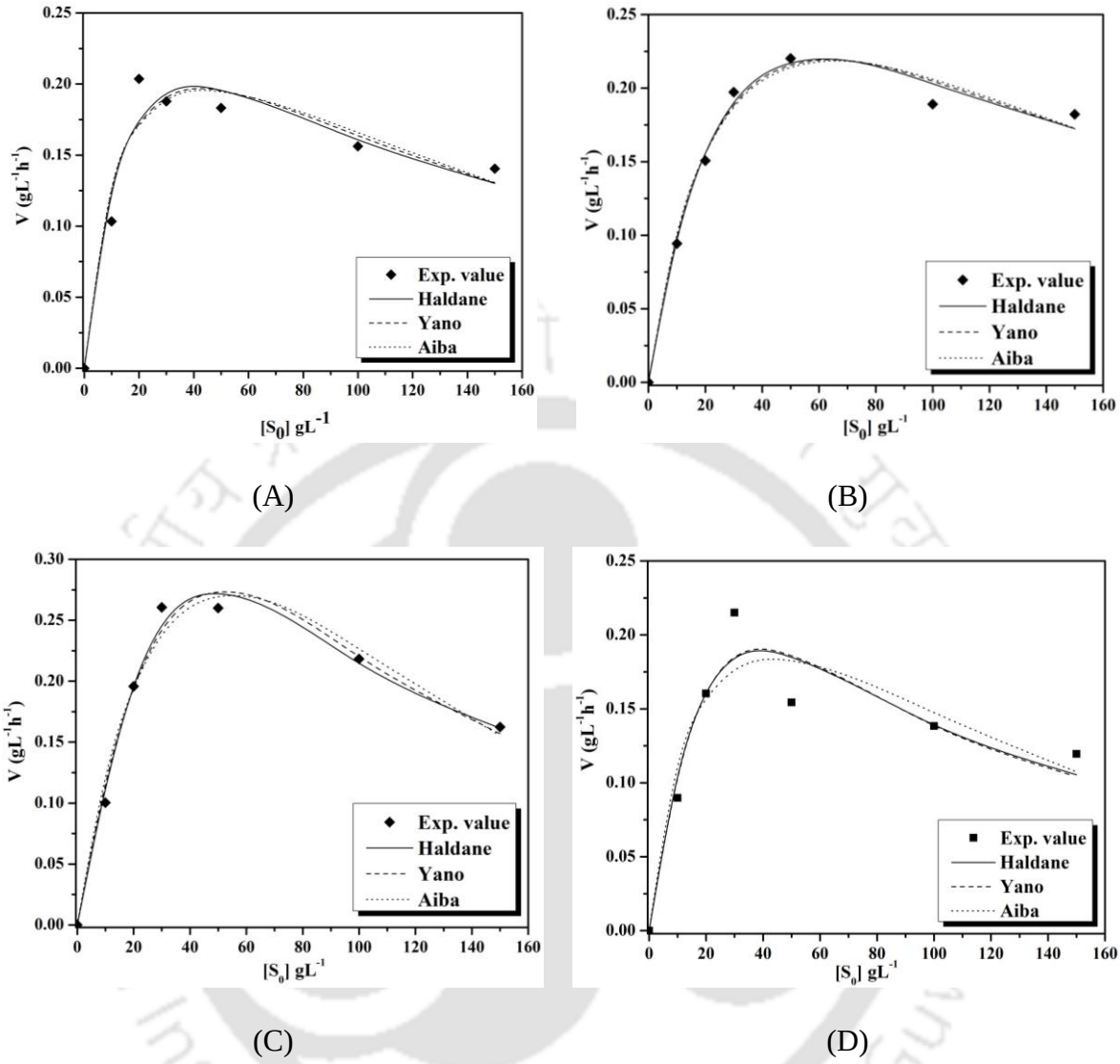

Figure 2.7. Results of fitting of various substrate-inhibition kinetic models to data of reaction velocity versus initial substrate concentration. (A) Free cells with pure glycerol as substrate; (B) Free cells with crude glycerol as substrate; (C) Immobilized cells with pure glycerol as substrate; (D) Immobilized cells with crude glycerol as substrate.

Table 2.1. Results of preliminary kinetic analysis of DHA formation by *G. oxydans* MTCC 904

(A) Kinetic parameters for free cells

Mathematical model	Pure glycerol as substrate				Crude glycerol as substrate			
	V_{max}	K_S	K_I	RMSE	V_{max}	K_S	K_I	RMSE
Haldane model	0.421	22.902	72.076	0.0150	0.559	46.662	77.613	0.0074
Yano model	0.340	16.491	135.741	0.0159	0.447	34.528	144.632	0.0084
Aiba model	0.337	15.208	176.180	0.0165	0.471	34.385	188.344	0.0091

(B) Kinetic parameters for immobilized cells

Mathematical model	Pure glycerol as substrate				Crude glycerol as substrate			
	V_{max}	K_S	K_I	RMSE	V_{max}	K_S	K_I	RMSE
Haldane model	5.774	486.699	4.457	0.0085	0.782	61.409	24.968	0.0181
Yano model	1.015	76.143	51.802	0.0106	0.861	69.411	22.365	0.0181
Aiba model	1.161	76.456	93.809	0.0128	0.387	22.413	131.369	0.0207

The units of V_{max}, K_S, and K_I are g $L^{-1}h^{-1}$, g L^{-1}, and g L^{-1}, respectively. RMSE – Root Mean Square Error

***Analysis with modified Haldane kinetics model*:** The preliminary analysis and also previous studies revealed that kinetics of glycerol bioconversion was best described by the Haldane kinetics model (Khanna et al., 2012, 2013). For further analysis, we consider the modified Haldane kinetics model given by Neufeld et al. (1980). This model is essentially of Monod basic form for substrate utilization, which is modified for substrate inhibition:

$$V = \frac{V_{\max}}{1 + \left(\frac{K_S}{[S_o]}\right) + \left(\frac{[S_o]}{K_I}\right)^n} \tag{2.4}$$

The value of n determines the order of inhibition, while K_I is the inhibition constant. The approach used for evaluation of the parameters V_{max}, K_S, K_I and n is necessarily that of curve fitting. The solution for any set of experimental data can, however, be simplified by an understanding of the influence of these parameters on curve shape. Equation 2.4 may be inverted as follows:

$$\frac{1}{V} = \frac{1}{V_{\max}} + \left(\frac{K_S}{V_{\max}}\right)\left(\frac{1}{[S_o]}\right) + \frac{[S_o]^n}{K_I^n V_{\max}} \tag{2.5}$$

At low values of $[S_o]$, the term $([S_o]/K_I)^n$ is negligible and the equation reduces to:

$$\frac{1}{V} = \frac{1}{V_{\max}} + \left(\frac{K_S}{V_{\max}}\right)\frac{1}{[S_o]} \tag{2.6}$$

By plotting $(1/V)$ versus $(1/[S_o])$, values of K_S and V_{max} can be estimated by slope and intercept as $1/[S_o] \to 0$. By taking first derivative of equation 2.5 we get:

$$\frac{d(1/V)}{d[S_o]} = \left(-\frac{K_S}{V_{\max}}\right)\frac{1}{[S_o]^2} + \frac{n[S_o]^{n-1}}{K_I^n\ V_{\max}} \tag{2.7}$$

At the minima of equation 2.7 or maxima of equation 2.4, $d(1/V)/d[S_o] = 0$, which gives:

$$[S_o]\big|_{V=V_{\max}} = \left[\frac{(K_S K_I^n)}{n}\right]^{1/(n+1)} \quad \text{and} \quad K_I\big|_{V=V_{\max}} = \left[\left(\frac{n}{K_S}\right)[S_o]^{n+1}\right]^{-n}$$

Dwyer et al. (1986) have proposed that for immobilized cells, the available (or accessible) substrate concentration, [S_o'], may be decreased from [S_o] because of diffusion–limited mass transport. The extent of limitation depends upon the type of immobilization matrix used, and the presence of other constituents in the matrix (e.g. cells, organic matter etc.), and the physical properties of the substrate. As per this proposition, Dwyer et al. (1986) have altered the equation of Neufeld et al. (1980) to describe utilization of an inhibitory substrate by either native or immobilized microorganism as follows:

$$V = \frac{V_{\max}}{\left[1 + \frac{K_S}{\left([S_o]\cdot X\right)} + \left(\frac{[S_o]}{K_I}\right)^n\right]} \qquad (2.8)$$

X is the empirical parameter ranging from 0 to 1 that changes [S_o] to [S_o'] to reflect the limited or fractional substrate available to immobilized cells ([S_o']) such that [S_o'] = [S_o]·X. For native cells, X = 1.

The kinetic data of reaction velocity *vs*. initial glycerol concentration shown in Fig. 2.8C was fitted to the modified Haldane kinetics model in equation 2.8 using nonlinear regression method using MATLAB® 7.10. Prior to fitting of the entire range of reaction velocity *vs*. initial substrate concentration to the equation 2.8, Lineweaver–Burk plots were obtained for both free and immobilized cells with pure and crude glycerol as substrate for low concentrations of 10, 20 and 30 g/L using equation 2.6. These plots are shown in Fig. 2.8A and B, and the values of parameters K_S and V_{max} obtained with these plots are listed in Table 2.2A. The results of Lineweaver–Burk analysis depicted in Table 2.2A revealed that the reaction velocity was higher for immobilized cells in case for both pure and crude glycerol as substrate. However, the value of K_S, indicative of the substrate affinity, was also higher for immobilized cells. Using these initial estimates of V_{max} and K_S, the main

substrate–inhibition model of Dwyer et al. (1986) was fitted to the complete range of V verses [S_o] depicted in Fig. 2.8C. The results of this analysis are shown in Table 2.2B.

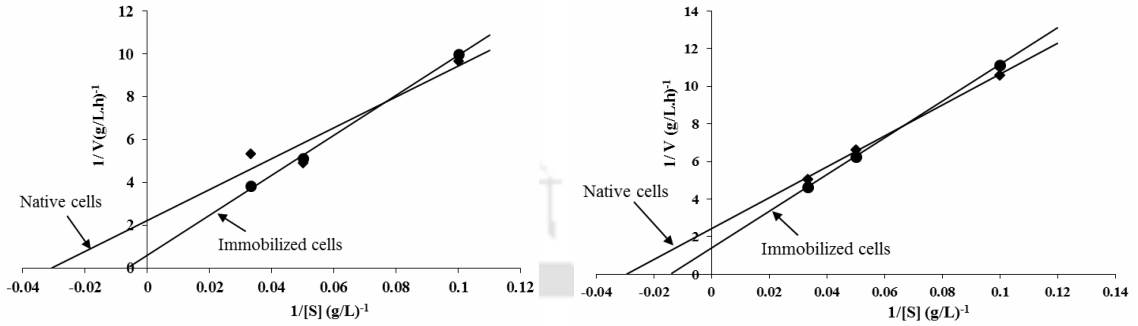

(A) (B)

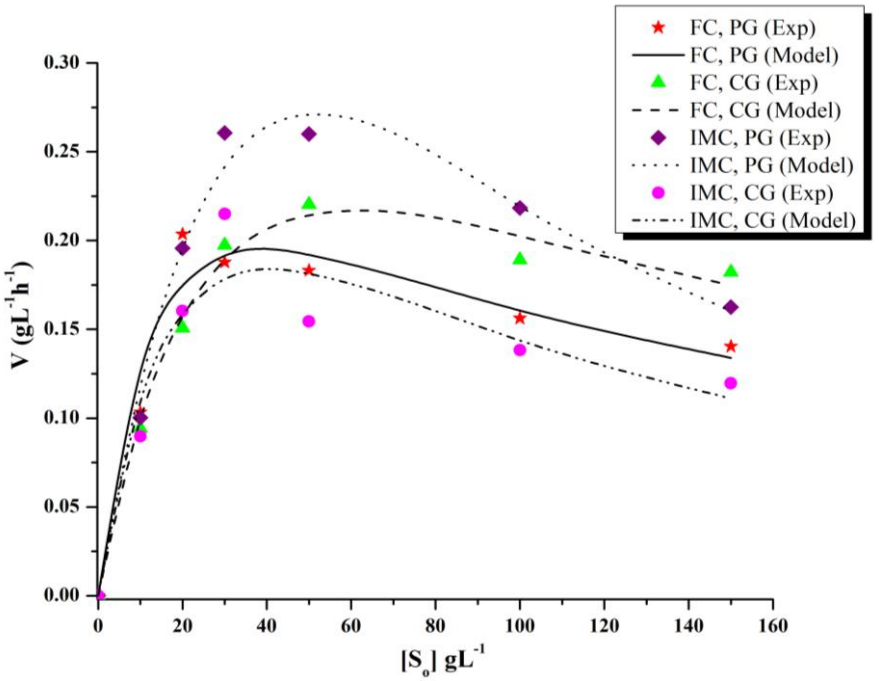

(C)

Figure 2.8. Lineweaver-Burk plots of DHA production rate by native (♦) and immobilized cells (●) in presence of (A) pure glycerol (B) crude glycerol. The initial glycerol concentration was 10, 20, 30 g/L. (C) Fitting of modified Haldane model for different experimental categories. Abbreviations: FC – Free cells, IMC – Immobilized cells, PG – Pure glycerol, CG – Crude glycerol

Table 2.2. Results of kinetic analysis with modified Haldane substrate-inhibition model

(A) Results of Lineweaver-Burk plots at low initial concentrations of glycerol

Experimental category	Pure glycerol as substrate			Crude glycerol as substrate		
	V_{max} (g $L^{-1}h^{-1}$)	K_S (g L^{-1})	R^2	V_{max} (g $L^{-1}h^{-1}$)	K_S (g L^{-1})	R^2
Free cells	0.45	32.49	0.90	0.42	34.08	0.99
Immobilized cells	1.64	152.87	0.99	0.73	70.88	1

(B) Results of kinetic analysis using modified Haldane substrate-inhibition model (in complete form)

Experimental category	S_{max} (g L^{-1})	V_{max} (g $L^{-1}h^{-1}$)	K_S (g L^{-1})	K_I (g L^{-1})	X	n	R^2
FC + PG	39.09	0.45	23.54	57.94	1	0.84	0.949
FC + CG	60.79	0.49	38.47	95.31	1	0.99	0.989
IMC + PG	31.21	0.78	17.46	60.01	0.31	1.37	0.985
IMC + CG	30.13	0.39	12.62	72.52	0.52	1.16	0.906

Abbreviations: FC – Free cells; IMC – Immobilized cells; PG – Pure glycerol; CG – Crude glycerol

The kinetic parameters in modified Haldane–substrate–inhibition model (Dwyer et al., 1986) have shown following salient features:

(1) For both pure and crude glycerol, the value of *X* was less than 1 for immobilized cells. This is indicative of the limited substrate concentration available to immobilized cells, as noted earlier. This is attributed to mass transport limitation in the immobilization matrix. Interestingly, the value of *X* for crude glycerol was higher, which represents faster transport of crude glycerol through PU foam. This effect is possibly a consequence of the impurities present in crude glycerol, which may reduce its viscosity, due to which crude glycerol is able to penetrate deeper and faster into porous structure of the PU foam.

(2) Comparing the kinetic parameters K_S and K_I between native and immobilized cells, we found that K_S was smaller for immobilized cells for both pure and crude glycerol. This effect is also attributed to restriction of substrate transport across PU foam, which causes retention of the substrate within matrix. This is reflected in reduction of value of K_S.

The inhibition constant, K_I, is practically same for free and immobilized cells in case of pure glycerol. However, for crude glycerol K_I is lower for immobilized cells, indicating that cells are more prone to inhibition. This effect is also attributed to mass transport limitation in immobilization matrix leading to retention of substrate and the impurities (alcohol + alkali) in it within matrix.

(3) The order of inhibition, n, shows interesting variations. Comparing the value of n between pure or crude glycerol as substrate for the two types of cells, we found higher inhibition for crude glycerol in case of free cells, while for immobilized cells reverse is true. We attribute this results to higher interaction between the cells and crude substrate in case of free cells, and lesser retention (or faster transport) of crude substrate across immobilization matrix for immobilized cells.

Comparing the order of inhibition between free and immobilized cells for a particular type of glycerol, we find that immobilized cells had higher inhibition for both pure and crude glycerol than free cells. This effect is again a manifestation of retention of impure or crude substrate in immobilization matrix due to which the inhibition effect of the impurities is enhanced.

(4) V_{max} and S_{max} (the substrate concentration corresponding to maximum reaction velocity) for different combination of type of cells and substrate are essentially manifestation of the values of K_S, K_I, X and n for that combination. For free cells rise in both K_S and K_I, indicating lesser substrate affinity and lesser inhibition as pure glycerol is replaced by crude glycerol, lead to practically similar values of V_{max}. However, for immobilized cells, a drop

in V_{max} is seen as pure glycerol is replaced by crude version. We attribute this effect to reduction in K_S and increase in X for crude glycerol as compared to pure glycerol. Higher X value in case of crude glycerol not only indicates greater accessibility of crude glycerol, but also higher retention of crude glycerol in the immobilization matrix, due to which the inhibition effect of the impurities is augmented. Higher substrate affinity in addition to greater to access to substrate containing impurities, cause reduction in reaction velocity despite higher inhibition constant and lesser order of inhibition.

An additional manifestation of the relative variations in kinetic parameters is in term of the S_{max} value. For the free cells, S_{max} for crude glycerol (60.79 g/L) is significantly higher than pure glycerol (39.09 g/L). On the other hand, the S_{max} values for immobilized cultures for both pure and crude version of glycerol are practically similar (31.21 and 30.13 g/L).

2.4. CONCLUSIONS

The present study has revealed interesting accounts of kinetics of crude glycerol bioconversion to dihydroxyacetone using immobilized cells of *G. oxydans*. Parameters of the modified substrate–inhibition kinetic model have shown following trends (as compared to free cells and pure glycerol as substrate):

1. Reduction in substrate concentration K_S at $V_{max}/2$.
2. Reduction in inhibition constant K_I.
3. Increase in order of inhibition n.
4. Reduction in maximum reaction velocity, V_{max}.

These facets are essentially implications of the mass transfer limitations across immobilization matrix, which results in protection of cells from substrate inhibition in addition to retention of substrate in matrix.

REFERENCES

Agarwal, M., Dikshit, P.K., Bhasarkar, J.B., Borah, A.J., Moholkar, V.S., 2016. Physical insight into ultrasound–assisted biodesulfurization using free and immobilized cells of *Rhodococcus rhodochrous* MTCC 3552. Chem. Eng. J. 295, 254–267.

Basak, B., Bhunia, B., Dutta, S., Chakraborty, S., Dey, A., 2014. Kinetics of phenol biodegradation at high concentration by a metabolically versatile isolated yeast *Candida tropicalis* PHB5. Environ. Sci. Pollut. Res. Int. 21, 1444–1454.

Bhasarkar, J.B., Dikshit, P.K., Moholkar, V.S., 2015. Ultrasound assisted biodesulfurization of liquid fuel using free and immobilized cells of *Rhodococcus rhodochrous* MTCC 3552: A mechanistic investigation. Bioresour. Technol. 187, 369–378.

Chen, J., Chen, J., Zhou, C., 2008. HPLC methods for determination of dihydroxyacetone and glycerol in fermentation broth and comparison with a visible spectrophotometric method to determine dihydroxyacetone. J. Chromatogr. Sci. 46, 912–916.

Claret, C., 1993. Inhibitory effect of dihydroxyacetone on *Gluconobacter oxydans*: Kinetic aspects and expression by mathematical equations. J. Ind. Microbiol. 11, 105–112.

Claret, C., Bories, A., Soucaille, P., 1992. Glycerol inhibition of growth and dihydroxyacetone production by *Gluconobacter oxydans*. Curr. Microbiol. 25, 149–155.

Dwyer, D.F., Krumme, M.L., Boyd, S.A., Tiedje, J.M., 1986. Kinetics of phenol biodegradation by an immobilized methanogenic consortium. Appl. Environ. Microbiol. 52, 345–351.

Flickinger, C., Perlman, D., 1977. Application of oxygen–enriched aeration in the conversion of glycerol to dihydroxyacetone by *Gluconobacter oxydans* IFO 3293. Appl. Environ. Microb. 33, 706–712.

Hekmat, D., Bauer, R., Fricke, J., 2003. Optimization of the microbial synthesis of dihydroxyacetone from glycerol with *Gluconobacter oxydans*. Bioprocess Biosyst. Eng. 26, 109–116.

Hu, Z.–C., Liu, Z.–Q., Zheng, Y.–G., Shen, Y.–C., 2010. Production of 1,3–dihydroxyacetone from glycerol by *Gluconobacter oxydans* ZJB09112. J. Microbiol. Biotechnol. 20, 340–345.

Khanna, S., Goyal, A., Moholkar, V.S., 2013. Mechanistic investigation of ultrasonic enhancement of glycerol bioconversion by immobilized *Clostridium pasteurianum* on silica support. Biotechnol. Bioeng. 110, 1637–1645.

Khanna, S., Jaiswal, S., Goyal, A., Moholkar, V.S., 2012. Ultrasound enhanced bioconversion of glycerol by *Clostridium pasteurianum*: A mechanistic investigation. Chem. Eng. J. 200–202, 416–425.

Lowry, O.H., Rosenbrough, N.J., Farr, A.L., Randall, R.J., 1951. Protein measurement with the Folin Phenol Reagent. J. Biol. Chem. 193, 265–275.

Loyarkat, S., Cheirsilp, B., Prasertsan, P., 2015. Two–stage repeated–batch fermentation of immobilized *Clostridium beijerinckii* on oil palm fronds for solvents production. Process Biochem. 50, 1167–1176.

Malani, R.S., Khanna, S., Moholkar, V.S., 2013. Sonoenzymatic decolourization of an azo dye employing immobilized horse radish peroxidase (HRP): a mechanistic study. J. Hazard. Mater. 256–257, 90–97.

Neufeld, R. D., Mack, J. D., Strakey, J. P., 1980. Anaerobic Phenol Biokinetics. Journal WPCF, 52, 2367–2377.

Rocha–Martin, J., Acosta, A., Berenguer, J., Guisan, J.M., Lopez–Gallego, F., 2014. Selective oxidation of glycerol to 1,3–dihydroxyacetone by covalently immobilized glycerol dehydrogenases with higher stability and lower product inhibition. Bioresour. Technol. 170, 445–453.

Rollini, M., Manzoni, M., 2005. Bioconversion of D–galactitol to tagatose and dehydrogenase activity induction in *Gluconobacter oxydans*. Process Biochem. 40, 437–444.

Stasiak–Różańska, L., Błażejak, S., Gientka, I., 2014. Effect of glycerol and dihydroxyacetone concentrations in the culture medium on the growth of acetic acid bacteria *Gluconobacter oxydans* ATCC 621. Eur. Food Res. Technol. 239, 453–461.

Underkofler, L.A., Fulmer, E.I., 1937. The production of dihydroxyacetone by the action of *Acetobacter suboxydans* upon glycerol. J. Am. Chem. Soc. 59, 301–302.

White, S.A., Claus, G.W., 1982. Effect of intracytoplasmic membrane development on oxidation of sorbitol and other polyols by *Gluconobacter oxydans*. J. Bacteriol. 150, 934–943.

CHAPTER 3

OPTIMIZATION OF MEDIUM COMPONENTS FOR DHA PRODUCTION

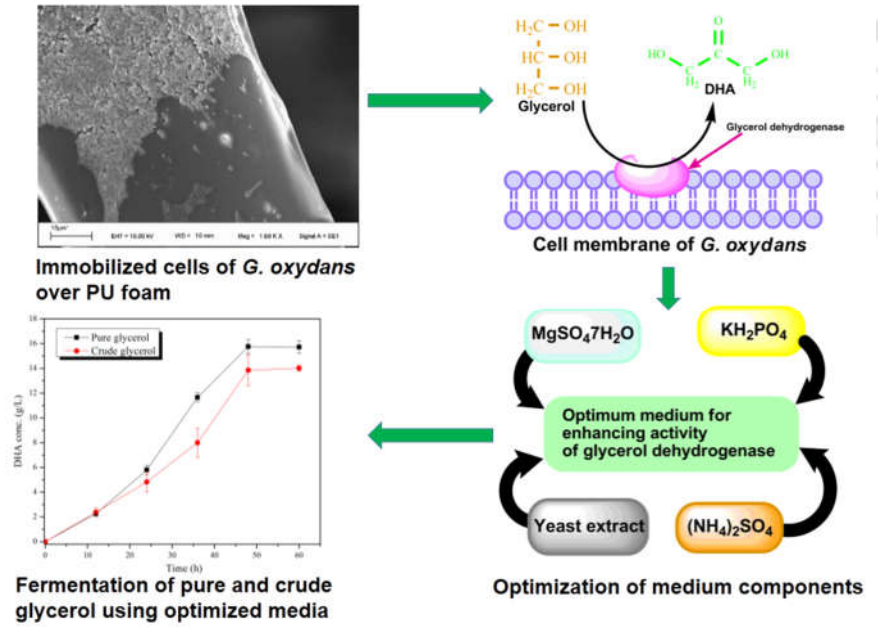

CHAPTER 3

OPTIMIZATION OF MEDIUM COMPONENTS FOR DHA PRODUCTION

3.1 INTRODUCTION

Although several earlier authors have addressed the matter of glycerol bioconversion to DHA, studies using biodiesel–derived crude glycerol are limited. Alkali, alcohol and salt contaminations in crude glycerol could have significant effect on DHA production by microbial cells, which needs to be properly investigated. Moreover, most of the previous studies have employed free cells of *G. oxydans* for the synthesis. However, immobilized cells – which give higher and more effective control over cell density in the medium – are suitable for large scale applications. In the present study, we addressed the matter of optimization of DHA production from crude glycerol using immobilized and cross–linked cells of *G. oxydans* over reticulated polyurethane foam as support. Polyurethane foam has highly porous structure with large surface area, and cells can easily get immobilized over the surface as well as inside the pores. Our approach to optimization of the DHA production by immobilized cells of *G. oxydans* essentially comprises statistical optimization of different medium components using Plackett–Burman and Central Composite Design (CCD). The metabolism of the cells could possibly change after

immobilization (Kourkoutas et al., 2010), and hence, the optimum medium composition for the two types of cell cultures could vary significantly. To ascertain this conjecture, we have also conducted fermentation of glycerol using the optimized medium employing immobilized cultures.

3.2 MATERIALS AND METHODS

3.2.1 Materials

Microbial culture of *Gluconobacter oxydans* MTCC 904 was procured from Microbial Type Culture Collection (MTCC), Chandigarh, India. DHA and pure glycerol were procured from Merck, Germany. Reticulated polyurethane foam was procured from local market. All other medium components and chemicals used in this study were procured from HiMedia Pvt. Ltd., India.

Crude glycerol was produced through biodiesel synthesis from alkali (NaOH) catalyzed transesterification reaction using soybean oil and methanol. The details of transesterification reaction are as follows: alcohol: oil molar ratio = 12:1, volume of oil = 60 ml, volume of alcohol = 30 ml, catalyst = 0.54 g (1% w/v), temperature = 65^{o}C, time = 1 h. After completion of the reaction, the reaction mixture was kept in the separating funnel for 18–20 h. The mixture separated into two layers, viz. upper layer of biodiesel and lower layer of glycerol. Approximately, 27 ml of crude glycerol was produced from the transesterification reaction. The quantities of alkali and alcohol contaminants in crude glycerol were determined as follows: 0.85% w/v of sodium hydroxide (calculated by acid base titration) and 0.26% w/v methanol (determined using gas chromatograph).

3.2.2 Growth and maintenance of *G. oxydans* culture

The lyophilized cells of *G. oxydans* were revived in MRS medium and kept in a

rotary incubator shaker (Make: Lab Companion; Model: SI–300R) at 30ºC, 150 rpm for 24 h. The revived cells were grown on agar slant and kept at 4ºC. The cultures were sub–cultured every month. The composition of MRS medium in 1 L of distilled water was as follows: peptone 10.0 g, beef extract 10.0 g, yeast extract 5.0 g, glucose 10.0 g, tween–80 1 mL, Na_2HPO_4 2.0 g, sodium acetate 5.0 g, triammonium citrate 2.0 g, $MgSO_4 \cdot 7H_2O$ 0.2 g, $MnSO_4 \cdot 4H_2O$ 0.2 g. The pH of the medium was adjusted to 6.0 ± 0.2 using 1 N HCl. The agar plates and slants were prepared by adding 15 g/L of agar in MRS medium.

3.2.3 Seed culture and fermentation medium compositions

The composition of seed culture medium was as follows: yeast extract 5.0 g/L, peptone 3 g/L, $K_2HPO_4 \cdot 3H_2O$ 3 g/L, $(NH_4)_2SO_4$ 2 g/L, $MgSO_4 \cdot 7H_2O$ 0.51 g/L, mannitol 10 g/L. The initial pH of the medium was adjusted to 6.0 ± 0.2. The fermentation was carried out with varying different medium composition with a fixed crude glycerol concentration of 20 g/L. The pH of the medium was adjusted to 5.0 ± 0.2 with 1N HCl. The medium was autoclaved prior to inoculation at 121ºC, 15 psi for 20 min. Three PU foam cubes (optimized in preliminary experiments, data not shown) with immobilized cells of *G. oxydans* were added to fermentation broth for experiments. Aliquots of the fermentation broth were withdrawn periodically to assess the quantity of DHA in the broth.

3.2.4 Immobilization and cross–linking of cells on PU foam

The cells of *G. oxydans* were immobilized over PU foam support using following method as described in previous chapter. The commercial grade polyurethane foam was cut into cubical pieces of appropriate size (1 cm × 1 cm × 1 cm), and were washed 3–4 times with d–H_2O and autoclaved prior to addition. The PU foam pieces were added to the broth at the onset of log phase of the culture, i.e. after 10 h (as per growth profile determined in

preliminary experiments). PU foam pieces were incubated for 50 h at 30ºC with shaking at 150 rpm. After incubation, polyurethane cubes with immobilized cells (immobilized supports) were separated from the medium, and were added to phosphate buffer (50 mM, pH 6.0) with shaking for 10 min. The foam pieces were then washed with phosphate buffer and dried at room temperature. The dried PU foam pieces were added to 0.1% gluteraldehyde solution for cross–linking of cells and incubated again for 1 h, followed by washing with phosphate buffer and subsequently drying at room temperature for 24 h. The preliminary confirmation of immobilization of the cells on the support was done by Lowry assay (Lowry et al., 1951). Four pieces of PU foam were added to 20 ml of 50 mM phosphate buffer of pH 6.0. The immobilized system was kept in ice bath to control the overheating and sonicated at 20 kHz (Make – Sonics and Materials Inc., Model: VCX 500) for releasing cells proteins. 1 mL of this extract was used for Lowry assay to determine all the cell proteins. A positive test confirms the presence of proteins, which were released from disruption of the cells immobilized on the surface of the support. Immobilization of the microbial cells on PU foam was also confirmed from scanning electron microscope analysis (SEM, Make – Leo, Model – 1430vp).

3.2.5 Analytical methods

The optical density of *G. oxydans* cells in fermentation broth was monitored with a UV–Vis spectrophotometer by measuring absorbance at 660 nm (Make: Perkin Elmer, Model: LAMBDA 35). The DHA in the aliquots withdrawn from the broth was quantified after centrifugation (10,000 rpm, 20 min) and proper dilution of the aliquot. DHA was assayed with diphenylamine reagent (Liu et al., 2008; Rocha–Martin et al., 2014), which comprised of diphenylamine (0.6 g), sulfuric acid (6 mL) and acetic acid (54 mL). 0.5 mL of the aliquot of fermentation broth was mixed with 4.5 mL of diphenylamine reagent

before incubation in closed tubes for 20 min in boiling water bath. The samples were cooled to room temperature and absorbance was recorded at 615 nm immediately. The concentration of DHA in the sample was determined using the standard graph of concentration versus absorbance.

3.2.6 Experimental design for medium optimization

Optimization of the fermentation medium was carried out using two–step procedure, viz. Plackett–Burman design followed by central composite design (CCD).

3.2.6.1 Plackett–Burman design

Published literature on DHA synthesis from glycerol (either pure or crude version) reports use of many medium components (Bauer et al., 2005; Bauer et al., 2006; Flickinger and Perlman, 1977; Hekmat et al., 2003; Hekmat et al., 2007; Wethmar and Deckwer, 1999). On the basis of published literature, 6 potential components, viz. yeast extract, K_2HPO_4, KH_2PO_4, $(NH_4)_2SO_4$, $MgSO_4 \cdot 7H_2O$, $CaCl_2 \cdot 2H_2O$, have been selected in present study for optimization of fermentation medium. The concentration limits of these medium components were also decided on the basis of published literature. Plackett–Burman experimental design with six possible medium components (or variables) comprised of twelve experimental (or fermentation) runs. Two concentration levels were selected for each medium component – coded as (–1) for lower level and (+1) for higher level, as given in Table 3.1. MINITAB (Release 15.1, PA, USA, Trial Version) was used for devising the Plackett–Burman experimental design, and also for analysis and processing of the data. Placket–Burman design is a two–level factorial design that follows first–order polynomial equation:

$$Y = \beta_o + \sum_{i=1}^{n} \beta_i X_i \qquad (3.1)$$

Notations: Y – response variable (DHA yield), β_o – model intercept, β_i – linear coefficient and X_i – optimization variable (or medium component) (Plackett and Burman, 1946). The concentration of DHA in the fermentation broth was measured up to 60 h. Each experimental run was carried out in triplicate to access reproducibility, and the average response value in each experiment was considered for analysis. The analysis of variance was carried out with a confidence interval of 95%. The significant variables from this result were further analyzed using central composite design (CCD) of experiments.

Table 3.1. Factors and levels used in Plackett–Burman design matrix

Factors	Levels	
	Low (–1)	High (+1)
(X_1) – Yeast extract (g/L)	2	10
(X_2) – K_2HPO_4 (g/L)	0.1	0.5
(X_3) – KH_2PO_4 (g/L)	0.1	0.9
(X_4) – $(NH_4)_2SO_4$ (g/L)	1	5
(X_5) – $MgSO_4 \cdot 7H_2O$ (g/L)	0.1	1
(X_6) – $CaCl_2 \cdot 2H_2O$ (g/L)	1	3

3.2.6.2 Central composite design (CCD)

The central composite design is commonly used to get insight into the interactions among individual variables while influencing the response (or target) variable. The CCD experimental design in present study comprised of three significant medium components identified from the previous Plackett–Burman design, viz. $MgSO_4 \cdot 7H_2O$, KH_2PO_4 and $(NH_4)_2SO_4$. These variables were used at five coded levels ($-\alpha$, –1, 0, +1, $+\alpha$) in the experimental design. The experimental design constituted 20 individual runs (

$= 2^k + 2k + n_o$), where k is the number of independent variables, and n_o is the number of replicate runs at the center point of the variable. The exact experimental design with permutation–combination of levels of different parameters was generated using Minitab statistical software (Release 15.1, Trial Version).

3.2.6.3 Statistical analysis and model fitting

The experimental data obtained was fitted to the following quadratic model containing coefficients corresponding to individual and interactive effects of parameters:

$$Y = \beta_0 + \sum_{i=1}^{k} \beta_i X_i + \sum_{i=1}^{k} \beta_{ii} X_i^2 + \sum_{i \neq j} \sum_{i} \beta_{ij} X_i X_j \qquad (3.2)$$

Notation: Y – measured response variable (DHA yield), k – number of factors or medium components, β_o – intercept (or regression constant), β_i – linear coefficient, β_{ii} – quadratic coefficient and β_{ij} – interaction coefficient. The coded values (x) of the actual experimental variables were determined using eq. 3.3:

$$X = (x_i - x_o)/\Delta x \qquad (3.3)$$

where, i = 1, 2, 3…, X is the dimensionless value of the variables; x_o is the value of the variable x at center point; and Δx is the step change. The analysis of variance (ANOVA) was done to determine the significance of each factor in fitted model and also to determine the goodness of fit. ANOVA of the linear, quadratic and interaction regression coefficients (i.e., F– value and p– value. The F– and p– values of linear and interaction coefficients essentially exhibit the individual and interactive effects of the independent variables on the response variable, i.e. DHA yield. p– values of linear and interaction coefficients indicate nature of interaction between independent variables.

3.2.7 Validation experiments

For the assessment of the accuracy of the optimum medium composition predicted by the statistical analysis, glycerol fermentation experiments have been conducted using the medium composition resulting from statistical analysis. Fermentation experiments have been carried out using both pure as well as crude glycerol to ascertain as whether impurities present in glycerol have any effect on fermentation kinetics DHA yield. Reproducibility of fermentation results was checked by performing all validation experiments in triplicate.

3.3 RESULTS AND DISCUSSION

3.3.1 Plackett–Burman experimental design

The results of initial screening of medium components using Plackett–Burman design are given in Table 3.2. It could be inferred from Table 3.2 that experimental and predicted (from eq. 3.1) values for DHA yield match very well. In the 12 experiments of Placket–Burman design, the DHA concentration varied from 7.721 to 13.081 g/L. The statistical analysis of Plackett–Burman design is given in Table 3.3A and B. The first–order model coefficients for all six variables along with *t*– and *p*–values are depicted in Table 3.3A, while the ANOVA of the model is given in Table 3.3B. The Pareto plot of the Placket–Burman analysis is shown in Fig. 3.1, which shows that *t*–value limit for this analysis is 2.57. The *t*–value for $MgSO_4 \cdot 7H_2O$ (X_5), $(NH_4)_2SO_4$ (X_4) and KH_2PO_4 (X_3) are higher than this limit, which points towards their significance. It also reported that the DHA production is affected by the change in concentration of KH_2PO_4 (Underkofler and Fulmer, 1937). However, K_2HPO_4 shows negative effect on the DHA yield as indicated by the negative Placket–Burman model coefficient. The overall regression coefficient (R^2) for the model is 0.971, with adjusted R^2 of 0.935. This indicates that model fits very well to the data.

Table 3.2. Plackett–Burman design matrix with coded values and DHA yield (g/L)

Run order	X_1	X_2	X_3	X_4	X_5	X_6	DHA yield (g/L)	
							Experimental	Predicted
1	1	–1	1	1	–1	1	12.216 ± 0.045	12.154
2	–1	–1	–1	–1	–1	–1	7.721 ± 0.142	7.872
3	1	1	1	–1	1	1	12.981 ± 0.224	13.346
4	–1	1	1	1	–1	1	11.611 ± 0.052	11.459
5	–1	–1	–1	1	1	1	13.081 ± 0.339	12.718
6	–1	1	–1	–1	–1	1	8.135 ± 0.067	8.482
7	1	1	–1	1	–1	–1	10.150 ± 0.241	10.034
8	1	1	–1	1	1	–1	12.632 ± 0.112	12.748
9	–1	–1	1	1	1	–1	12.987 ± 0.205	13.564
10	–1	1	1	–1	1	–1	12.602 ± 0.043	12.042
11	1	–1	–1	–1	1	1	12.025 ± 0.156	11.890
12	1	–1	1	–1	–1	–1	10.189 ± 0.028	10.021

Table 3.3. Results of Plackett–Burman experimental design

(A) Model coefficients, *t*– and *p*–value for the optimization variables

Model term	Coefficient Estimate	Computed *t*–value	*p*–value
Intercept	11.361	81.9	0.000*
X_1	0.338	2.44	0.059
X_2	–0.008	–0.06	0.951
X_3	0.737	5.31	0.003*
X_4	0.752	5.42	0.003*
X_5	1.357	9.78	0.000*
X_6	0.314	2.26	0.073

* Significant p values, $p \leq 0.05$; $R^2 = 0.971$; Predicted $R^2 = 0.829$; Adjusted $R^2 = 0.935$

(B) ANOVA for the model

Term	SS	DF	Mean square	*F*–value	*p*–value
Model	37.961	6	6.327	27.39	0.001
X_1	1.371	1	1.371	5.94	0.059
X_2	0.001	1	0.001	0.00	0.951
X_3	6.516	1	6.516	28.21	0.003
X_4	6.786	1	6.786	29.38	0.003
X_5	22.104	1	22.104	95.7	0.000
X_6	1.183	1	1.183	5.12	0.073
Residual error	1.155	5	0.231	--	--
Total	39.116	11	--	--	--

DF – degrees of freedom; SS – sum of squares; MS – mean square

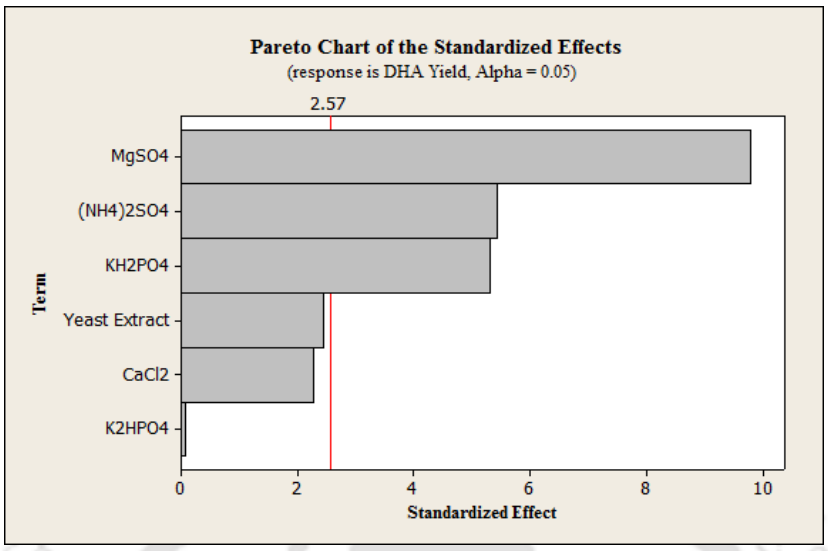

Figure 3.1. Pareto plot for Plackett–Burman analysis

It should be noted that the *p*– value of yeast extract (X_1) is 0.059, which is slightly above the significance limit of 0.05. Moreover, the *t*–value of yeast extract is 2.44, which is again, slightly lower than the Pareto plot limit of 2.57. Neglecting the insignificant variables, the model equation for DHA production could be written as:

$$Y_{yield} = 11.361 + 0.737X_3 + 0.752X_4 + 1.357X_5 \quad (3.4)$$

These results indicate that yeast extract is not a completely insignificant component of the fermentation medium, and a minimum concentration of yeast extract is required in the fermentation medium. Underkofler and Fulmer (1937) have stated that fermentation medium for DHA production from glycerol must contain at least 0.5% of yeast extract. Flickinger and Perlman (1977) have also reported that the growth of *Gluconobacter* strains is stimulated by the concentration of yeast extract in the fermentation medium.

3.3.2 Central composite design for optimization of medium components

The Placket–Burman experimental design identified $MgSO_4 \cdot 7H_2O$, $(NH_4)_2SO_4$ and KH_2PO_4 as the significant variables or medium components affecting the DHA yield. The central composite design (CCD) was used to optimize the actual values (or concentrations) of the significant variables (or medium components) from Plackett–Burman design. Preliminary fermentation experiments with only $MgSO_4 \cdot 7H_2O$, $(NH_4)_2SO_4$ and KH_2PO_4 as medium components resulted in very low DHA yield (< 8 g/L), which was lower than the yield in any of the 12 experiments in the Placket–Burman design. Therefore, as per the results of Placket–Burman design stated in previous section, and observations of Flickinger and Perlman (1977) and Underkofler and Fulmer (1937), yeast extract was also included in the fermentation medium. The concentration of yeast extract in the fermentation medium, however, was maintained at a constant value of 2 g/L (i.e. the lowest value in the optimization range given in Table 3.1), and has not been considered in the CCD experimental design. The full factorial CCD matrix of these variables is given in Table 3.4 along with the response variable of actual and predicted DHA yield.

The coefficients of the quadratic response model (given in eq. 3.2) along with the *p*– and *t*–values of linear, quadratic and interaction coefficients are given in Table 3.5A. The second–order regression equation for the fitted data is as follows:

$$Y_{yield} = 13.8444 + 1.1964X_5 + 0.816X_3 - 0.2884X_4 - 0.0762X_5^2 - 0.6946X_3^2 - 0.6958X_4^2 - 0.3192X_3X_5 - 0.6947X_4X_5 + 0.5047X_3X_4 \quad (3.5)$$

Table 3.4. Central composite design matrix of three medium components

Run order	$MgSO_4 \cdot 7H_2O$ (X_5)*	KH_2PO_4 (X_3)*	$(NH_4)_2SO_4$ (X_4)*	DHA yield (g/L)	
				Experimental	Predicted
1	0 (0.55)	0 (0.5)	0 (3)	13.983 ± 0.12	13.844
2	–1 (0.28)	–1 (0.26)	–1 (1.81)	10.236 ±0.083	10.145
3	–1 (0.28)	–1 (0.26)	+1 (4.19)	9.926 ±0.056	9.948
4	0 (0.55)	0 (0.5)	+α (5)	11.289 ±0.105	11.392
5	0 (0.55)	0 (0.5)	–α (1)	12.351 ±0.012	12.361
6	0 (0.55)	0 (0.5)	0 (3)	13.913 ±0.137	13.844
7	+1 (0.82)	+1 (0.74)	+1 (4.19)	11.581 ±0.061	11.593
8	0 (0.55)	–α (0.1)	0 (3)	10.413 ±0.085	10.508
9	0 (0.55)	0 (0.5)	0 (3)	13.806 ±0.171	13.844
10	–α (0.1)	0 (0.5)	0 (3)	10.464 ±0.091	10.470
11	0 (0.55)	0 (0.5)	0 (3)	13.842 ±0.116	13.844
12	0 (0.55)	0 (0.5)	0 (3)	13.710 ±0.028	13.844
13	–1 (0.28)	+1 (0.74)	+1 (4.19)	13.326 ±0.043	13.228
14	+1 (0.82)	+1 (0.74)	–1 (1.81)	12.651 ±0.063	12.549
15	0 (0.55)	0 (0.5)	0 (3)	13.832 ±0.142	13.844
16	+1 (0.82)	–1 (0.26)	+1 (4.19)	9.762 ±0.045	9.589
17	0 (0.55)	+α (0.9)	0 (3)	13.234 ±0.174	13.252
18	+1 (0.82)	–1 (0.26)	–1 (1.81)	12.547 ±0.076	12.565
19	0 (0.28)	+1 (0.74)	–1 (1.81)	11.313 ±0.113	11.406
20	+α (1)	0 (0.5)	0 (3)	11.024 ±0.034	11.131

* Coded and actual (in parenthesis, g/L) values of the parameter

The values of the regression coefficients, viz. R^2 = 0.997, predicted R^2 = 0.979, adjusted R^2 = 0.994, not only indicates that the model fits well to the experimental data, but also that 99.7% of the effect on DHA yield was explained by variation of the optimization parameters (or medium components). The ANOVA for the fitted model is described in Table 3.5B.

Table 3.5. Results of central composite design for medium optimization

(A) Model coefficients, *t*– and *p*– values for second order regression model

Model term	Coefficient	*t*–value	*p*–value Prob > *F*
Intercept (β_o)	13.844	284.387	0.000*
Linear coefficients			
$MgSO_4 \cdot 7H_2O$ (X_5)	1.196	6.080	0.000*
KH_2PO_4 (X_3)	0.816	25.265	0.000*
$(NH_4)_2SO_4$ (X_4)	–0.288	–8.928	0.000*
Square coefficients			
$MgSO_4 \cdot 7H_2O$ (X_5^2)	–0.076	–34.228	0.000*
$KH_2PO_4 \times KH_2PO_4$ (X_3^2)	–0.695	–22.09	0.000*
$(NH_4)_2SO_4$ (X_4^2)	–0.696	–22.129	0.000*
Interaction coefficients			
$MgSO_4 \cdot 7H_2O$ and KH_2PO_4 ($X_5 \times X_3$)	–0.319	–7.565	0.000*
$MgSO_4 \cdot 7H_2O$ and $(NH_4)_2SO_4$ ($X_5 \times X_4$)	–0.695	–16.463	0.000*
KH_2PO_4 and $(NH_4)_2SO_4$ ($X_3 \times X_4$)	0.505	11.961	0.000*

* Significant *p* values, $p \leq 0.05$; $R^2 = 0.997$; Predicted $R^2 = 0.979$; Adjusted $R^2 = 0.994$

(B) ANOVA for quadratic model

Source	DF	SS	MS	*F*–value	*p*–value Prob > *F*
Regression	9	43.404	4.823	338.500	0.000
Linear	3	10.756	3.585	251.660	0.000
Square	3	25.933	8.644	606.730	0.000
Interaction	3	6.715	2.238	157.100	0.000
Residual (Error)	10	0.143	0.014		
Lack of fit	5	0.098	0.019	2.270	0.106
Pure error	5	0.044	0.009		
Total	19	43.546			

DF – degree of freedom; SS – sum of squares; MS – mean square

(C) Analysis of the contour plots

Parameter space for maximum DHA yield				
Contour plot	Range of concentration (g/L)			
	KH_2PO_4	$(NH_4)_2SO_4$	$MgSO_4 \cdot 7H_2O$	DHA yield (g/L)
a. KH_2PO_4 vs. $MgSO_4 \cdot 7H_2O$	0.44-0.9	3#	0.38-0.66	13
b. $(NH_4)_2SO_4$ vs. KH_2PO_4	0.51-0.9	2.64- 3.92	0.55#	13
c. $(NH_4)_2SO_4$ vs. $MgSO_4 \cdot 7H_2O$	0.5#	2.03 – 3.44	0.39-0.68	13
Global optimum values of variable parameters: a. $MgSO_4 \cdot 7H_2O$ = 0.545 g/L; b. KH_2PO_4 = 0.641 g/L; c. $(NH_4)_2SO_4$ = 3.02 g/L Maximum DHA yield: 14.084 g/L				

Center point values of third variable parameter

It should be noted that the quadratic equation fitted to the experimental data is in terms of the coded values (and not absolute values) of optimization variables. The *t*–test, *F*–values and *p*–values of these coefficients are indicative of the significance of these variables. A large *t*–stat value and *p*–value < 0.05 indicates significance of the coefficient and the optimization variable (or medium component) to which the coefficient belongs. Relative *F*–values of linear interaction and quadratic coefficient indicate the significance of the individual effect of the optimization variable and the magnitude of interaction between them. As per ANOVA results given in Table 3.5B, *F*–value of overall regression is 338.5, while *F*–value of linear coefficient is 251.6. *p*–values of all linear, quadratic and interaction coefficients are < 0.05, which indicates their significance. The Lack of Fit *F*–value of 2.27 and *p*–value of 0.106 implies that Lack of Fit is not significant as compared to the pure error or in other words the model was significant. It should however be noted that the quadratic regression model is valid only within the experimental range applied in the present study.

Figs. 3.2A, B, C show the contour plots indicating effect of interactive effect of any two variables on the DHA yield from glycerol fermentation. The contour plots (which essentially are graphical representation of regression equation) represent infinitive number of combinations of two test variables with the third variable maintained at its zero (or center point) level. The shape or nature of the response surface contours, whether elliptical, circular, or saddle point depicts the magnitude interaction between the optimization variables (Ravikumar et al., 2005; Tanyildizi et al., 2005). If the independent variables have good interaction between them, perfectly elliptical contours are obtained. The surface confined in the smallest ellipse in the contour diagram corresponds to parameter space for which the maximum response of the target variable – or maximum DHA yield in present context – is seen. The contour plots in Figs. 3.2A (KH_2PO_4 vs $MgSO_4$) and 3.2B (KH_2PO_4

vs. $(NH_4)_2SO_4$) have distorted elliptical shape which points to relatively insignificant interaction between the parameters. This is also corroborated by the negative *t*–value of the interaction coefficients between these variables, as noted earlier. Contour plot in Fig. 3.2C ($(NH_4)_2SO_4$ vs. $MgSO_4$) has elliptical nature indicating significant interaction between the parameters. This is also confirmed by the *p*– and *t*–values of their interaction coefficient. The contour plots help us identify range of parameters for which the highest yield of DHA synthesis through glycerol fermentation is obtained. The parameter space corresponding to maximum DHA yield for any two variables (with value of the third variable held at its center point) is given in Table 3.5C. The values of all three optimization variables corresponding to maximum DHA yield (global optimum) are also listed in Table 3.5C. A maximum DHA yield of 13 g/L was obtained for all three combinations of two optimization variables. Maximum DHA yield corresponding to optimization of all three medium components is 14.08 g/L. The values of medium components concentrations corresponding to maximum DHA yield are: a. $MgSO_4 \cdot 7H_2O$ = 0.545 g/L; b. KH_2PO_4 = 0.641 g/L; c. $(NH_4)_2SO_4$ = 3.02 g/L.

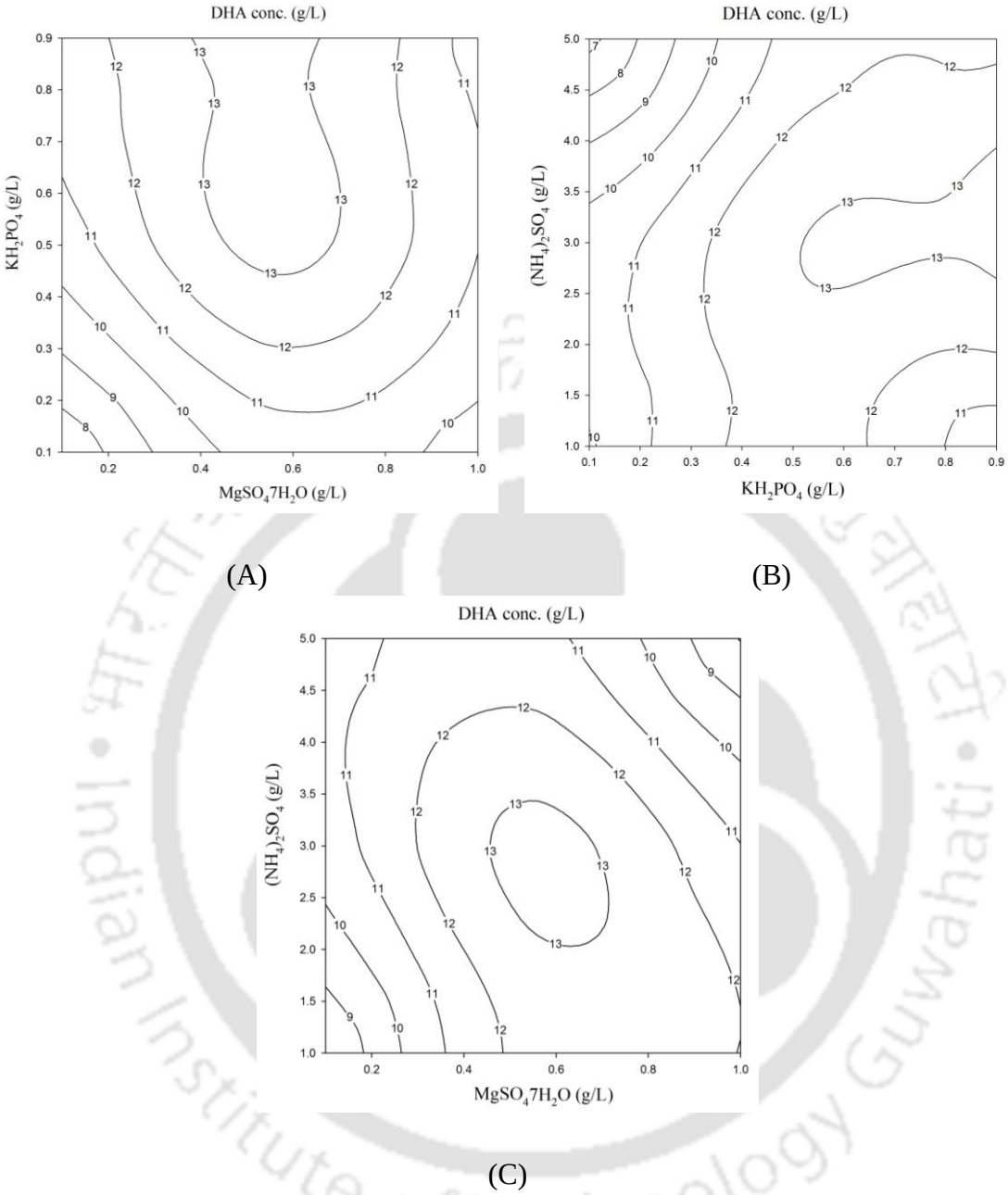

Figure 3.2. Contour plots depicting interactions among different optimization parameters for DHA production (A) $MgSO_4 \cdot 7H_2O$ and KH_2PO_4 (B) KH_2PO_4 and $(NH_4)_2SO_4$ (C) $MgSO_4 \cdot 7H_2O$ and $(NH_4)_2SO_4$

3.3.3 Validation of experiments of glycerol fermentation with optimized medium

The desirability function plot showing optimum concentration of medium components is shown in Fig. 3.3A. As noted earlier, the validation of the statistical analysis of medium composition for glycerol fermentation was done by conducting fermentation experiments with optimum medium compositions predicted by the CCD analysis. Fig. 3.3B depicts the profile of production of DHA in these experiments using pure and crude glycerol as substrate with immobilized cells of *G. oxydans*. The final DHA concentration achieved with crude glycerol was 14.01 g/L, which is in close agreement with the prediction of CCD analysis (14.08 g/L). On the other hand, final DHA concentration in experiments with pure glycerol was 15.728 g/L, which was only 12.33% higher than crude glycerol. These results essentially indicate that optimization of the fermentation medium helps in reducing the adverse effect of the impurities in glycerol on fermentation process.

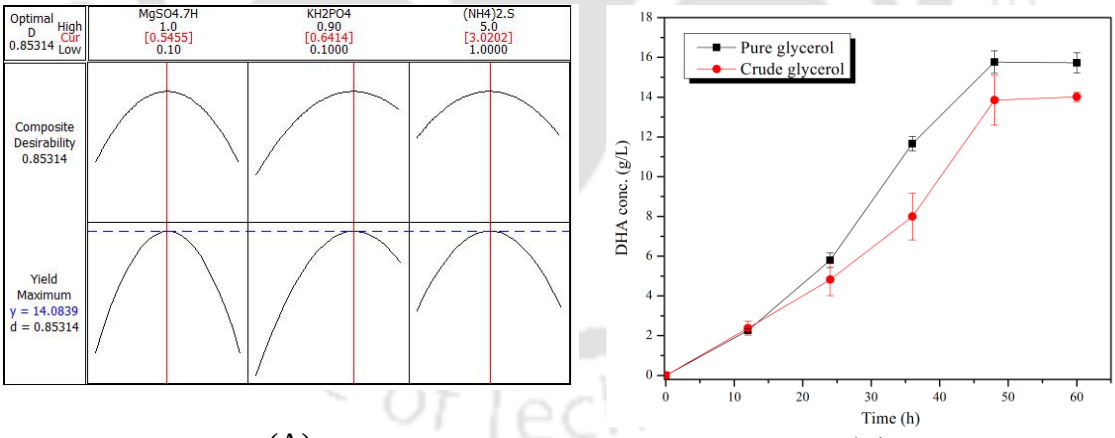

(A) (B)

Figure 3.3. Validation of experiments (A) Desirability function plot showing the optimum levels of medium components (B) Profile for production of DHA using pure and crude glycerol as substrate (concentration 20 g/L) by immobilized *G. oxydans*.

3.3.4 Analysis of effect of medium components

The statistical optimization of fermentation medium components has revealed $MgSO_4 \cdot 7H_2O$, $(NH_4)_2SO_4$ and KH_2PO_4 as the significant components. In this section, an attempt is made to identify their influence on the glycerol fermentation process. As noted earlier, glycerol dehydrogenase is a key enzyme in the pathway of glycerol metabolism to dihydroxyacetone. This enzyme is a member of medium chain alcohol dehydrogenases, which essentially are metalloenzymes. Glycerol dehydrogenase is a zinc–dependent metalloenzyme. Substitution of metal ions of the metalloenzyme is an efficient technique for enhancing activity and stability of enzyme. Wang et al. (2013) recently published a study on improving the stability, activity and substrate promiscuity of glycerol dehydrogenase substituted by divalent metal ions like Mg^{2+} and Mn^{2+}. The study of Wang et al. (2013) has revealed that catalytic efficiency of glycerol dehydrogenase (in terms of substrate binding, catalytic sites and substrate promiscuity) shows marked improvement with addition of Mg^{2+}. Magnesium substitution also improved the thermo-stability with 6–fold extension of half–life at 60 & 70ºC.

$(NH_4)_2SO_4$ essentially acts as a source of assimilable nitrogen for cell growth, in addition to providing assimilable sulfur (Yalcin and Ozbas, 2008). It was revealed in the experiments of central composite design (CCD), that ammonium salt itself was not sufficient for fermentation, and a small quantity (2 g/L) of yeast extract was also required. Yeast extract provides growth factors such as amino acids, vitamins, nucleotides and fatty acids that have specific role in catalytic and structural reactions. Li et al. (2011) have demonstrated that three amino acids (glycine, serine and tyrosine) in yeast extract accelerate the production of alcohol–dependent enzymes.

The role of KH_2PO_4 in the medium is twofold, viz. potassium and phosphate are important growth enhancing nutrients. Moreover, KH_2PO_4 also acts as a buffering agent

and it helps in maintenance of pH of the fermentation broth at a desired value (Yalcin and Ozbas, 2008).

3.4 CONCLUSIONS

This study attempted to optimize production of DHA from crude glycerol using immobilized *G. oxydans*. DHA production was revealed to be influenced by medium components that augment activity and substrate promiscuity of glycerol dehydrogenase (inorganic salt of $MgSO_4 \cdot 7H_2O$), provide nitrogen and sulfur source for cell growth [$(NH_4)_2SO_4$], and help maintain pH of the medium (buffer KH_2PO_4). Yeast extract, which provides growth factors and amino acids accelerating production of alcohol degrading enzyme, was also revealed as essential component of the medium. With optimized medium, fermentation of crude glycerol resulted in DHA yield at par with yield for pure glycerol.

REFERENCES

Bauer, R., Hekmat, D., 2006. Development of a transient segregated mathematical model of the semicontinuous microbial production process of dihydroxyacetone. Biotechnol. Prog. 22, 278–284.

Bauer, R., Katsikis, N., Varga, S., Hekmat, D., 2005. Study of the inhibitory effect of the product dihydroxyacetone on *Gluconobacter oxydans* in a semi–continuous two–stage repeated–fed–batch process. Bioprocess Biosyst. Eng. 28, 37–43.

Flickinger, C., Perlman, D., 1977. Application of oxygen–enriched aeration in the conversion of glycerol to dihydroxyacetone by *Gluconobacter melanogenus* IFO 3293. Appl. Environ. Microb. 33, 706–712.

Hekmat, D., Bauer, R., Fricke, J., 2003. Optimization of the microbial synthesis of dihydroxyacetone from glycerol with *Gluconobacter oxydans*. Bioprocess Biosyst. Eng. 26, 109–116.

Hekmat, D., Bauer, R., Neff, V., 2007. Optimization of the microbial synthesis of dihydroxyacetone in a semi–continuous repeated–fed–batch process by in situ immobilization of *Gluconobacter oxydans*. Process Biochem. 42, 71–76.

Kourkoutas, Y., Manojlovic, V., Nedovic, V.A., 2010. Immobilization of microbial cells for alcoholic and malolactic fermentation of wine and cider. In: Encapsulation Technologies for Active Food Ingredients and Food Processing (Editors: N.J. Zuidam, V.A. Nedovic), Springer Science + Business Media LLC, New York. pp. 327–344.

Li, M., Liao, X., Zhang, D., Du, G., Chen, J., 2011. Yeast extract promotes cell growth and induces production of polyvinyl alcohol–degrading enzymes. Enzyme Res. 2011, 179819. doi:10.4061/2011/179819.

Liu, Z., Hu, Z., Zheng, Y., Shen, Y., 2008. Optimization of cultivation conditions for the production of 1,3–dihydroxyacetone by *Pichia membranifaciens* using response surface methodology. Biochem. Eng. J. 38, 285–291.

Lowry, O.H., Rosenbrough, N.J., Farr, A.L., Randall, R.J., 1951. Protein measurement with the Folin Phenol Reagent. J. Biol. Chem. 193, 265–275.

Plackett, R.L., Burman, J.P., 1946. The design of optimum multifactorial experiments. Biometrika. 33, 305–325.

Ravikumar, K., Pakshirajan, K., Swaminathan, T., Balu, K., 2005. Optimization of batch process parameters using response surface methodology for dye removal by a novel adsorbent. Chem. Eng. J. 105, 131–138.

Rocha–Martin, J., Acosta, A., Berenguer, J., Guisan, J.M., Lopez–Gallego, F., 2014. Selective oxidation of glycerol to 1,3–dihydroxyacetone by covalently immobilized glycerol dehydrogenases with higher stability and lower product inhibition. Bioresour. Technol. 170, 445–453.

Tanyildizi, M.S., Ozer, D., Elibol, M., 2005. Optimization of α–amylase production by *Bacillus sp*. using response surface methodology. Process Biochem. 40, 2291–2296.

Underkofler, L.A., Fulmer, E.l., 1937. The production of dihydroxyacetone by the action of *Acetobacter suboxydans* upon glycerol. J. Am. Chem. Soc. 59, 301–302.

Wang, S., Wang, J., Zhou, X., Guo, Y., Fang, B., 2013. The improvement of stability, activity, and substrate promiscuity of glycerol dehydrogenase substituted by divalent metal ions. Biotechnol. Bioprocess Engg. 18, 796–800.

Wethmar, M., Deckwer, W., 1999. Semisynthetic culture medium for growth and dihydroxyacetone production by *Gluconobacter oxydans*. Biotechnol. Tech. 13, 283–287.

Yalcin, S.K., Ozbas, Z.Y., 2008. Effects of ammonium sulfate concentration on growth and glycerol production kinetics of two endogenic wine yeast strains. Indian J. Biotechnol. 7, 89–93.

भारतीय प्रौद्योगिकी संस्थान गुवाहाटी
Indian Institute of Technology Guwahati

CHAPTER 4

PROCESS OPTIMIZATION AND ANALYSIS OF PRODUCT INHIBITION KINETICS

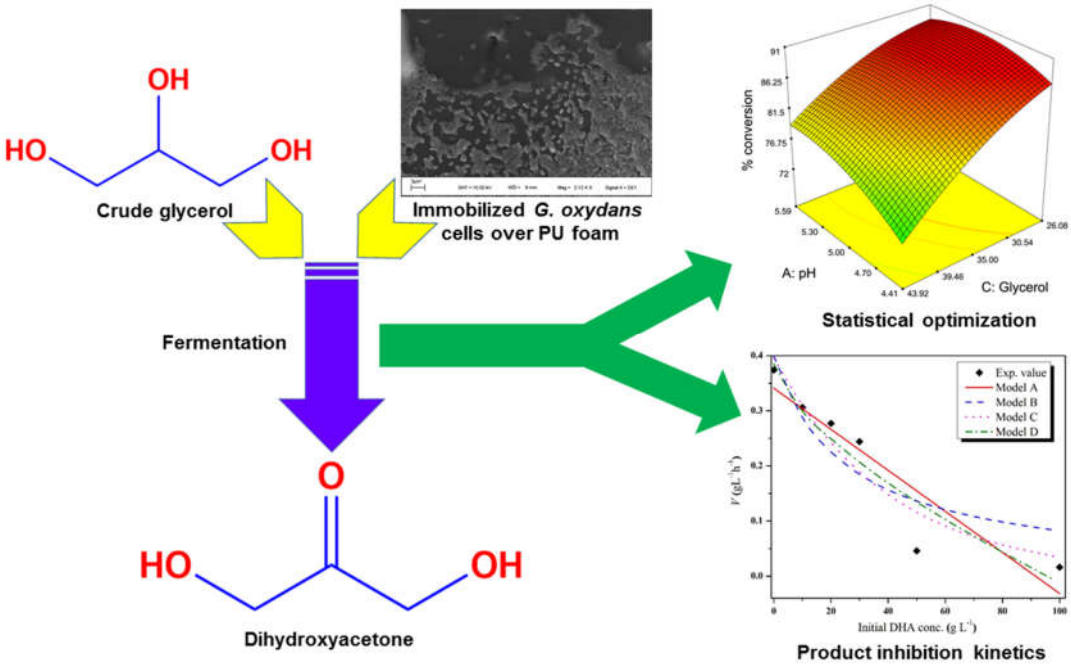

CHAPTER 4

PROCESS OPTIMIZATION AND ANALYSIS OF PRODUCT INHIBITION KINETICS

4.1 INTRODUCTION

In previous chapter, we optimized the fermentation medium for DHA production from crude glycerol using immobilized *G. oxydans*. Four media components, viz. yeast extract, KH_2PO_4, $MgSO_4 \cdot 7H_2O$ and $(NH_4)_2SO_4$, were determined as most significant for DHA production using immobilized cells. In Chapter 2, we reported the substrate inhibition kinetics of DHA production from crude glycerol. In present study, we have taken ahead this theme with optimization of the process parameters of glycerol fermentation, viz. pH, temperature and initial glycerol concentration. Moreover, we also studied the product inhibition kinetics of the glycerol bioconversion by *G. oxydans*. This facet of glycerol metabolism by *G. oxydans* has been addressed by very few previous authors. Claret et al. (1993) showed that limiting inhibitory concentrations of DHA for microbial growth and glycerol fermentation were 67 g/L and 85 g/L, respectively. Beyond these concentrations, no microbial growth or no glycerol metabolism was observed. Lesser inhibitory DHA concentration for the biomass growth indicated higher sensitivity of biomass synthesis to DHA concentration. Stasiak–Rozanska et al. (2014) have shown that mitotic activity of *G. oxydans* was inhibited by DHA even at relatively low concentration of 20–30 g/L, while the microbial cell mass production stopped at DHA concentration of 70 g/L. It should be

mentioned that results of both Claret et al. (1993) and Stasiak–Rozanska et al. (2014) are restricted for free cells and pure glycerol as substrate.

In the present study, *G. oxydans* cells were immobilized over polyurethane foam, which has highly porous structure and large surface area. The microbial cells can bind over the surface as well as inside the pores of the immobilization matrix resulting in high density (Bhasarkar et al., 2015; Padhi and Gokhale, 2016). The process optimization of crude glycerol fermentation has been done using statistical central composite design (CCD) of experiments. Moreover, we have fitted the experimental data on product inhibition to several biokinetic models previously reported in literature. We have also proposed a new product inhibition model based on modified Haldane kinetic model. The values of the model parameters obtained after data fitting essentially give insight into the inhibitory effect of dihydroxyacetone (DHA) on glycerol bioconversion.

4.2 MATERIALS AND METHODS

4.2.1 Materials

The micro–organism, *Gluconobacter oxydans* MTCC 904 was procured from Microbial Type Culture Collection (MTCC), Chandigarh, India. Dihydroxyacetone (DHA) and pure glycerol were procured from Merck, Germany. Reticulated polyurethane foam was procured from local market. Crude glycerol was produced in our laboratory through transesterification reaction. The details of transesterification reaction are as follows: alcohol molar ratio = 12:1, refined soybean oil = 20 mL, methanol = 10 mL, NaOH catalyst = 0.18 g (1% w/v). The catalyst was added to methanol at 65°C and stirred for 15–20 min prior to addition. This mixture was mixed at 250 rpm with soybean oil 65°C for 1 h in a round bottom flask equipped with reflux condenser. After completion of reaction, mixture of glycerol and biodiesel was kept standing in a separating funnel for 18–20 h. The reaction

mixture separated into two layers in separating funnel, viz. the upper biodiesel layer, and lower glycerol layer. Approximately, 30 mL of crude glycerol was produced from a reaction mixture of total volume of 100 mL. The alkali and alcohol impurities in crude glycerol were determined as: 0.85% w/v of sodium hydroxide (calculated by acid base titration) and 0.26% w/v methanol. All other medium components and chemicals used in this study were procured from HiMedia Pvt. Ltd., India.

4.2.2 Growth and maintenance of *G. oxydans* culture

The lyophilized microbial cells were revived in MRS medium and kept in a rotary incubator shaker (Make: Lab Companion; Model: SI–300R) at 30ºC, 150 rpm for 24 h. The revived cells were grown on agar slant and kept at 4ºC. The cultures were sub–cultured every month. The composition of MRS medium (in 1 L of distilled water) is as follows: Peptone = 10.0 g, beef extract = 10.0 g, yeast extract = 5.0 g, glucose = 10.0 g, tween–80 = 1 mL, Na_2HPO_4 = 2.0 g, sodium acetate = 5.0 g, triammonium citrate = 2.0 g, $MgSO_4 \cdot 7H_2O$ = 0.2 g, $MnSO_4 \cdot 4H_2O$ = 0.2 g. The pH of medium was adjusted to 6.0 ± 0.2 with the help of 1 N HCl. The agar plates and slants were prepared by adding 15 g/L of agar in MRS medium.

4.2.3 Seed culture and fermentation medium compositions

The composition of seed culture medium is as follows: yeast extract = 5.0 g/L, peptone – 3 g/L, $K_2HPO_4 \cdot 3H_2O$ – 3 g/L, $(NH_4)_2SO_4$ – 2 g/L, $MgSO_4 \cdot 7H_2O$ – 0.51 g/L, mannitol – 10 g/L. The initial pH of the medium was adjusted to 6.0 ± 0.2. The fermentation was carried out with previously optimized medium with composition: yeast extract – 2 g/L, $MgSO_4 \cdot 7H_2O$ – 0.55 g/L, KH_2PO_4 – 0.62 g/L, $(NH_4)_2SO_4$ – 3 g/L. The medium was autoclaved prior to inoculation at 121ºC, 15 psi for 20 min. Three number of PU foam cubes

(optimized in preliminary study) with immobilized and cross–linked *G. oxydans* cells were added to the fermentation medium. The immobilization of cell over PU foam was achieved using previously reported procedure.

4.2.4 Experimental design for process parameter optimization

4.2.4.1 Central composite design

Central composite design is a commonly employed statistical experimental design for studying both individual and interaction effects of optimization variables on the response variable. The lower and upper limiting values of the optimization variables, viz. pH, temperature and initial glycerol concentration, are listed in Table 4.1A. Five coded levels or values of these variables, noted as $-\alpha$, –1, 0, +1, $+\alpha$ and listed in Table 4.1B, were used for devising the experimental sets. The CCD experimental design constituted 20 individual runs ($=2^k+2k+n_0$), where 'k' is the number of independent variables, and n_o is the number of replicate runs at the center point of the variable. The complete CCD experimental design (with permutation/combinations of optimization variables) was generated using Minitab statistical software (Release 15.1, Trial Version).

Percentage conversion of crude glycerol to DHA was considered as the response variable and was calculated using the following formula:

$$\text{Percentage conversion of glycerol (\%)} = \frac{\text{Final DHA conc. (g/L)}}{\text{Initial glycerol conc. (g/L)}} \times 100 \qquad (4.1)$$

Table 4.1. Details of experiments for optimization of DHA production

(A) Factors and levels used in Central Composite Design matrix for DHA fermentation

Factors	Coded value	Levels	
		Low (–α)	High (+α)
pH	P	4	6
Temperature (°C)	T	25	35
Crude glycerol conc. (g/L)	G	20	50

(B) Central Composite Design matrix of optimization variables with coded and actual values (in parenthesis) along with response variable (glycerol conversion)

Run order	pH	Temperature	Glycerol conc.	Glycerol conversion (%)	
				Experimental	Predicted
1	0 (5)	0 (30)	0 (35)	87.683 ±0.31	85.796
2	+1 (5.59)	+1 (33)	–1 (26.08)	79.603 ±0.96	77.663
3	0 (5)	0 (30)	0 (35)	83.783 ±0.12	85.796
4	0 (5)	0 (30)	–α (20)	88.055 ±0.66	90.709
5	+1 (5.59)	–1 (27)	+1 (43.92)	83.347 ±0.92	85.451
6	–1 (4.41)	–1 (27)	–1 (26.08)	76.959 ±0.27	76.082
7	–1 (4.41)	+1 (33)	+1 (43.92)	61.622 ±0.93	60.800
8	–α (4)	0 (30)	0 (35)	75.637 ±0.79	76.961
9	0 (5)	+α (35)	0 (35)	55.889 ±0.40	58.477
10	0 (5)	–α (25)	0 (35)	75.795 ±0.58	73.639
11	+α (6)	0 (30)	0 (35)	84.443 ±0.89	83.552
12	+1 (5.59)	–1 (27)	–1 (26.08)	85.318 ±0.81	85.834
13	–1 (4.41)	+1 (33)	–1 (26.08)	87.025 ±0.92	84.615
14	–1 (4.41)	–1 (27)	+1 (43.92)	69.027 ±0.72	70.661
15	0 (5)	0 (30)	0 (35)	86.591 ±0.94	85.796
16	0 (5)	0 (30)	0 (35)	86.885 ±0.38	85.796
17	0 (5)	0 (30)	0 (35)	84.561 ±0.45	85.796
18	0 (5)	0 (30)	+α (50)	72.582 ±0.72	70.361
19	+1 (5.59)	+1 (33)	+1 (43.92)	58.314 ±0.66	58.885
20	0 (5)	0 (30)	0 (35)	85.348 ±0.27	85.796

4.2.4.2 Statistical analysis and model fitting

The experimental data given in Table 4.1B was fitted to the following quadratic model containing coefficients corresponding to individual and interactive effects of parameters:

$$Y = \beta_0 + \sum_{i=1}^{k} \beta_i X_i + \sum_{i=1}^{k} \beta_{ii} X_i^2 + \sum_{i \neq j} \sum_{i} \beta_{ij} X_i X_j \qquad (4.2)$$

Notation: Y – measured response variable (percentage conversion), k – number of factors or process variable, β_0 – regression constant, β_i – linear coefficient, β_{ii} – quadratic coefficient and β_{ij} – interaction coefficient. The coded values (x) of the actual experimental variables were found from Eq. (4.3):

$$X = (x_i - x_0)/\Delta x \qquad (4.3)$$

where, $i = 1, 2, 3\ldots$, X are the dimensionless values of the variables; x_i is the dimensionless value of the variables; x_o is the value of x_i at center point; and Δx is the step change. The analysis of variance (ANOVA) was also done to determine the significance of each factor in fitted model and also to determine the goodness of fit. ANOVA of the linear, quadratic and interaction regression coefficients (i.e., F–value and p–value) are given in Table 4.2B. The F– and p–values essentially exhibit the significance of individual and interactive effects of the optimization (independent) variables on the response variable.

4.2.5 Validation of experiment

The result of the statistical experimental design, i.e. optimum combination of the process parameters for which the glycerol conversion or DHA yield is maximum, was validated with an independent experiment conducted at the conditions predicted by the CCD design. The validation experiments were carried out in triplicate in order to check the reproducibility of the results.

4.2.6 Kinetic studies of DHA inhibition

The effect of DHA concentration on cell growth and glycerol fermentation was assessed by varying the initial DHA concentration in the fermentation broth in range: 10 to 100 g/L at fixed initial glycerol concentration of 20 g/L. For these experiments, DHA was added externally to the broth prior to fermentation. The control experiment was crude glycerol fermentation with no initial DHA concentration in the broth. All experiments were conducted using pre–optimized fermentation medium (as mentioned in Chapter 3). The experimental parameters of pH and temperature were fixed at their optimum values yielded by the statistical experimental design in this study. 5% v/v inoculum was added to the fermentation mixture for experiments employing free cells, while 3 PU foam cubes with immobilized cells, were added to fermentation mixture for experiments employing immobilized cells. Fermentation was carried out for 96 h with samples of fermentation broth withdrawn and analyzed every 8 h for quantification of glycerol and DHA concentration. The time profiles of DHA production and glycerol conversion were fitted to various biokinetic models accounting for product inhibition reported in literature (Claret et al., 1993; Luong, 1985; Mulchandani and Luong, 1989) listed below:

Ghose et al. model: $$V = V_{\max} \cdot \frac{[S_0]}{K_S + [S_0]} \cdot (1 - P_0 / P_m) \quad (4.4)$$

Egamberdiev model: $$V = V_{\max} \cdot \frac{[S_0]}{K_S + [S_0]} \cdot \frac{K_{ip}}{P_0 + K_{ip}} \quad (4.5)$$

Aiba model: $$V = V_{\max} \cdot \frac{[S_0]}{K_S + [S_0]} \cdot \exp(-P_0 / K_{ip}) \quad (4.6)$$

Luong model: $$V = V_{\max} \cdot \frac{[S_0]}{K_S + [S_0]} \cdot \left(1 - (P_0 / P_m)^{\alpha}\right) \quad (4.7)$$

Various notations are: V – rate of reaction (DHA production); V_{max} – maximum rate of reaction; $[S_0]$ – initial substrate (glycerol) concentration; P_0 – initial product (DHA)

concentration in the medium; K_S – substrate concentration at which $V = V_{max}/2$; K_{ip} – product inhibition constant; P_m – threshold concentration beyond which no biological activities occurred; α – empirical constant. The experimental data was fitted to these models using the Curve Fitting module of MATLAB® 7.10.0 to obtain the numerical values of the model parameters.

In addition to the above conventional biokinetic models, we have proposed a new modified Haldane kinetic model of product inhibition given as:

$$\frac{dP}{dt} = \frac{V_{max}}{1 + \frac{K_S}{[S_0]} + \left(\frac{[S_0]}{K_I}\right)^n} \cdot \left[1 - \left(\frac{[P_0 + P]}{P_m}\right)^{\alpha}\right] \tag{4.8}$$

The new model simultaneously accounts for the substrate and product inhibition. Secondly, unlike the previous models that are based on the initial concentration of product in fermentation mixture, the new model also accounts for the product formed during fermentation due to which the product concentration in the broth changes continuously. The time profiles of product formation in the fermentation broth were fitted to this model using Runge–Kutta 4th order solver coupled with Genetic Algorithm (GA) optimization module in MATLAB® 7.10.0. The experimental and simulated profiles of DHA production were matched to determine the optimum values of the six model parameters, viz. V_{max}, K_S, K_I, n, P_m, and α. Optimization of the model parameters (within pre–defined upper and lower bounds) was done by minimizing the root mean square error between experimental and simulation results using the GA module. Variations in the values of the model parameters for different initial product concentrations provide physical insight into the inhibition kinetics.

4.2.7 Analytical methods

The concentrations of glycerol and DHA in the samples withdrawn from fermentation mixture were quantified using HPLC. A Rezex RCM monosaccharide calcium–column (300 mm × 8 µm × 7.8 mm, Phenomenex, India) thermostated at 35°C with help of external column oven (Make: PCI analytics Pvt. Ltd., India, Model: HCO–02) (Hekmat et al., 2007) was used for measurements. The HPLC system (series 200, Perkin Elmer) comprised of a pump, a refractive index detector and a vacuum degasser. Ultra–pure water (18.2 MΩ·cm resistivity at 25°C) was used as the mobile phase at a flow rate of 0.5 mL/min. Reaction mixture samples were centrifuged (12,000 rpm, 20 min) followed by filtration through a 0.2 µm membrane filter, and appropriate dilution prior to injection into HPLC. Standard calibration plots were prepared to determine concentrations of both glycerol and DHA.

For the experiments using free cells of *G. oxydans*, the concentration of cell mass (or growth profile of the microbial cells) was monitored by measuring absorbance at 660 nm with a UV–visible spectrophotometer.

4.3 RESULTS AND DISCUSSION

4.3.1 Optimization of process variables with central composite design (CCD)

The full factorial matrix of the CCD of experiments (comprising 20 runs) is given in Table 4.1B along with actual and predicted values of response variable (glycerol conversion, %). The results given in Table 4.1B indicate that the glycerol conversion (%) ranged from 55.89% (run number 9) to 88.06% (run number 4). The coded values optimization variables and corresponding response variables for the 20 runs were fitted to a quadratic model. The linear, square and interaction coefficients of the quadratic response model (given in Eq. (4.9)) along with *p*– and *t*– values of the coefficients are given in Table

4.2A. The second–order regression equation for the fitted data is as follows:

$$Y_{yield} = 85.796 + 1.959P - 4.508T - 6.05G - 1.959P^2 - 6.978T^2 - 1.86G^2 - 4.176P \times T + 1.259P \times G - 4.599T \times G \quad (4.9)$$

Analysis of variance (ANOVA) of the quadratic model is given in Table 4.2B. The regression coefficient (R^2) value of 0.97 indicates that the quadratic model fits well to the experimental data. ANOVA results show that regression model was highly significant ($p < 0.01$), while the lack of fit was not significant ($p > 0.05$) which is essentially corroboration of best fit of the quadratic model to experimental data. The values of regression coefficients, viz. $R^2 = 0.97$, predicted $R^2 = 0.82$, adjusted $R^2 = 0.95$, indicate that 97.1% variations in the response variable could be explained using the model.

The *t*–test, *F*–value and *p*–value of quadratic model coefficients represents their relative significance. A large *t*–stat value and *p*–value < 0.05 indicates greater significance of the coefficient and response variable. Relative *F*–values of linear and interaction coefficients indicate the relative significance of the individual effect of the parameter and interactive effects between the parameters in describing the response variable. The ANOVA results given in Table 4.2B show that *F*–value of linear coefficients is 49.63 and interactive coefficient is 19.22. This indicates that the influence of the optimization variables on the response variable is more of independent type with minor interactions.

4.3.2 Interaction effects of process variables

Fig. 4.1 shows the surface plots and corresponding contour plots indicating the interaction effect of any two process parameters on glycerol fermentation while the third variable is maintained at its zero or center point level. The surface confined in the innermost contour represents the parameter space corresponding to maximum value of the response variable.

Table 4.2. Summary of statistical optimization of DHA fermentation

(A) Values of coefficients for second order regression model

Optimization variable	Coefficient estimate	Computed *t*–value	*p*–value Prob > *F*
Intercept	85.796	89.111	0.000
pH	1.959	3.067	0.012
Temperature	–4.508	–7.057	0.000
Glycerol conc.	–6.050	–9.470	0.000
pH × pH	–1.959	–3.150	0.010
Temperature × Temperature	–6.978	–11.222	0.000
Glycerol conc. × Glycerol conc.	–1.860	–2.991	0.014
pH × Temperature	–4.176	–5.004	0.001
pH × Glycerol conc.	1.259	1.509	0.162
Temperature ×Glycerol conc.	–4.599	–5.510	0.000

* Significant *p* values, $p \leq 0.05$; $R^2 = 0.97$; Predicted $R^2 = 0.82$; Adjusted $R^2 = 0.96$

(B) ANOVA for quadratic model

Source	DF	SS	MS	*F*–value	*p*–value Prob > *F*
Regression	9	1892.53	210.281	37.73	0.000
Linear	3	829.76	276.586	49.63	0.000
Square	3	741.39	247.128	44.35	0.000
Interaction	3	321.39	107.129	19.22	0.000
Residual (Error)	10	55.73	5.573		
Lack of fit	5	44.57	8.914	4.00	0.077
Pure error	5	11.16	2.231		
Total	19	1948.26			

DF– degree of freedom; SS– sum of squares; MS– mean square

(C) Statistical analysis of experimental results. Analysis of contour plots*

Fixed parameter (center point value)	Variable parameters		Glycerol conversion (%)
pH = 5	Temp = 30°C	Glycerol conc. = 26.1 g/L	89.99
Temperature = 30°C	pH = 5.1	Glycerol conc. = 26.1 g/L	90.05
Glycerol conc. = 35 g/L	pH = 5.6	Temp = 28.1°C	88.49
Global optimum values for variable parameters: a. pH = 4.7; b. Temp = 31°C; Glycerol conc. = 20 g/L Maximum percentage conversion = 91.32% (predicted), 89.16% (experimental, DHA =17.83 g/L.)			

* The contour plots are given in the supplementary material provided with the paper.

The ranges of the parameters corresponding to center point values of optimization variables, viz. pH = 5, temperature = 30°C, glycerol concentration = 35 g/L, are given in Table 4.2C. The glycerol conversion in each case is ~ 89 – 90%. The global optimum values of the process parameters are: pH = 4.7, temperature = 31°C and initial crude glycerol concentration = 20 g/L. The desirability function plot showing optimum values of variables is shown in Fig. 4.2.

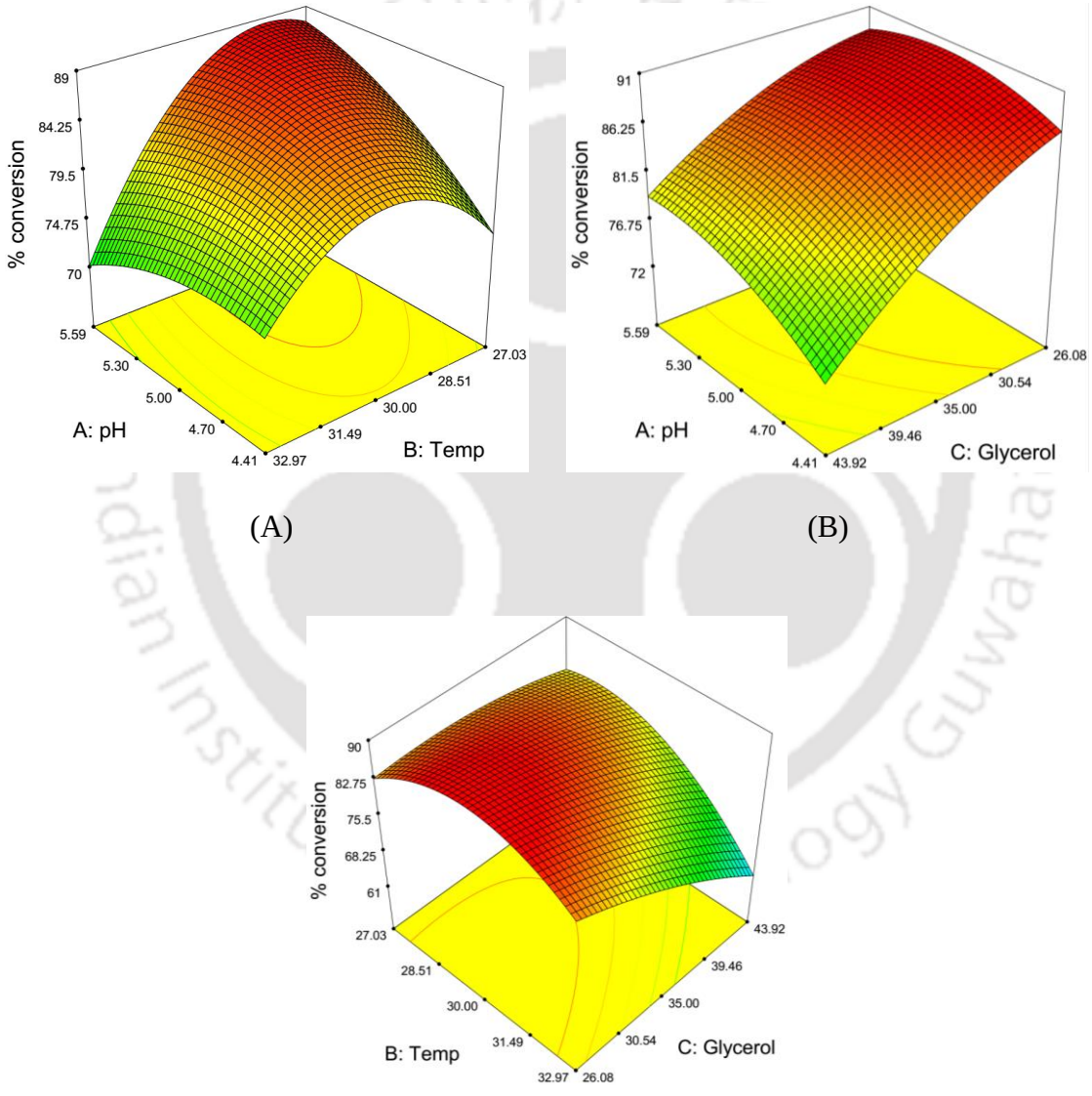

Figure 4.1. Surface plot and corresponding contour plot for effect of different parameters on the percentage conversion of glycerol to DHA (A) temperature and pH (A) glycerol conc.(g/L) and pH (C) glycerol conc.(g/L) and temperature

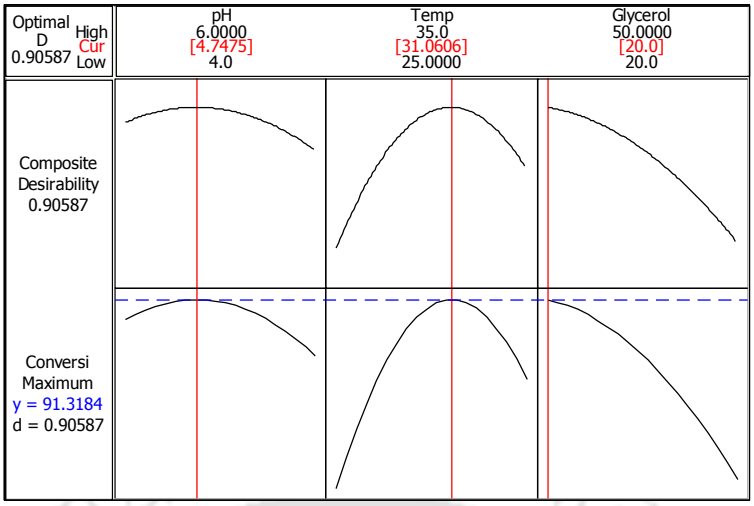

Figure 4.2. Desirability function plot showing the optimum levels of process parameters.

4.3.3 Validation of the CCD optimization of glycerol bioconversion

Validation of the results predicted by statistical optimization of glycerol fermentation was done by conducting experiments at the global optimum conditions of pH, temperature and initial crude glycerol concentration. Simultaneously, fermentation experiments with pure glycerol (in triplicate to assess the reproducibility) were also conducted to assess the adverse effect of impurities in the crude glycerol on fermentation yield. The time profiles of glycerol consumption and DHA formation are shown in Fig. 4.3. For crude glycerol as substrate, experimental glycerol conversion corresponding to these values is 89.16% which matches closely with the predicted glycerol conversion of 91.32%. On the basis of concentration, 17.83 g/L of DHA was produced from fermentation of crude glycerol (with initial concentration of 20 g/L), whereas for pure glycerol fermentation the final DHA concentration reached in the broth was 18.79 g/L. It is noteworthy that after optimization of both fermentation medium (Chapter 3) and fermentation parameters (present study), the difference in DHA yields from fermentation of crude and pure glycerol is ~5%.

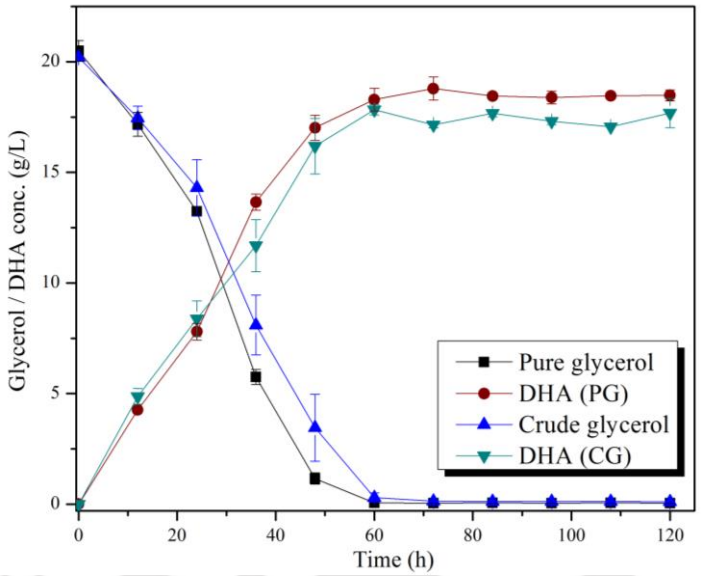

Figure 4.3. Profile of DHA production using pure and crude glycerol as substrate (concentration 20 g/L) by immobilized *G. oxydans* cells. PG – Pure glycerol, CG – Crude glycerol

Optimum values of the process variables obtained in this study have physical relevance to glycerol fermentation process. pH is one of the vital parameters that influence kinetics and yield of microbial fermentation. It has been reported that low pH is more beneficial for glycerol fermentation with *G. oxydans*, as these microbes belong to the class of acetic acid bacteria (Hekmat et al., 2003; Svitel and Sturdik, 1994; Wethmar and Deckwer, 1999). Hu et al. (2011) reported higher DHA production in the pH range of 4.5 to 5.0 (with optimum pH being 5.0) by resting cells of *G. oxydans*. In another study, Hu et al. (2010) carried out experiments with *G. oxydans* ZJB09112 strain in which maximum DHA production occurred at pH 5.0. The optimum pH obtained in present study is 4.74, which concurs with previous literature, which reports that low pH favors DHA production. The optimum initial crude glycerol concentration determined in this study is 20 g/L, which is in concurrence with our previous work on kinetics of glycerol fermentation, in which the substrate inhibition showed marked rise after initial glycerol concentration of 20 g/L.

In a previous Chapter 3, we reported optimization of the fermentation medium for crude glycerol fermentation by immobilized cells of *G. oxydans*. The maximum DHA yield obtained after optimization was 14.08 g/L for initial crude glycerol concentration of 20 g/L. After optimization of process parameters in present study, the DHA yield increased to 17.83 g/L. With approach of one–variable–at–a–time (OVAT), Wei et al. (2007) reported 30°C to be most suitable temperature for immobilized cells *G. oxydans* in terms of their stability and activity. Moreover, immobilized cells were found to be more resistant towards higher temperature. Several other previous authors also reported 30°C as the optimum temperature for glycerol fermentation for DHA production (Hekmat et al., 2007; Hu et al., 2017; Wei et al., 2007). The optimum temperature obtained in present study (using approach of statistical design of experiments) concurs with the results of previous authors.

4.3.4 Experimental profiles with initial DHA concentration

The time profiles of glycerol consumption with varying initial concentration of DHA (0–50 g/L) are shown in Fig. 4.4A and 4.4B, for free and immobilized *G. oxydans* cells, respectively. The time profiles of microbial cell growth with varying initial concentration of DHA are shown in Fig. 4.4C. Comparing Fig. 4.4A and 4.4B, greater inhibition effect of DHA for immobilized cells is clearly evident, as the rate of glycerol consumption reduces faster in case of immobilized cells. Nonetheless, for 96 h of fermentation, the consumption of glycerol is almost complete till initial glycerol concentration of 30 g/L. At the highest initial glycerol concentration of 50 g/L, the glycerol consumption rate reduces sharply for immobilized cells, and more than half of initial glycerol remains unconsumed. For the free cells, however, the inhibition effect of DHA is marginal for initial glycerol concentration of 50 g/L. This result essentially shows greater susceptibility of immobilized cells towards product inhibition. The time profile of cells

mass concentration for varying initial DHA concentration also reveal marked reduction in growth rate and final concentration at the end of 96 h fermentation. This reduction is proportional to the initial DHA concentration.

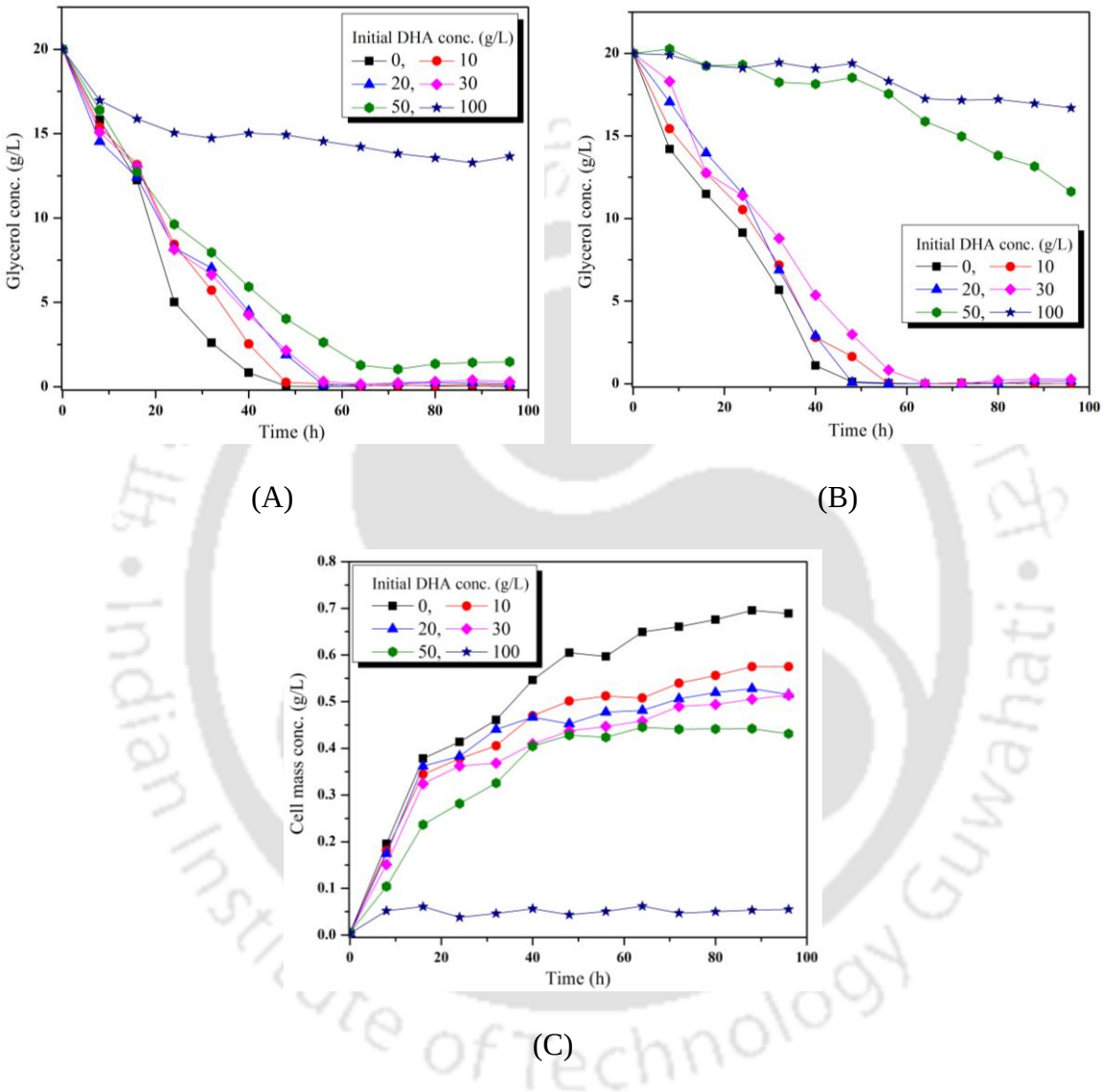

Figure 4.4. Experimental results of DHA fermentation with varying initial DHA concentration. Time profiles for glycerol consumption: (A) Free cells, (B) Immobilized cells; (C) Time profile of cell mass production (for free cells).

4.3.5 Data fitting to biokinetic models

The results of fitting of experimental profiles of DHA production and glycerol consumption to conventional biokinetic models (viz. Ghose et al. model, Egamberdiev model, Aiba model and Luong model) are shown in Fig. 4.5. The results of fitting of experimental profiles of DHA and glycerol to the modified Haldane kinetic model for product inhibition are depicted in Fig. 4.6. Tables 4.3A and 4.3B summarize the values of kinetic parameters obtained after fitting of experimental profiles. Among the conventional models, the model of Ghose et al. and Luong fits well to the time profiles of glycerol and DHA in case of free cells, while for the immobilized cells, the experimental profiles are best described by the Aiba model, as indicated by the values of regression coefficient. Certain trends in the kinetic parameters of these models are evident from Table 4.3A as follows:

1. The range of P_m for free cells (102–105 g/L) is higher than immobilized cells (91–95 g/L). Relatively lesser value of P_m indicates greater susceptibility of the cells to product inhibition in immobilized form. The probable cause underlying this effect is that the cells trapped inside the support have access to the medium present only in the immobilization matrix, and not complete fermentation mixture. Moreover, the concentration of product in medium present in the immobilization matrix is likely to be higher due to restricted transport of fermentation mixture across the porous matrix.

2. K_{ip} theoretically represents the product concentration for which the specific rates are 2 or 2.7 times lower (for Egamberdiev model and Aiba model, respectively) than the maximum specific rates obtained without product inhibition. The range of K_{ip} for the free cells is 36.8–56.5 g/L, while that for immobilized cells is 25.9–40.7 g/L. Smaller range of K_{ip} values for immobilized cells also represents greater susceptibility of the cells towards product inhibition. Again, this result is too a probable consequence of higher local

concentration of the product in the immobilization matrix due to restricted transport across the matrix.

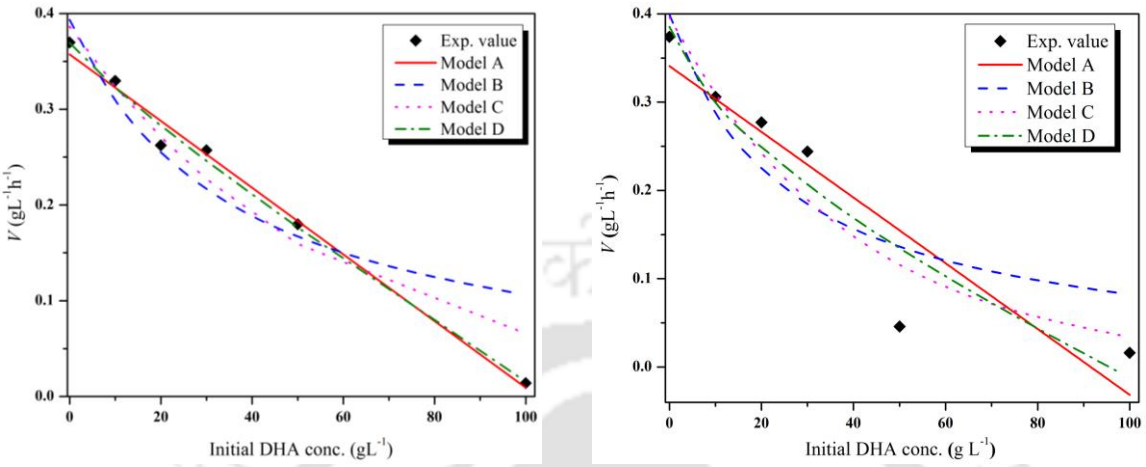

(A) (B)

Figure 4.5. Results of fitting of various product-inhibition models to data of reaction velocity versus initial DHA concentrations. (A) Free cells; (B) Immobilized cells. Model term: A – Ghose et al. model, B – Egamberdiev model, C – Aiba model, D – Luong model

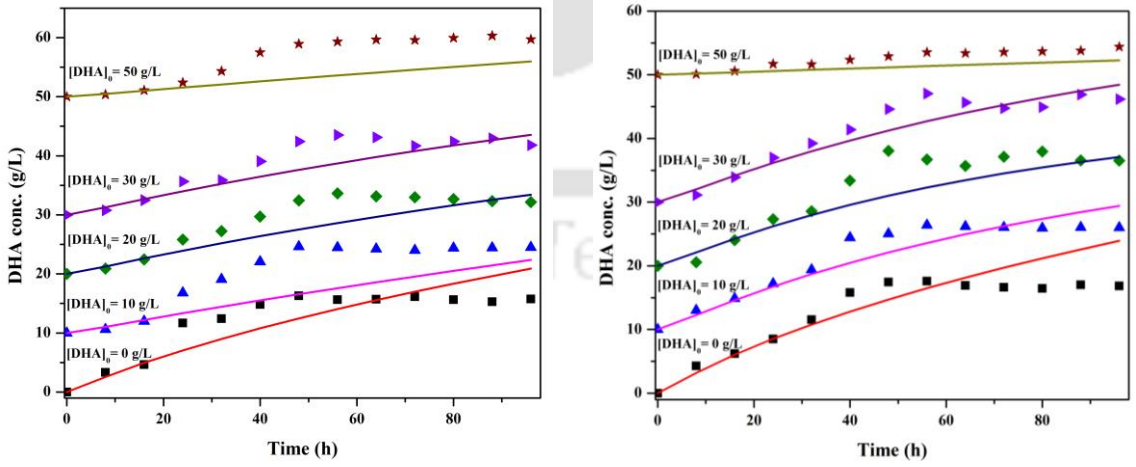

(A) (B)

Figure 4.6. Results of fitting of DHA production profiles (for different initial DHA concentrations) to modified Haldane product-inhibition model. (A) Free cells; (B) Immobilized cells.

Table 4.3. Kinetic analysis of product (DHA) inhibition of DHA fermentation

(A) Fitting of experimental data to kinetic models reported in literature

Models	Kinetic constants					Correlation coefficient (R^2)
	V_{max} ($g \cdot L^{-1} \cdot h^{-1}$)	K_S ($g \cdot L^{-1}$)	P_m ($g \cdot L^{-1}$)	K_{ip} ($g \cdot L^{-1}$)	α (-)	
Free cells						
Ghose et al.	0.93	31.85	102.60	–	–	0.99
Egamberdiev	0.95	28.55	–	36.88	–	0.86
Aiba	0.95	29.28	–	56.49	–	0.95
Luong	0.91	28.96	105.00	–	0.88	0.99
Immobilized cells						
Ghose et al.	0.83	28.92	91.54	–	–	0.85
Egamberdiev	0.96	27.97	–	25.89	–	0.82
Aiba	0.97	28.97	–	40.67	–	0.91
Luong	0.93	28.20	95.42	–	0.67	0.89

(B) Fitting of experimental data to modified Haldane model for product inhibition (proposed in this study)

[DHA] ($g \cdot L^{-1}$)	V_{max} ($g \cdot L^{-1} \cdot h^{-1}$)	K_S ($g \cdot L^{-1}$)	K_I ($g \cdot L^{-1}$)	n (-)	P_m ($g \cdot L^{-1}$)	A (-)
Free cells						
0	1.53	28.43	64.61	0.74	70.65	0.27
10	0.97	26.66	89.97	0.19	60.31	0.21
20	0.96	20.04	85.09	0.69	50.15	0.28
30	0.91	20.08	81.59	0.81	84.48	0.38
50	0.48	21.26	42.86	0.85	88.75	0.11
Immobilized cells						
0	1.88	26.39	99.24	0.97	64.93	0.25
10	1.14	23.48	93.71	0.59	71.11	0.35
20	1.12	21.18	82.65	0.96	51.99	0.27
30	1.15	24.69	99.38	0.91	62.96	0.26
50	0.30	42.35	99.54	0.85	69.62	0.12

Table 4.4. Summary of fermentation experiments with varying initial DHA concentration

Initial DHA conc. (g/L)	0	10	20	30	50
Net DHA production (free cells, g/L)	15.75	14.62	13.64	13.51	10.32
Net DHA production (immobilized cells, g/L)	17.59	16.41	18.06	17.05	4.34

3. The model that didn't account for product inhibition predicted large discrepancy in the K_S values for free and immobilized cells as reported in our previous Chapter (Chapter 2). The immobilized cells had higher substrate affinity, as indicated by lesser K_S value (12.62 g/L). The conventional models accounting for product inhibition, however, predict almost similar K_S values for both free and immobilized cells, as revealed by data presented in Table 4.3A.

4. The values of V_{max} predicted by the conventional models were almost similar for both free and immobilized cells.

Before analyzing the results of data fitting using modified Haldane model, we would like to ponder over the kinetic expression for product inhibition used in this model. In the Luong (1985) model, velocity of the reaction (V) was related to maximum velocity (V_{max}) through relation: $\left(1-\left(P_o/P_m\right)^{\alpha}\right)$. This essentially means that value of reaction velocity $V \rightarrow 0$, as product concentration in fermentation mixture $P \rightarrow P_m$. The magnitude of constant α will indicate the type of relation between V and P. For $\alpha < 1$, a rapid initial drop in the reaction rate followed by a slow decrease to zero occurs. On the other hand, for $\alpha > 1$, a slow initial drop in reaction velocity is seen followed by rapid decrease to zero. The model of Luong et al. (1985), however, does not account for the substrate inhibition effect on cellular activity, and assumes a regular Michaelis–Menten relation, viz. $S/\left(S+K_S\right)$, for the substrate dependence of kinetics. In the modified Haldane model we have essentially combined the Haldane type expression for substrate dependence, i.e. $1/\left(1+K_S/[S_o]+\left([S_o]/K_I\right)^n\right)$ with the Levenspiel model of product inhibition. Mulchandani and Luong (1989) noted that the retention for product inhibition $\left(1-\left(P_o/P_m\right)^{\alpha}\right)$ fits well to many microbial systems. However, the inhibitory product

concentration P_m must be determined a priori. The other approach for determination of P_m is graphical, in which the P_m value is guessed until a linear plot is obtained between $\ln(V/V_{max})$ and $\ln(1-P/P_m)$. Levenspiel has reported the values of P_m resulting from two approaches are quite different. In order to obviate this numerical limitation, we have used the Genetic Algorithm for fitting of the experimental profiles, which essentially considers simultaneous optimization of all parameters within the prescribed bound (i.e. global optimization), instead of local optimization (as done in Levenberg–Marquardt technique). For both free and immobilized cells, the value of α in Luong model is less than 1, which indicates susceptibility of the glycerol dehydrogenase to product inhibition. Lesser α value for immobilized cells than free cells essentially a consequence of retention of the product in the immobilization matrix, due to which the inhibition effect is enhanced.

As revealed by data in Table 4.3B, the ranges of P_m predicted by modified Haldane model for free and immobilized cells are 50–88 g/L and 52–71 g/L, respectively. Thus, although immobilization of cells does not alter the lower limit of the inhibitory DHA concentration, the upper limit of P_m shows marginal reduction for immobilized cells which indicates greater susceptibility of the cells towards inhibition.

Comparing α values predicted by Luong model and modified Haldane kinetic model for product inhibition, significantly lower values of α for the latter model indicates greater susceptibility of glycerol dehydrogenase for product inhibition. This essentially indicates that in presence of substrate inhibition, the product inhibition is more marked. For very high product concentration, α value drops very sharply for both free and immobilized cells (~ 0.11) indicating intense inhibition by product.

The modified Haldane model proposed in present study predicts marginal reduction in K_S, with increasing initial product concentration in the fermentation mixture. For very high initial product concentration (50 g/L), the K_S value for immobilized cells shows sharp

rise to 42.3 g/L indicating severe reduction in substrate affinity. The modified Haldane model shows marked drop in V_{max} as initial product concentration increases from 0 to 10 g/L. Thereafter, till initial DHA concentration of 30 g/L the values of V_{max} remains practically unaltered. For the highest initial DHA concentration of 50 g/L, V_{max} shows sharp drop for both free and immobilized cells. Comparing between free and immobilized cells, the free cells have higher V_{max} of 0.48 $g \cdot L^{-1} \cdot h^{-1}$, as compared to immobilized cells (0.3 $g \cdot L^{-1} \cdot h^{-1}$).

The values of the K_I (inhibitory substrate concentration) and n (the order of inhibition) don't show any particular trend with initial DHA concentration for both free and immobilized cells. On relative basis, K_I values are slightly higher for immobilized cells indicating higher resistance of cells towards substrate inhibition. The values of n for most initial DHA concentration are ~1 for free and immobilized cells. This essentially indicates linear nature of substrate inhibition effect, i.e. the velocity of reduces linearly with increasing substrate concentration.

The net DHA production by glycerol fermentation for the free and immobilized cells of *G. oxydans* depicted in Table 4.4 concurs with the above trends in the parameters of different biokinetic models. The final DHA concentration for both free and immobilized cells shows marginal variations (15–18 g/L) till initial DHA concentration of 30 g/L. comparing between the two types of cells, the DHA production for immobilized cells is higher than the free cells. A plausible explanation for this can be given in terms of the reduction in substrate utilized for cell maintenance and growth. As the immobilized cells do not grow, all glycerol uptake is utilized towards DHA production. For the highest initial DHA concentration of 50 g/L, the net DHA yield shows sharp reduction for both free (10.32 g/L) and immobilized (4.34 g/L) cells. Significantly lower yield for immobilized cells is essentially a consequence of the smallest V_{max} and the largest K_S value, indicating reduced

substrate affinity in presence of high concentration of product. Moreover, retention of fermentation mixture in the immobilization matrix augments the inhibition effect of product. Stasiak–Rozanska et al. (2014) have reported complete inhibition of glycerol fermentation by *G. oxydans* (in free form) at DHA concentration of 85 g/L This experimental value matches closely with the range of P_m value (92–95 g/L) predicted by the Ghose et al. model, Aiba model and Luong model.

4.4 CONCLUSIONS

At statistically optimized parameters of pH = 4.74, initial substrate concentration = 20 g/L and temperature = 31°C, crude glycerol fermentation by immobilized *G. oxydans* resulted in DHA yield of 17.83 g/L. Analysis of time profiles of glycerol consumption with biokinetic model revealed that *G. oxydans* cells could tolerate DHA inhibition till concentration of 30 g/L. Immobilized cells were more susceptible to product inhibition due to retention of fermentation mixture in the immobilization matrix. For DHA concentration ≥ 50 g/L, sharp drop in reaction velocity and substrate affinity of immobilized cells resulted in marked reduction in DHA yield.

REFERENCES

Bhasarkar, J.B., Dikshit, P.K., Moholkar, V.S., 2015. Ultrasound assisted biodesulfurization of liquid fuel using free and immobilized cells of *Rhodococcus rhodochrous* MTCC 3552: A mechanistic investigation. Bioresour. Technol. 187, 369–378.

Claret, C., Bories, A., Soucaille, P., 1993. Inhibitory effect of dihydroxyacetone on *Gluconobacter oxyd*ans: Kinetic aspects and expression by mathematical equations. J. Ind. Microbiol. 11, 105–112.

Hekmat, D., Bauer, R., Fricke, J., 2003. Optimization of the microbial synthesis of dihydroxyacetone from glycerol with *Gluconobacter oxydans*. Bioprocess Biosyst. Eng. 26, 109–116.

Hekmat, D., Bauer, R., Neff, V., 2007. Optimization of the microbial synthesis of dihydroxyacetone in a semi–continuous repeated–fed–batch process by in situ immobilization of *Gluconobacter oxydans*. Process Biochem. 42, 71–76.

Hu, Z.–C., Tian, S.–Y., Ruan, L.–J., Zheng, Y.–G., 2017. Repeated biotransformation of glycerol to 1,3–dihydroxyacetone by immobilized cells of *Gluconobacter oxydans* with glycerol– and urea–feeding strategy in a bubble column bioreactor. Bioresour. Technol. 233, 144–149.

Hu, Z.–C., Zheng, Y.–G., Shen, Y.–C., 2010. Dissolved–oxygen–stat fed–batch fermentation of 1,3–dihydroxyacetone from glycerol by *Gluconobacter oxydans* ZJB09112. Biotechnol. Bioprocess Eng. 15, 651–656.

Hu, Z.–C., Zheng, Y.–G., Shen, Y.–C., 2011. Use of glycerol for producing 1,3–dihydroxyacetone by *Gluconobacter oxydans* in an airlift bioreactor. Bioresour. Technol. 102, 7177–7182.

Luong, J.M.Y., 1985. Kinetics of ethanol inhibition in alcohol fermentation. Biotechnol. Bioeng. 29, 242–248.

Mulchandani, A., Luong, J.M.T., 1989. Microbial inhibition revisited. Enzyme Microbiol. Technol. 11, 66–73.

Padhi, S.K., Gokhale, S., 2016. Benzene control from waste gas streams with a sponge–medium based rotating biological contactor. Int. Biodeter. Biodegr. 109, 96–103.

Stasiak–Różańska, L., Błażejak, S., Gientka, I., 2014. Effect of glycerol and dihydroxyacetone concentrations in the culture medium on the growth of acetic acid bacteria *Gluconobacter oxydans* ATCC 621. Eur. Food Res. Technol. 239, 453–461.

Svitel, J., Sturdik, E., 1994. Product yield and by–product formation in glycerol conversion to dihydroxyacetone by *Gluconobacter oxydans*. J. Ferment. Bioeng. 78, 351–355.

Wei, S., Song, Q., Wei, D., 2007. Repeated use of immobilized *Gluconobacter oxydans* cells for conversion of glycerol to dihydroxyacetone. Prep. Biochem. Biotechnol. 37, 67–76.

Wethmar, M., Deckwer, W., 1999. Semisynthetic culture medium for growth and dihydroxyacetone production by *Gluconobacter oxydans*. Biotechnol. Tech.13, 283–287.

भारतीय प्रौद्योगिकी संस्थान गुवाहाटी
Indian Institute of Technology Guwahati

CHAPTER 5

BATCH AND REPEATED-BATCH FERMENTATION FOR DHA PRODUCTION

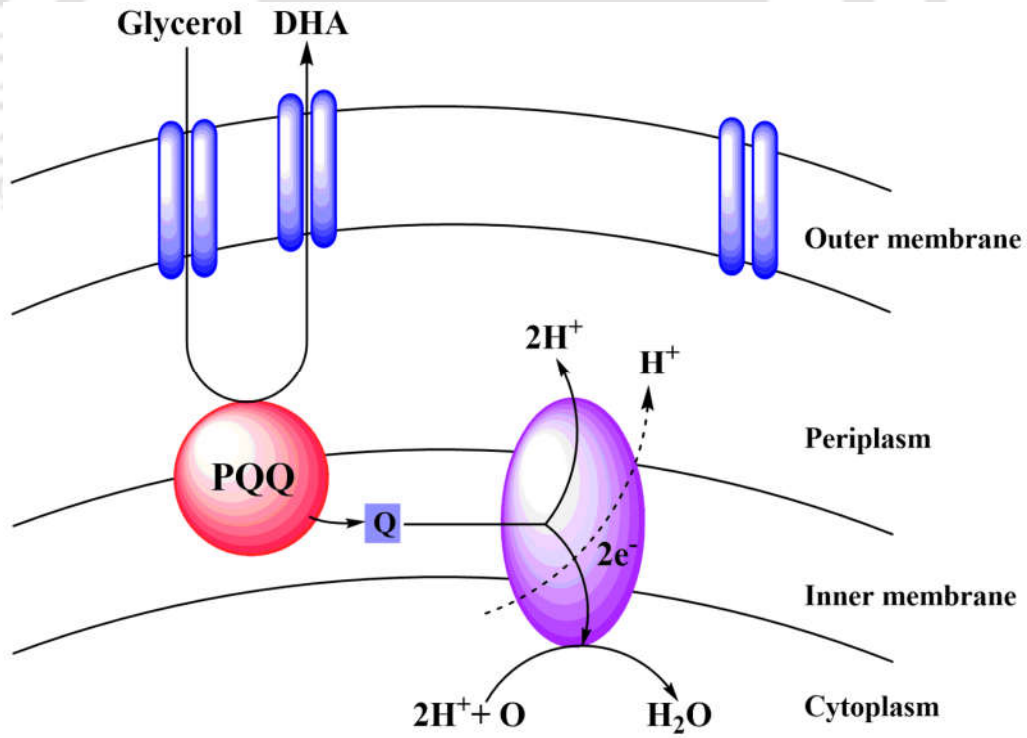

CHAPTER 5

BATCH AND REPEATED–BATCH FERMENTATION FOR DHA PRODUCTION

5.1 INTRODUCTION

In previous chapters, it was revealed that high initial concentrations of glycerol and DHA inhibit growth of *G. oxydans* cells, leading to decrease in DHA yield and productivity (Claret et al., 1992; 1993). Chapter 2 dealt with optimization of initial glycerol concentration and kinetic aspects of DHA production for different initial glycerol concentration. The results of Chapter 2 indicated that glycerol concentration > 20 g/L has inhibitory effect on *G. oxydans* cells causing reduction in cell growth and DHA production. In Chapter 5, effect of initial DHA concentrations on glycerol metabolism was studied by analysis of experimental results with different product inhibition models. The inhibitory product concentration (P_m) beyond which no biological activity and glycerol conversion was observed, was in the range of 90–100 g/L for both free and immobilized cells. For enhancing DHA yield, previous authors have reported adoption of numerous strategies to overcome the inhibitory effect of substrate and product. A review of literature in this area has been presented in Chapter 1. Hu et al. (2010) have reported influence of glycerol feeding strategy on DHA formation in fed–batch operations in bubble column reactor. Hu et al. (2010) used pure glycerol as substrate with different protocols of glycerol feeding. In another study, Liu et al. (2013) have used both crude and pure glycerol as substrate for the

DHA production in batch fermentation (7 L stirred bioreactor) using free cells of *Gluconobacter frateurii* and observed 11% higher DHA yield in presence of pure glycerol as compared to crude glycerol. The authors have carried out fed–batch fermentation in 7 L stirred tank bioreactor, maintaining glycerol concentration in the broth < 5–15 g/L. DHA productivity of 2.6 $g \cdot L^{-1} \cdot h^{-1}$ was obtained in fed–batch process, which was higher than productivity in batch fermentation (1.7 $g \cdot L^{-1} \cdot h^{-1}$). Enhancement in DHA productivity was attributed to elimination of substrate inhibition. Final DHA concentration of 125.8 g/L and 90.5% yield was observed at the end of 48 h fermentation.

Present study is aimed towards enhancing the DHA yield with intermittent feeding of glycerol so as to maintain the glycerol concentration far below the minimum inhibitory concentration. Both pure and biodiesel derived crude glycerol were used as substrate for the fermentation experiments. Batch and repeated–batch fermentation with free and immobilized cells were conducted using optimized medium and process parameters (basically results of previous chapters). Repeated–batch fermentations with intermittent feeding of glycerol were carried out in Erlenmeyer flask. This study was further extended using resting cells of *G. oxydans* as catalyst for glycerol conversion. For resting/whole cell experiments, the cells were harvested from unspent growth medium after completion of immobilization process. With this approach *G. oxydans* cells could be reused for biotransformation process apart from the immobilized cells. The results of this study provided insight into optimum substrate feeding strategy for achieving high DHA yield while obviating the substrate inhibition effect.

5.2 MATERIALS AND METHODS

5.2.1 Materials

Gluconobacter oxydans MTCC 904 was procured from Microbial Type Culture Collection (MTCC), Chandigarh, India. DHA and pure glycerol were procured from Merck, Germany. Reticulated polyurethane foam was procured from local market. All other medium components and chemicals used in this study were procured from HiMedia Pvt. Ltd., India. Crude glycerol was produced through biodiesel synthesis from alkali (NaOH) catalyzed transesterification reaction using soybean oil and methanol as described in previous chapter.

5.2.2 Growth and maintenance of *G. oxydans* culture

The lyophilized cells of *G. oxydans* were revived in MRS medium and kept in a rotary incubator shaker (Make: Lab Companion; Model: SI–300R) at 30ºC, 150 rpm for 24 h. The revived cells were grown on agar slant and kept at 4ºC. The cultures were sub–cultured every month. The composition of MRS medium in 1 L of distilled water was as follows: peptone – 10.0 g, beef extract – 10.0 g, yeast extract – 5.0 g, glucose – 10.0 g, tween–80 – 1 mL, Na_2HPO_4 – 2.0 g, sodium acetate – 5.0 g, triammonium citrate – 2.0 g, $MgSO_4 \cdot 7H_2O$ – 0.2 g, $MnSO_4 \cdot 4H_2O$ – 0.2 g. The pH of the medium was adjusted to 6.0 ± 0.2 using 1 N HCl. The agar plates and slants were prepared by adding 15 g/L of agar in MRS medium.

5.2.3 Seed culture medium and immobilization of cells over PU foam support

The composition of seed culture medium was as follows: yeast extract – 5.0 g/L, peptone – 3 g/L, $K_2HPO_4 \cdot 3H_2O$ – 3 g/L, $(NH_4)_2SO_4$ – 2 g/L, $MgSO_4 \cdot 7H_2O$ – 0.51 g/L, mannitol – 10 g/L. The initial pH of the medium was adjusted to 6.0 ± 0.2. The medium

was autoclaved prior to inoculation at 121ºC, 15 psi for 20 min. The cells of *G. oxydans* were immobilized over PU foam support following the method described in previous chapter.

5.2.4 Preparation of resting/whole–cell catalyst

After separation of the PU foam cubes from the growth medium, large number of cells still remained suspended in the growth medium. These cells were harvested from the broth by centrifugation (10,000 × g, 20 min, 4°C) for further use in glycerol fermentation. The harvested cells were washed thrice with phosphate buffer (pH 6.0, 50 mM) and diluted with the same buffer to final concentration of 1 g/mL. The cells were stored at 4°C.

5.2.5 Batch fermentation by free and immobilized cells

Batch fermentation was carried out with free and immobilized cells of *G. oxydans* using pure and crude glycerol as substrate. Initial glycerol concentration in the fermentation medium was 20 g/L (based on optimization studies reported in previous chapters). In fermentation using immobilized cultures, 3 PU foam cubes (as per optimization results) with immobilized and cross–linked *G. oxydans* cells were added to fermentation broth.

The fermentation medium for batch experiments had optimized composition as: yeast extract – 2 g/L, $(NH_4)_2SO_4$ – 3.02 g/L, KH_2PO_4 – 0.64 g/L, $MgSO_4 \cdot 7H_2O$ – 0.55 g/L. The pH of the medium was adjusted to 4.7 prior to sterilization using 1 N HCl. 100 mL of fermentation media was taken in 250 mL Erlenmeyer flask and was kept in rotary shaker (Make – Lab Companion, Model – SI–300R) at 150 rpm, 31°C for 120 h. The optimized process variables such as pH, temperature and initial glycerol concentration were maintained at their optimum levels as reported in previous chapters. Samples of fermentation broth were withdrawn at regular interval for analysis.

5.2.6 Biotransformation of glycerol to DHA by resting cells

Batch glycerol fermentation with resting cells were carried out in 250 mL Erlenmeyer flask with two different initial substrates (crude glycerol) concentration, viz. 10 and 20 g/L, as substrate. Prior to fermentation, preliminary studies were conducted for optimization of initial resting cell concentration and pH of fermentation mixture.

Initial biocatalyst (or resting cell) concentration: Initial concentration of resting cells was varied as 5, 10, 15, 20 g/L. Initially, pure glycerol (20 g/L) was added to phosphate buffer (50 mM, pH – 5.0) in Erlenmeyer flask and autoclaved, prior to addition of resting cells. Different concentrations of resting cells were resuspended in the sterilized solution containing substrate, and fermentation was carried out in rotary shaker (Make – Lab Companion, Model – SI–300R) at 150 rpm, 30°C for a period of 42 h. Samples were withdrawn at regular intervals for the analysis of glycerol and DHA.

Initial pH of buffer: Fermentation was carried out at three different pH viz. pH 5.0, 5.5, 6.0 with buffer concentration of 50 mM. Potassium phosphate was used for preparation of buffers with pH of 5.5 and 6.0, while sodium acetate was selected for preparation of buffer with pH 5.0. Initial glycerol concentration was 20 g/L in all experiments. The flasks were kept in rotary shaker at 150 rpm, and 30°C for 96 h. Samples of fermentation mixture were withdrawn at regular interval for analysis.

Batch experiments with resting cells: Batch fermentation with resting cells was carried out at two initial concentrations of crude glycerol (i.e. 10 and 20 g/L). The values of other parameters (viz. cell concentration and pH of buffer) was maintained at their optimum levels, as determined in previous experiments. Fermentation was conducted in an incubator

shaker at 150 rpm, 30°C for 72 h. Samples were withdrawn every 12 h for analysis.

5.2.7 Repeated–batch fermentation by shake flask

Repeated–batch fermentations were carried out in 250 mL Erlenmeyer flask with prescribed initial substrate concentration (either 10, 15 or 20 g/L). The glycerol feeding strategy was decided on the basis of maintaining substrate concentration ≥ 5 g/L. The pulses of glycerol were also fed at pre–described levels, viz. 10, 15 and 20 g/L. The time for glycerol pulses were 48 and 96 h after commencement of fermentation. The initial glycerol concentrations and the strategy for glycerol pulses in different experiments is described in Table 5.2. Total fermentation duration was 216 h and samples of fermentation mixture were withdrawn in regular interval for analysis.

5.2.8 Analytical methods

The growth of *G. oxydans* cells in fermentation broth (for free cells) was monitored by measuring absorbance at 660 nm with a UV–Vis spectrophotometer (Make: Perkin Elmer, Model: LAMBDA 35). Glycerol and DHA in the samples of fermentation mixture were quantified by HPLC analysis using a Rezex RCM Monosaccharide calcium–column (300 mm × 8 µm × 7.8 mm, Phenomenex, India) thermostated at 35°C with the help of external column oven (Model: HCO–02, Make: PCI Analytics Pvt. Ltd., India) (Hekmat et al., 2007). The HPLC apparatus comprised of a pump (Series 200, Perkin Elmer), a refractive index detector (Series 200, Perkin Elmer) and a vacuum degasser (Series 200, Perkin Elmer). HPLC grade water (Mili–Q, ≥ 18mΩ resistivity) was used as the mobile phase at a flow rate of 0.5 mL/min. Samples of fermentation mixture were centrifuged (12,000× g, 20 min) and filtered through a 0.2 µm membrane filter, and diluted appropriately prior to analysis. Standard calibration plots were used to determine

concentrations of both substrate and product.

5.3 RESULTS AND DISCUSSION

5.3.1 Results of preliminary experiments for resting cells

The results of preliminary experiments with varying initial resting cell concentration and pH of the buffer are shown in Fig. 5.1. The initial resting/whole cell concentration in the reaction mixture was varied from 5 to 20 g/L (with initial glycerol concentration fixed at 20 g/L), as shown in Fig. 5.1A. Maximum DHA concentration of 14.9 g/L was observed with initial resting cell concentration of 5 g/L. As cell concentration increased from 5 to 20 g/L, final DHA concentration was reduced. The residual (or unconverted) glycerol in fermentation mixture was 1.7 and 5.7 g/L for initial resting cell concentration of 5 and 20 g/L, respectively. Based on these results, the initial cell concentration for further experiments was fixed as 5 g/L.

The pH optimization experiments were carried out in presence of two different buffer (i.e. phosphate buffer and acetate buffer) at 3 pH levels, viz. 5, 5.5, and 6. As *G. oxydans* culture belongs to class of acetic acid bacteria, higher glycerol conversion and DHA production was favored in acidic pH (Hekmat et al., 2003; Svitel and Sturdik, 1994; Wethmar and Deckwer, 1999). The results of fermentation at various initial pH are shown in Fig. 5.1B. As expected, maximum DHA concentration 17.5 g/L observed at the lowest pH 5.0.

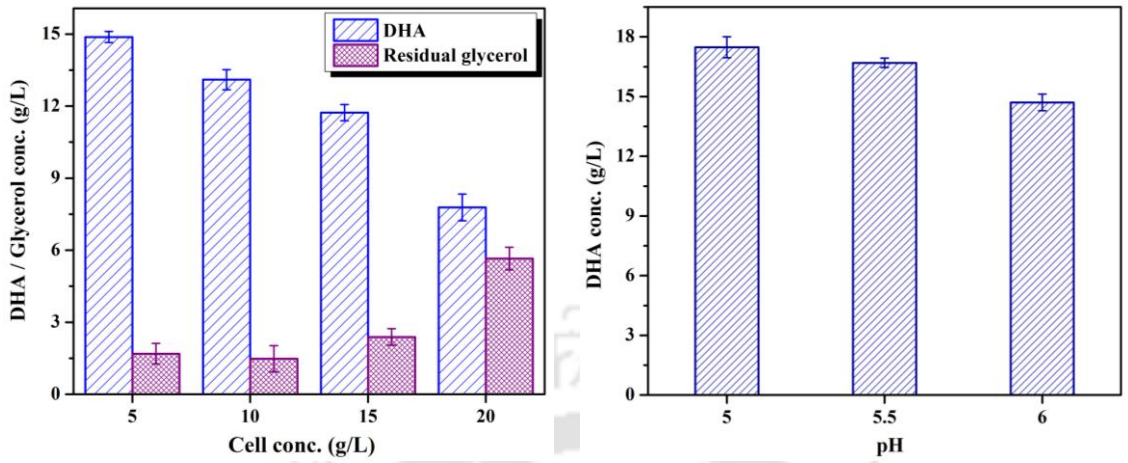

(A) (B)

Figure 5.1. Preliminary experiments for optimization of initial resting cell concentration and pH of buffer for glycerol conversion. (A) Optimization of resting cell conc. for DHA production; (B) effect of initial pH on DHA production under different initial pHs at 30°C

5.3.2 Batch fermentation for DHA production

Batch fermentations with pure glycerol and biodiesel–derived crude glycerol were carried out to ascertain the influence of impurities on DHA production. The time profiles of glycerol consumption and DHA formation in these experiments are depicted in Fig. 5.2. The summary of the results is given in Table 5.1.

For fermentation with free cells (Figs. 5.2A and B), the maximum DHA concentration attained in 60 h of the fermentation was 17.04 and 16.24 g/L for pure and biodiesel–derived crude glycerol, respectively. Moreover, complete glycerol consumption in fermentation mixture was observed in these experiments. The cell concentration in broth reached 0.69 g/L for both pure and crude glycerol. No significant increase in DHA yield and productivity was observed in case of pure glycerol as substrate in comparison with crude glycerol. The highest DHA concentrations attained in 3–day fermentation using

immobilized cells were 18.79 and 17.83 g/L with pure and crude glycerol as substrate, respectively. Fermentation with resting cells was conducted with initial crude glycerol concentration of 10 and 20 g/L. Maximum DHA yield attained in these experiments was 8.46 and 16.32 g/L, respectively. The time profiles of glycerol consumption and DHA formation in these experiments are depicted in Figs. 5.2E and F. Similar DHA yields with free and resting cells essentially indicate similar catalytic activity. This result is also a corroboration that activity of the key enzyme glycerol dehydrogenase responsible for glycerol oxidation in *G. oxydans* is not altered by the procedure of resting cell preparation. Although the glycerol was completely consumed from the fermentation media (Fig. 5.2), the reaction efficiency did not reach 100%. A plausible explanation for this discrepancy is utilization of glycerol in other metabolic reactions than DHA oxidation. A probable alternate route of glycerol conversion is oxidation to sodium glycerate due to the alkali impurities present in glycerol from transesterification reaction (Gupta et al., 2001; Stasiak–Różańska and Błażejak, 2012).

Table 5.1. Summary of batch fermentation using free, immobilized and resting cells as catalyst

Experimental category	Initial glycerol conc. ($g \cdot L^{-1}$)	Initial rate of reaction ($g \cdot L^{-1} \cdot h^{-1}$)	Final DHA conc. ($g \cdot L^{-1}$)	DHA productivity ($g \cdot L^{-1} \cdot h^{-1}$)	$Y_{P/S}$ (g/g)	Fermentation time (h)
FC, PG	20	0.31	17.04 ± 0.04	0.28	0.854	60
FC, CG	20	0.34	16.24 ± 0.34	0.27	0.824	60
IMC, PG	20	0.35	18.79 ± 0.53	0.26	0.940	72
IMC, CG	20	0.40	17.83 ± 0.23	0.28	0.833	60
RC, CG	10	0.64	8.46 ± 0.46	0.23	0.846	36
RC, CG	20	0.58	16.32 ± 0.42	0.27	0.816	60

Notation: FC – Free cells; IMC – Immobilized cells; RC – Resting cells; PG – Pure glycerol; CG – Crude glycerol

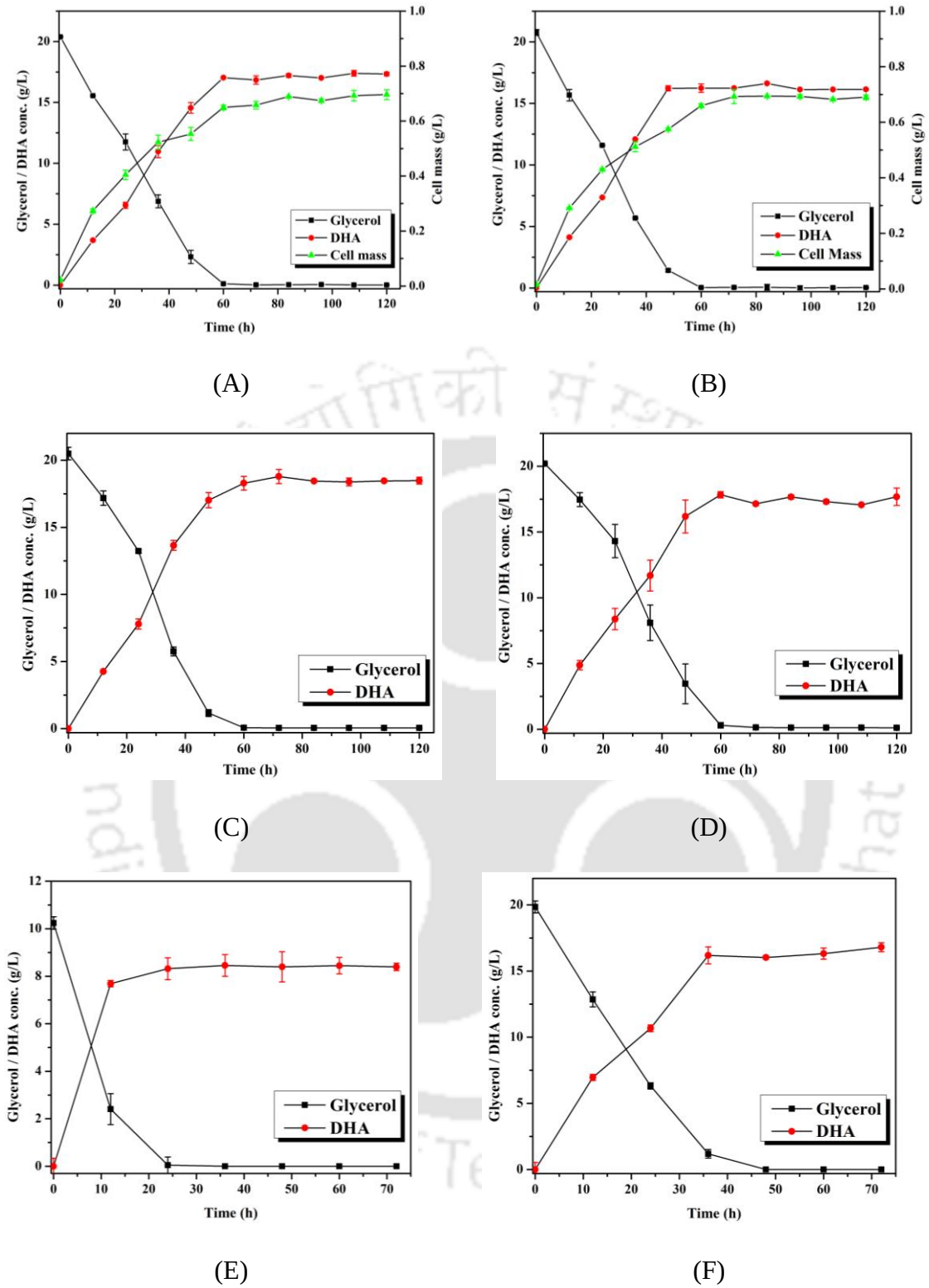

Figure 5.2. Results of batch fermentation with pure and crude glycerol as substrate using free, immobilized and resting cells of *G. oxydans* (A) Free cells with pure glycerol; (B) Free cells with crude glycerol; (C) Immobilized cells with pure glycerol; (D) Immobilized cells with crude glycerol; (E) Resting cells with crude glycerol = 10 g/L; (F) Resting cells with crude glycerol = 20 g/L.

5.3.3 Repeated–batch fermentation for DHA production

G. oxydans cells are prone to substrate inhibition at higher glycerol concentration that leads to reduction in DHA production (Claret et al., 1992; Claret et al., 1994). An alternative to batch fermentation with high initial glycerol concentration, is the fed–batch route in which prescribed quantities of glycerol are added to the fermentation broth at regular intervals. In this protocol, it is possible to maintain the glycerol concentration below the inhibitory level. The quantities and time interval of glycerol doses are decided on the basis of rate of consumption of glycerol. Nonetheless, this strategy cannot maintain constant substrate concentration in fermentation mixture, and variations are expected.

Repeated batch fermentation experiments were carried out using pulse–feeding strategy, where glycerol was added intermittently to the fermentation broth at discrete intervals. Volume of fermentation mixture was maintained constant during entire process, and in the time interval between the glycerol feeds, the system operated in batch mode. First glycerol pulse (or feed) was administered at 48 h after commencement of fermentation, followed by another 48 h of fermentation during which the residual glycerol concentration dropped < 5 g/L. The second glycerol feed pulse was given at this time. Different combinations of pulse–feeding strategies were implemented for glycerol fermentation using free, immobilized, and resting cells. The results of repeated–batch fermentation with pulse–feeding of glycerol are given in Table 5.2. The fermentation profiles in representative fed–batch experiments employing free, immobilized, and resting cells with pure and crude glycerol as substrates are shown in Fig. 5.3. The summary of all fed–batch experiments is given in Table 5.2. Results depicted in Table 5.2 reveal that cumulative DHA concentration increases with total glycerol feed. Among all experimental runs (or protocols) with different strategies of glycerol feed, run F5 yielded maximum DHA concentration of 65.64 g/L. The final DHA concentration in protocol F5 was 33.88% higher

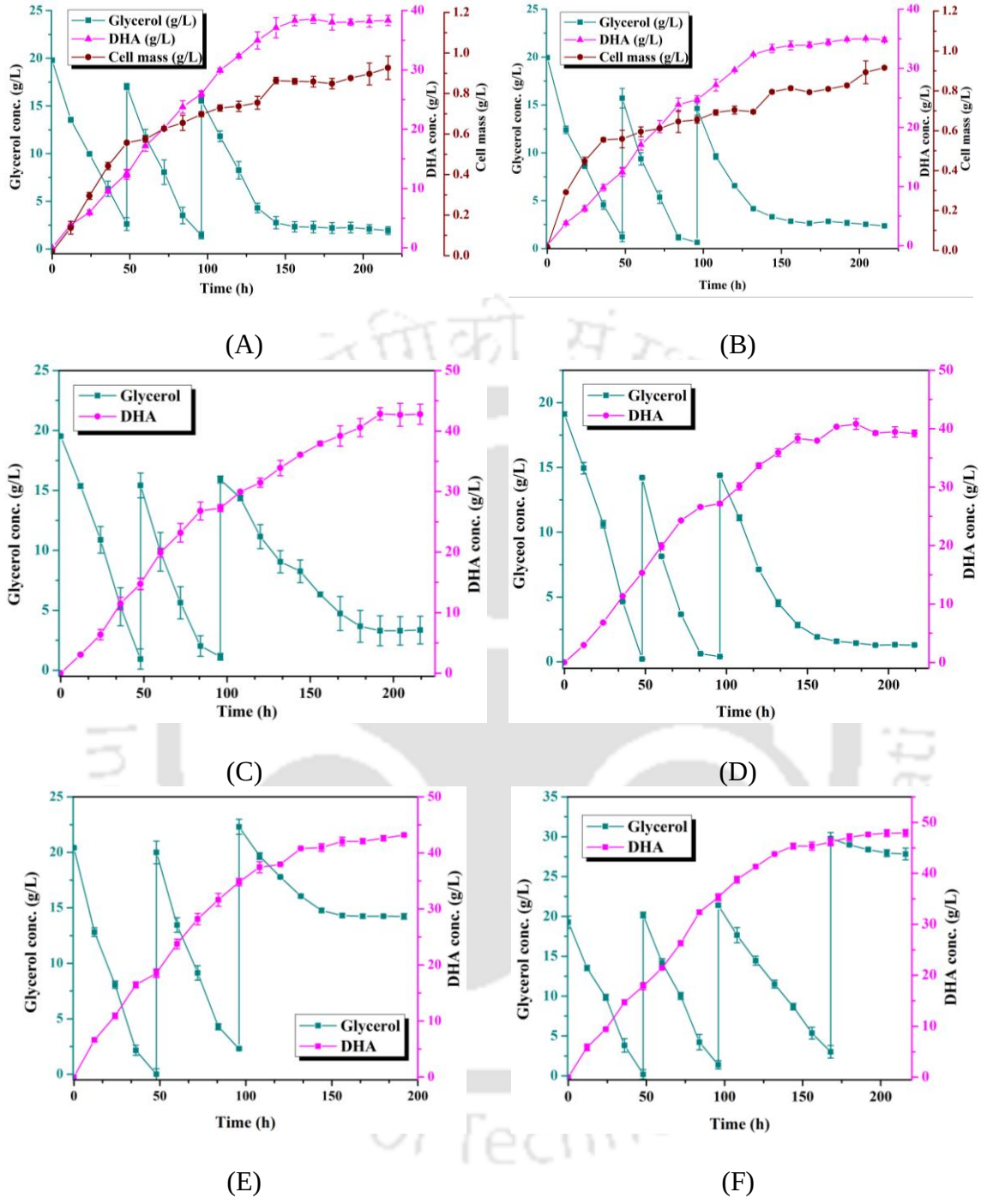

Figure 5.3. Results of repeated–batch fermentation with pure and crude glycerol as substrate using free, immobilized and resting cells of *G. oxydans* (A) FC, PG (20+15+15 g/L); (B) FC, CG (20+15+15 g/L); (C) IMC, PG (20+15+15 g/L); (D) IMC, CG (20+15+15 g/L); (E) RC, CG (20+20+20 g/L); (F) RC, CG (20+20+20+20 g/L).
FC – Free cells; IMC – Immobilized cells; PG – Pure glycerol; CG – Crude glycerol; RC – Resting cells

than that protocol F4 with a productivity of 0.228 $g \cdot L^{-1} \cdot h^{-1}$. However, conversion rate of glycerol to DHA in protocol F5 was 87.52%, which was 2.7% lower than protocol F2. The total fermentation period for protocols F4 and F5 was higher than protocol F2. The DHA productivity for protocol F2 was 83.33% and 64.04% higher than protocols F4 and F5, respectively. For both pure and crude glycerol, immobilized cells were revealed to yield higher DHA yield and productivity as compared to free and resting cells. The conversion rate of glycerol to DHA in this study (protocol F2) is close agreement with the results of Hu et al. (2010). Interestingly, microbial species *G. oxydans* ZJB09112 employed by Hu et al. (2010) is a mutant strain, and the reactor used for this study was vertical bubble column bioreactor.

Crude glycerol conversion rate with resting cells (in protocol F9) matched closely with free cells. However, this conversion rate was lesser than immobilized cells. On the basis of DHA productivity (0.374 $g \cdot L^{-1} \cdot h^{-1}$) and yield (35.95 g/L), glycerol conversion rate (89.88%) and total fermentation time (96 h), protocol F2 seems to be most optimum. Higher concentration of product (DHA) in the fermentation broth has detrimental effect over growth of *G. oxydans* cells, which further leads to decrease in DHA production. The minimum inhibitory concentration of DHA where the cell growth and DHA production ceases was determined by kinetic analysis in our previous study (Chapter 4). The inhibitory product concentration was found to be in the range of 90 – 100 g/L. However, the cell growth and DHA production was also affected moderately at lower concentration of product below 90 g/L. This conjecture was ascertained from the Fig. 5.3, where the duration of fermentation increases with increase in DHA concentration in the fermentation broth. The rate of glycerol consumption in second pulse cycle (administered after 96 h) was reduced than the previous pulse.

Table 5.2. Summary of results of repeated–batch experiments at various pulse feeding of substrate

Experiments	Initial glycerol concentration ($g \cdot L^{-1}$)	Glycerol feed strategy (pulses, $g \cdot L^{-1}$)	DHA concentration ($g \cdot L^{-1}$)	Glycerol conversion (%)	DHA productivity ($g \cdot L^{-1} \cdot h^{-1}$)	$Y_{P/S}$ (g/g)	Fermentation time (h)
F1 (CG, IMC)	20	15+15	40.81 ± 0.92	81.62	0.227	0.84	180
F2 (CG, IMC)	10	10+10+10	35.95 ± 0.42	89.88	0.374	0.90	96
F3 (CG, IMC)	10	10+10+10+10	41.71 ± 0.52	83.42	0.331	0.88	132
F4 (CG, IMC)	15	15+15+15	49.03 ± 1.21	81.72	0.204	0.86	240
F5 (CG, IMC)	15	15+15+15+15	65.64 ± 0.94	87.52	0.228	0.95	288
F6 (PG, IMC)	20	15+15	42.84 ± 1.03	85.68	0.223	0.92	180
F7 (PG, FC)	20	15+15	38.58 ± 0.73	77.16	0.229	0.81	168
F8 (CG, FC)	20	15+15	35.03 ± 0.11	70.06	0.171	0.74	204
F9 (CG,RC)	20	20+20	43.19 ± 0.15	71.98	0.224	0.94	192
F10 (CG,RC)	20	20+20+20	47.90 ± 0.27	59.88	0.222	0.92	216

Notation: PG – Pure glycerol; CG – Crude glycerol; IMC – Immobilized cells; FC – Free cells; RC – Resting cells

This reduction in glycerol consumption rate was attributed to the effect of product inhibition, as the product (DHA) gets accumulated in the broth with escalation of fermentation cycle.

Inhibitory effect of gradual increase in product (DHA) concentration in the fermentation broth on glycerol consumption rate was assessed by kinetic analysis. Time profiles of glycerol consumption for each pulse feed cycle were fitted to the pseudo 1st order rate equation for determination of first order rate constant (k_1). Each pulse cycle indicates the time interval between a glycerol feed to the next feed, i.e., 0–48 h, 48–96 h and so on. The rate constants for different categories of experiments (as shown in Fig. 5.3) were summarized in Table 5.3. Form the results shown in Table 5.3, it was observed that the k_1 value for free, and immobilized cell fermentation increased in the second pulse cycle (i.e. 48–96 h) as compared to the first cycle. This could be due to decrease in initial feed glycerol concentration (15 g/L) in second cycle, as compared to the first cycle (20 g/L). So the cells were less prone to initial substrate inhibition in the second phase. Significant decrease in rate constant value for the third pulse cycle than the first two cycles signifies, that the inhibition effect on *G. oxydans* cells is due to accumulation of end product (DHA). As reported in previous chapter (Chapter 4), low DHA concentration in the fermentation broth partially inhibit *G. oxydans* cells, which further decreases the activity of the enzyme glycerol dehydrogenase. Experiments using resting cells, for which crude glycerol concentration for each pulse was kept constant (i.e. 20 g/L), a decrease in the rate constant value was observed. For experimental run F9 and F10 using resting cells, a significant decrease in k_1 value was observed for pulse 3 and pulse 4 as compared to the previous pulses. This phenomenon clearly indicates the effect of substrate as well as product inhibition on *G. oxydans* cells, at high concentration of glycerol and DHA in fermentation broth. Higher rate constant value for immobilized cells essentially indicates faster reaction

rate as compared to free cells. Confinement of microbial cells within porous matrix increases the cell population within a defined space, which in turn increases the probability of interaction of the substrate molecules to the cells. Whereas, for experiments with free and resting cells, the microbial cells population are distributed throughout the reaction volume, which further decreases the local concentration as well as probability of interaction between substrate and cell.

Table 5.3. Results of fitting pseudo 1st order rate equation for determination of kinetic constants

Experiments	Glycerol feed	Pseudo 1st order rate constant = k_1 (h^{-1})			
		Pulse 1 (0–48 h)	Pulse 2 (48–96 h)	Pulse 3 (96–216 h)	Pulse 4 (144–192)
F7 (PG, FC)	20+15+15 g/L	0.037	0.046	0.022	–
F8 (CG, FC)	20+15+15 g/L	0.049	0.063	0.019	–
F6 (PG, IMC)	20+15+15 g/L	0.049	0.052	0.014	–
F1(CG, IMC)	20+15+15 g/L	0.067	0.074	0.024	–
F9 (CG, RC)	20+20+20 g/L	0.064	0.042	0.006	–
F10 (CG, RC)	20+20+20+20 g/L	0.071	0.047	0.015*	0.002

Notation: PG – Pure glycerol; CG – Crude glycerol; IMC – Immobilized cells; FC – Free cells; RC – Resting cells; * – Time duration for the pulse was from 96 – 144 h.

5.4 CONCLUSIONS

This chapter reports studies on batch fermentation of pure and crude glycerol using previously optimized media and process variables. Fermentation of both pure and crude glycerol was carried out using free, immobilized, and whole/resting cells as catalyst. Further, fermentation was also carried out using repeated–batch strategy aimed at obviating the effect of substrate inhibition. The strategy of pulse–feeding of glycerol has proven to be an alternate way to reduce the substrate inhibition effect and for achieving higher DHA yield. Immobilized cells have been revealed to give higher yield and productivity of DHA than free and resting cells. The effect of product inhibition on *G. oxydans* cells with increase

in DHA concentration in fermentation broth is corroborated by first order rate constant. Significant decrease in rate constant value for 3rd feed cycle attributes the decrease in activity of the enzyme glycerol dehydrogenase with increase in DHA concentration in the fermentation medium. Further optimization of the process variables such as dose of glycerol pulse, time interval of the dose and basic design of the bioreactor can boost DHA yield and productivity. In summary, the present study not only demonstrated a repeated fed–batch process to overcome substarte inhibition effect, but also has attempted an indepth study to the kinetic prospect of this process.

REFERENCES

Claret, C., 1993. Inhibitory effect of dihydroxyacetone on *Gluconobacter oxydans*: Kinetic aspects and expression by mathematical equations. J. Ind. Microbiol. 11, 105–112.

Claret, C., Bories, A., Soucaille, P., 1992. Glycerol inhibition of growth and dihydroxyacetone production by *Gluconobacter oxydans*. Curr. Microbiol. 25, 149–155.

Claret, C., Salmon, J.M., Romieu, C., Bories, A., 1994. Physiology of *Gluconobacter oxydans* during dihydroxyacetone production from glycerol. Appl. Microbiol. Biotechnol. 41, 359–365.

Gupta, A., Singh, V.K., Qazi, G.N., Kumar, A., 2001. *Gluconobacter oxydans*: Its biotechnological applications. J. Mol. Microbiol. Biotechnol. 3, 445–456.

Hekmat, D., Bauer, R., Fricke, J., 2003. Optimization of the microbial synthesis of dihydroxyacetone from glycerol with *Gluconobacter oxydans*. Bioprocess Biosyst. Eng. 26, 109–116.

Hekmat, D., Bauer, R., Neff, V., 2007. Optimization of the microbial synthesis of dihydroxyacetone in a semi–continuous repeated–fed–batch process by in situ immobilization of *Gluconobacter oxydans*. Process Biochem. 42, 71–76.

Hu, Z.–C., Liu, Z.–Q., Zheng, Y.–G., Shen, Y.–C., 2010. Production of 1,3–dihydroxyacetone from glycerol by *Gluconobacter oxydans* ZJB09112. J. Microbiol. Biotechnol. 20, 340–345.

Liu, Y.P., Sun, Y., Tan, C., Li, H., Zheng, X.J., Jin, K.Q., Wang, G., 2013. Efficient production of dihydroxyacetone from biodiesel-derived crude glycerol by newly isolated *Gluconobacter frateurii*. Bioresour. Technol. 142, 384-389.

Stasiak–Różańska, L., Błażejak, S., 2012. Production of dihydroxyacetone from an aqueous solution of glycerol in the reaction catalyzed by an immobilized cell preparation of acetic acid bacteria *Gluconobacter oxydans* ATCC 621. Eur. Food Res. Technol. 235, 1125–1132.

Svitel, J., Sturdik, E., 1994. Product yield and by–product formation in glycerol conversion to dihydroxyacetone by *Gluconobacter oxydans*. J. Ferment. Bioeng. 78, 351–355.

Wethmar, M., Deckwer, W., 1999. Semisynthetic culture medium for growth and dihydroxyacetone production by *Gluconobacter oxydans*. Biotechnol. Tech.13, 283–287.

CHAPTER 6

ULTRASOUND ENHANCED BIOCONVERSION OF GLYCEROL

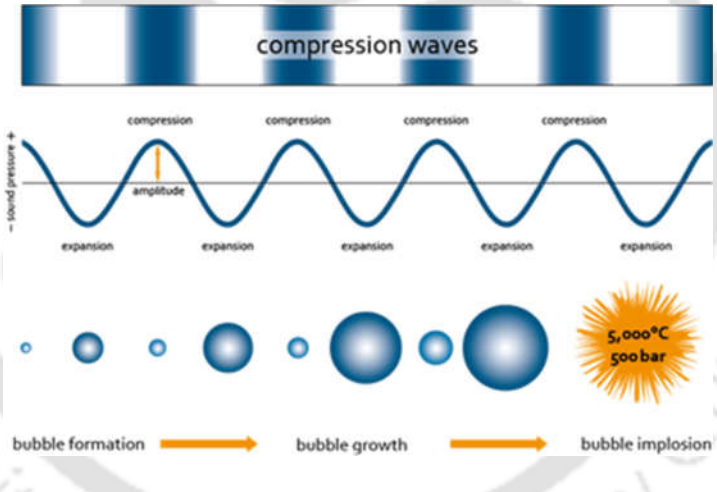

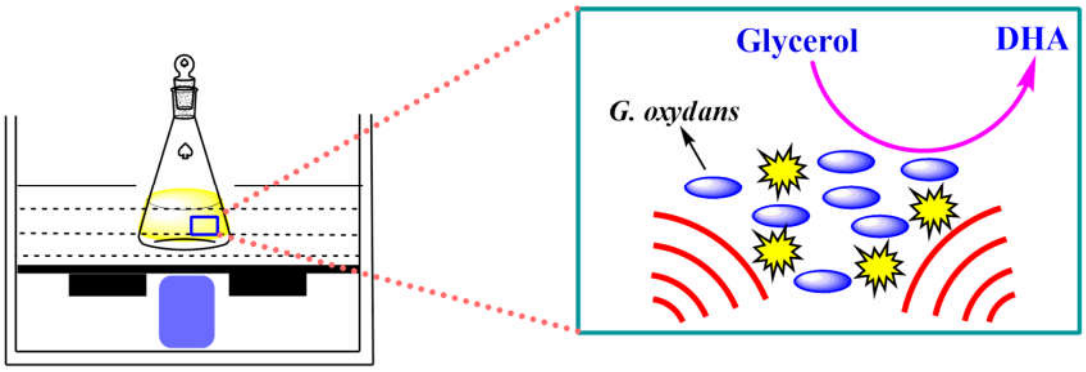

CHAPTER 6

INVESTIGATIONS IN SONICATION-INDUCED INTENSIFICATION OF CRUDE GLYCEROL FERMENTATION

6.1 INTRODUCTION

The major limitation of the fermentation–based processes (especially from viewpoint of large–scale manufacture of the product) is slow kinetics. Moreover, all fermentation systems have strong mass transfer limitations. In biotransformation of glycerol to DHA by *G. oxydans*, oxygen plays crucial role as final acceptor of electrons generated during the oxidation of glycerol (Claret et al., 1994; Hu et al., 2011; Wei et al., 2007). In case of aerobic fermentation (such as glycerol fermentation by *G. oxydans*), the oxygen needs to be transferred from air to the fermentation medium as dissolved oxygen (DO), and further to the microbial cells. Thus, maintenance of DO concentration in the fermentation mixture close to saturation is a possible means of enhancing the kinetics of glycerol metabolism.

Previous studies have adopted different strategies for maintaining DO concentration in the fermentation broth close to saturation. Primary process parameters influencing DO concentration during fermentation are flow rate of sparge gas through the fermentation mixture and oxygen partial pressure in this gas. Moreover, the degree of agitation provided

in the fermentation mixture is also an important factor, as it determines the distribution and residence time of the gas bubbles (Ertunc et al., 2009; Siegell and Gaden, 1962). You et al. (2013) have adopted 2–stage agitation speed strategy in a 7.5 L fermenter, viz. 800 rpm during cell (inoculum) growth and 600 rpm during the fermentation. In another study, Flickinger and Perlman (1977) reported 3fold rise in glycerol conversion in 25L batch fermenter by increasing the partial pressure of oxygen in sparge gas. Hu and Zheng (2011) followed a strategy of maintaining different DO concentrations in the three stages of fermentation using a mutant strain of *G. oxydans*. These concentrations (as percentages of air saturation) were as follows: 20% for first 24 h of fermentation, 30% until 60 h, and then 40% till end of fermentation. With this strategy, Hu and Zheng (2011) could obtain the highest DHA concentration of 209 g/L with productivity of 2.91 $g \cdot L^{-1} \cdot h^{-1}$.

The present study has dealt with a relatively new strategy for enhancing glycerol metabolism in *G. oxydans* with use of sonication (or ultrasound irradiation) of fermentation mixture. Sonication is a well–known means of intensification of chemical and biochemical processes. (Agarwal et al., 2016; Bar, 1988; Choudhury et al., 2013; Malani et al. 2017; Singh et al., 2015; Sulaiman et al., 2011; Zabaneh and Bar, 1991). A review on ultrasound–assisted biochemical processes has been published by Gogate and Kabadi (2009). Most of the biochemical processes are mass transfer limited operations, and the yield as well as kinetics of these processes increases with the level of convection or turbulence in the system. Ultrasound and its secondary effect, cavitation, which is nucleation, growth and implosive collapse of tiny gas bubbles (induced by variation of bulk pressure in the medium with passage of ultrasound wave) can induce high intensity convection in the medium on extremely small temporal (~ few tens nanoseconds) and spatial scale (~ 0.1 – 10 μm). This convection is generated through different mechanisms such as micro–streaming, micro convection, acoustic (or shock) waves and microjets developed during asymmetric collapse

of bubbles. These mechanisms have been explained in greater details in our previous papers (Kuppa and Moholkar, 2010; Moholkar and Warmoeskerken, 2003; Morya et al., 2008). As demonstrated in our previous studies (Agarwal et al., 2016; Bhasarkar et al., 2015a), the micro–convection generated by ultrasound and cavitation can induce changes in the secondary structure of the enzymes (present in free form in bulk medium), which essentially catalyze the biotransformation. These conformational changes essentially enhance substrate–enzyme affinity. Moreover, the microturbulence also enhances the probability of enzyme–substrate interaction, and the velocity of the enzymatic reactions. These phenomena essentially are manifested in terms of marked rise (of several folds) in the kinetics of enzymatic reactions. The system in the present context, i.e. biotransformation of glycerol to DHA by *G. oxydans*, is different in that the enzyme glycerol dehydrogenase is located inside the microbial cell. Glycerol fermentation has been carried out using both free and immobilized cells of *G. oxydans* on polyurethane foam. As explained in subsequent sections, we have demonstrated that micro–convection generated by sonication not only enhances cellular transport of glycerol (as it crosses the outer cell membrane to reach inner membrane bound PQQ), but also induces conformational changes in the glycerol dehydrogenase enzyme, which have been analyzed with circular dichroism spectra. Concurrent analysis of the experimental results has given interesting insight into biophysical aspects of ultrasound–induced enhancement in glycerol metabolism by *G. oxydans*.

6.1.1 Structure of glycerol dehydrogenase enzyme and binding sites

Pyrroloquinoline quinone (PQQ) is a prosthetic group found in several enzymes that work on dehydrogenation of the primary or secondary hydroxyl groups in alcohols and sugars. PQQ is non-covalently bound to apoenzyme (i.e. an inactive enzyme, which

requires binding of an organic or inorganic cofactor for activation). These enzymes also contain 1 mol Ca^{2+}/mol of PQQ, which is coordinated both by PQQ and by several amino acid side chain atoms and is required for activity. Alcohol dehydrogenases are found in wide range of organisms ranging from bacterial to mammals. There are two variants of ADH, viz. the NAD(P)-dependent enzyme present in the cytoplasm, and secondly, the PQQ-dependent ADH found in narrow range of bacterial species (i.e. α, β, and γ-proteobacteria). The latter type of ADH is localized only in the periplasmic fraction. These dehydrogenases include both quinoprotein and quinohemoprotein type enzyme. Some PQQ-dependent enzymes are soluble in periplasm and others are bound to outer surface of the cytoplasmic membrane. Thus, quino (hemo) protein ADH from a "periplasmic alcohol oxidase system" together with the membrane bound respiratory chain. These enzymes functions as primary dehydrogenase, which transfer reducing equivalents directly to the bacterial aerobic respiratory chain in periplasm. Due to this mechanism, these enzymes function as primary dehydrogenase that transfer reducing equivalent directly to the bacterial aerobic respiratory chain in the periplasm. Moreover, these enzymes have truncated, and less energy efficient respiratory chain that leads to direct oxidation of substrate without energy consuming cellular transport of substrate (i.e. uptake of substrate and excretion of the oxidized products).

PQQ-dependent alcohol dehydrogenases are classified into 3 groups, viz. type I, II and III. Type I ADH is found in limited number of proteobacteria. This is highly analogous to quinoprotein methanol dehydrogenase in methylotrophs. These enzymes are simple quinoproteins having PQQ as the only prosthetic group. The soluble enzyme of sorbose/sorbosone dehydrogenase and membrane bound glycerol dehydrogenase, even though their physiological substrate are not alcohols but polyols like glycerol. These enzymes can also oxidize several alcohols with high efficiency.

Structural characteristics and binding/reaction sites of quinohemoprotein ADH: Toyama et al. (2004) reported the basic structure of all PQQ-containing quinoproteins. All PQQ-containing quinoproteins have common basic structure of "propeller fold" superbarrel comprising eight 4-stranded anti-parallel β-sheets arranged with radial symmetry so as to resemble shape of blades of propeller (Fig. 6.1). The antiparallel β-sheets have shape of letter W. Each of these β-sheets has 11 amino acid residues with a typical sequence, viz. Ala (A) in 1st position, Asp (D) in 3rd, Gly (G) at 7th, Lys/Glu (i.e. K/E) at 8th and Trp (W) at the last position. This results in consensus sequence AxDxxxGK(E)xxW. This sequence also plays role in stabilizing the anti-parallel β-sheets. About 100 amino acids located between the consensus sequence of W-units have (relatively) low degree of sequence homology, and this segment appear to define the likely site of substrate entry into the alcohol dehydrogenases having broad substrate specificity. The basic crystal structures of the PQQ-containing quinoproteins are: (1) 3 methanol dehydrogenase (MDH, from methylotrophs), (2) quinoprotein ethanol dehydrogenase (qEDH), (3) quinohemoprotein ethanol dehydrogenase (qhEDH), and (4) ADH IIB. Amino acid residues involved in the binding of PQQ and the calcium ion in the active site are well conserved.

The volume of active site cavity, where the substrate binds and react on the top of PQQ, has been calculated from crystal structures of MDH, qEDH and ADH IIB as: 18, 62 and 120 Å^3, respectively (Fig. 6.2). The side chains of Leu 556 / Leu 547 in MDH and Trp 557 in qEDH form a lid-like cover. In crystal structure ADH IB and qhEDH, lid-like structures are formed by the side chains of residues Phe419 and Phe 425, and by residues Trp440 and Phe606, respectively (Fig. 6.2). In case of qEDH and MDH crystal structure, the heme domain is located above Phe419, Phe425, Phe606 and Trp440 residues.

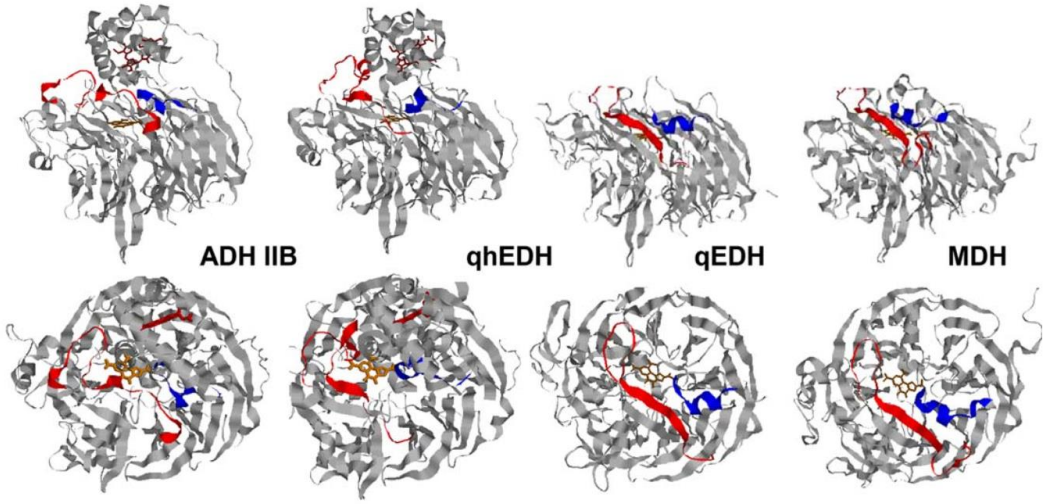

Figure 6.1. The overall structures of quinoprotein ADHs are drawn as ribbon models. The PQQ and heme c moieties are shown as stick models, colored orange and red, respectively. The S1 and S2 regions are colored red and blue, respectively. (adopted from Toyama et al. 2004)

Therefore, the substrate may not get access to active site in a similar manner as in qEDH and MDH. The alternate route for substrate is entry through the hydrophobic mouth of a channel leading to the active site cavity. This site is located on the side of PQQ domain in case of ADH IIB structure and between PQQ-and heme-domains in case qhEDH. In case of qhEDH, the amino acid residue Phe606 helps in forming a hydrophobic wall for the active site cavity located in heme domain. In case of ADH IIB structure, the hydrophobic wall is constituted by the residue Val593, which is located just above Phe410 in crystal structure. Other residues that appear in the hydrophobic channel leading to active site cavity are Met597 (in ADH IIB) and Val610 (in qhEDH). Among the quinoproteins MDH and qEDH, and PQQ-domain of ADH IIB and qhEDH, the amino acid sequences are highly identical. However, some segments in the structure of PQQ-domains are variable in conformation. These segments are located in the loop region between the strands of propeller blade type structures.

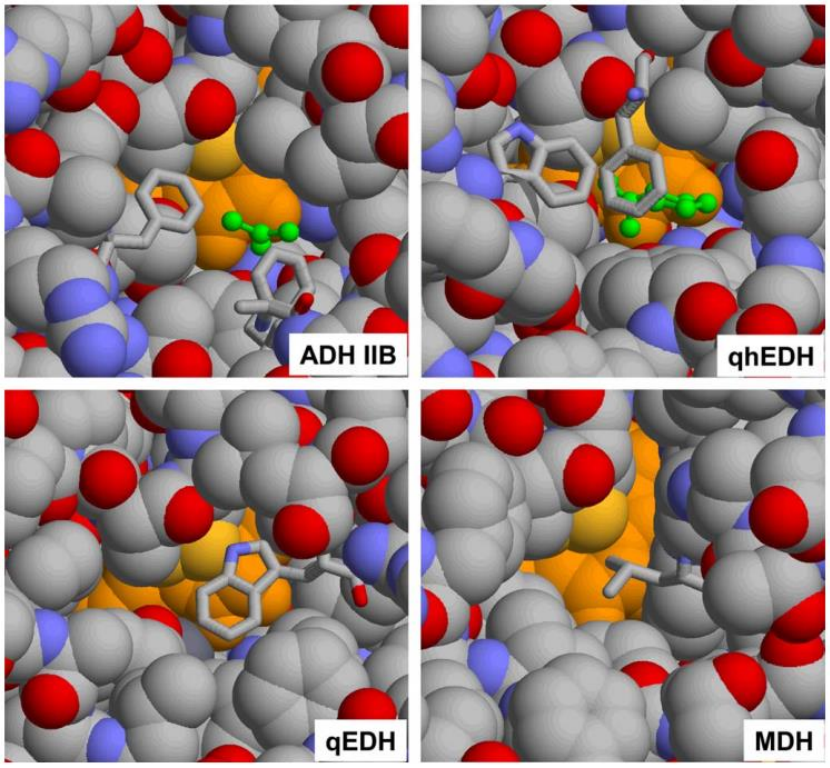

Figure 6.2. Active site cavity of quinoprotein ADHs. PQQ and the side chains of the quinoprotein domain that surround the cavity are represented as spacefilling models. PQQ is colored orange. The reaction products are shown as green ball-stick models (adopted from Toyama et al., 2004)

The loop region is open like a "mouth" in case of ADH IIB structure, whereas two corresponding segments in the loop region are closed in case of qhEDH. In these structures, the "mouth" accepting the substrate is provided by the "S1" portion of the loop and the cytochrome domain, which are the entrances surrounded by hydrophobic amino acid residues. The top view of the active site (as viewed down on to PQQ) gives the overall structure of the site in different quinoproteins. The residues of left side wall in the active site cavity are rather uniform in all quinoproteins (e.g. Cys105, Cys106, Glu173, Trp254, and Asp295) as shown in Fig. 6.2. The other residues making up the active site wall are variable in different segments (Phe 419 & Phe 425 in segment 1, Val 525 & Thr 529 in segment 2, Pro 377 & Phe 378 in case of ADB IIB). These variations in the residues lead to substrate specificity. Electron transfer during the oxidative half reaction differs among

three types of ADHs. Type I ADH, like MDH or glycerol dehydrogenase, have been shown to donate electrons directly to the soluble cytochrome c.

6.2 MATERIALS AND METHODS

6.2.1 Materials

Gluconobacter oxydans MTCC 904 was procured from Microbial Type Culture Collection (MTCC), Chandigarh, India. DHA and pure glycerol were procured from Merck, Germany. All other medium components and chemicals were procured from HiMedia Pvt. Ltd., India. Crude glycerol was synthesized in–house through alkali (NaOH) catalyzed transesterification of soybean oil (for greater details of procedure, refer to chapter 3). The alkali and alcohol contaminations in crude glycerol were quantified as follows: 0.85% w/v of sodium hydroxide (calculated by acid base titration) and 0.26% w/v methanol (determined using gas chromatograph).

6.2.2 Growth and maintenance of *G. oxydans* culture

The lyophilized cells of *G. oxydans* were revived in MRS medium and kept in a rotary incubator shaker (Make: Lab Companion; Model: SI–300R) at 30ºC, 150 rpm for 24 h. The revived cells were grown on agar slant and kept at 4ºC. The cultures were sub–cultured every month. The composition of MRS medium in distilled water (vol. = 1 L) was as follows: peptone – 10.0 g, beef extract – 10.0 g, yeast extract – 5.0 g, glucose – 10.0 g, Tween–80 – 1 mL, Na_2HPO_4 – 2.0 g, sodium acetate – 5.0 g, triammonium citrate – 2.0 g, $MgSO_4 \cdot 7H_2O$ – 0.2 g, $MnSO_4 \cdot 4H_2O$ – 0.2 g. The pH of the medium was adjusted to 6.0 ± 0.2 using 1 N HCl. The agar plates and slants were prepared by adding 15 g/L of agar in MRS medium.

6.2.3 Seed culture and fermentation media composition

The composition of seed culture medium was as follows: yeast extract – 5.0 g/L, peptone – 3 g/L, $K_2HPO_4 \cdot 3H_2O$ – 3 g/L, $(NH_4)_2SO_4$ – 2 g/L, $MgSO_4 \cdot 7H_2O$ – 0.51 g/L, mannitol – 10 g/L. The initial pH of the medium was adjusted to 6.0 ± 0.2. The medium was autoclaved prior to inoculation at 121ºC, 15 psi for 20 min. Previously optimized fermentation medium components were selected for carrying out batch experiments with a composition as follows: yeast extract – 2 g/L, $(NH_4)_2SO_4$ – 3.02 g/L, KH_2PO_4 – 0.641 g/L, $MgSO_4 \cdot 7H_2O$ – 0.545 g/L. The pH of the medium was adjusted to 4.7 prior to sterilization using 1N HCl. 100 mL of fermentation media was taken in 250 mL Erlenmeyer flask and was kept on a rotary shaker (Make – Lab Companion, Model – SI–300R) at 150 rpm, 31°C for 24 h. The optimum values of pH and temperature from our previous study were selected for fermentation experiments. Samples were withdrawn in regular interval to determine the concentration of substrate and product.

For glycerol fermentation using immobilized cells, three number of PU foam cubes (optimized in preliminary study) with immobilized and cross–linked *G. oxydans* cells were added to the fermentation medium. The immobilization of cell over PU foam was achieved using previously reported procedure (Bhasarkar et al., 2015b).

6.2.4 Apparatus and reaction setup

Experiments involving ultrasonic irradiation of glycerol fermentation were conducted in a dual frequency (37/80 kHz) ultrasonic bath (Model: P–30H, Elmasonic, Germany, capacity 2.75 L, power: 130 W). A schematic diagram of experimental set–up is shown in Fig. 6.3. This bath has the facility of automatic frequency tuning and amplitude

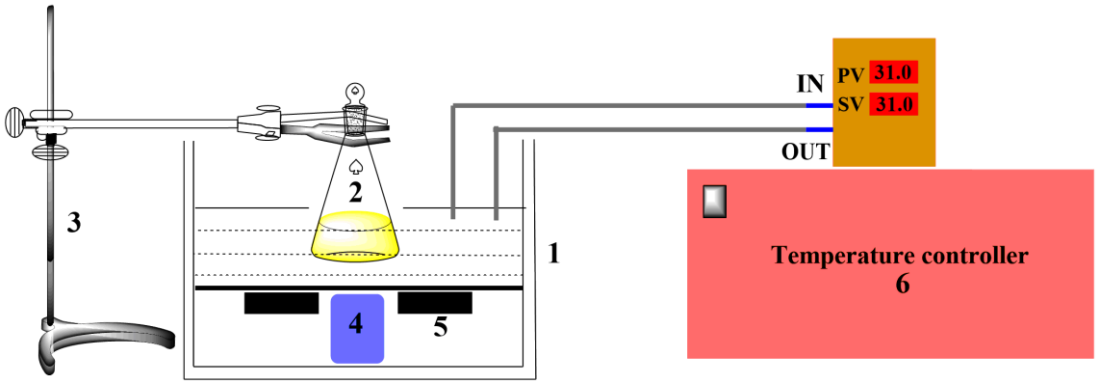

Figure 6.3. Schematic diagram of the experimental setup.
Legends: (1) ultrasound bath; (2) fermentation flask; (3) flask placement system (burette stand and holder); (4) bath controller (sonication time and frequency); (5) piezoelectric transducers; (6) temperature controlled water circulation bath.

compensation, which ensured constant power delivery to the reaction system during the sonication, despite changes occurring in reaction medium. The actual acoustic power input to the bath and pressure amplitude of the ultrasound waves generated thereby in the bath were determined using calorimetric technique (Chakma and Moholkar, 2014). Using calorimetric techniques (Chakma and Moholkar 2013; Sivasankar et al. 2007), the pressure amplitude of the ultrasound waves generated in the bath was calculated as 160 kPa. The bath was filled with water during sonication, which acts as the transmission medium for the ultrasound waves to the reaction mixture. Fermentation experiments were carried out in a 250 mL Erlenmeyer flask made of borosilicate glass. The flask containing fermentation broth was placed at central region of the ultrasound bath for all experiments to avoid the unequal distribution of the ultrasound waves. The temperature of the water in the bath was maintained at 31°C during treatment by circulating water through a copper coil immersed inside the bath from a temperature–controlled water bath (Model: WB2000, Amkette Analytics). The control experiments were carried out in flask of similar dimension and volume, as used in case of experiments with ultrasound irradiation. For control

experiments, the flask was kept in an incubator shaker (Make: Lab Companion; Model: SI–300R) at 31°C and 150 rpm. Both test and control samples were withdrawn after every 3 h up to 24 h.

6.2.5 Optimization of duty cycle of sonication

Continuous sonication of the fermentation mixture can cause damage (or disruption) to microbial cells due to shock waves generated by the transient cavitation bubbles. In order to avoid this phenomenon, sonication is applied in pulsed mode. The duty cycle of sonication (fractional periods of sonication and silent mode, respectively, in unit time interval) is an important parameter (Khanna et al., 2012; Singh et al., 2015). In order to optimize this parameter, three different duty cycles, viz. 10, 20 and 30% were applied to suspension of microbial cells in the seed culture medium, and the morphological changes in *G. oxydans* cells induced by sonication were studied. 10% duty cycle essentially refers to 1 min of sonication followed by 9 min of mechanical shaking in incubator shaker in every 10 min of treatment. The cells of *G. oxydans* were grown in seed culture medium containing mannitol as carbon source, and subjected to sonication at 10, 20 and 30% duty cycles for 12 h. The control experiment (against which the test experiments with sonication were compared), was carried out in a flask in incubator shaker at 30°C with shaking speed of 150 rpm for 12 h. After incubation, the cells were harvested by centrifugation (10,000× g, 20 min, 4°C) and diluted with phosphate buffer saline (PBS). Morphological changes of *G. oxydans* cells in both control (mechanical shaking only) and test samples (mechanical shaking with sonication) were studied by Flow cytometry (BD FACS caliber) analysis. Flow cytometry analysis was done using 488 nm laser and 530 nm emission filter. FSC (Forward Scattered Light) and SSC (Side Scattered Light) were used to evaluate the morphological changes in the cells.

6.2.6 Fermentation experiments

Fermentation experiments were carried out with three different initial substrate concentrations (viz. 20, 30, and 50 g/L), for both pure and crude glycerol. For experiments with free cells, 5% v/v of inoculum from 24 h grown seed culture medium was added to the fermentation mixture. For experiments with immobilized cells, 3 PU foam cubes with immobilized and cross–linked cells were added to the fermentation broth. Test experiments (sonication + mechanical shaking) were carried out with a duty cycle of 20%, which was optimized in preliminary experiments. Samples of fermentation mixture were withdrawn every 3 h (for total fermentation duration of 24 h) for both test and control experiments for analysis. The time profiles of glycerol consumption in all experiments were fitted to pseudo 1^{st} order kinetic model to obtain the rate constant for comparative evaluation.

6.2.7 Analysis

The concentrations of glycerol and DHA in the samples withdrawn from fermentation mixture were quantified using HPLC. A Rezex RCM monosaccharide calcium–column (300 mm × 8 µm × 7.8 mm, Phenomenex, India) thermostated at 35°C with help of external column oven (Make: PCI analytics Pvt. Ltd., India, Model: HCO–02) was used for measurements (Hekmat et al., 2007). The HPLC system (series 200, Perkin Elmer) comprised of a pump, a refractive index detector and a vacuum degasser. Ultra–pure water (18.2 MΩ·cm resistivity at 25°C) was used as the mobile phase at a flow rate of 0.5 mL/min. Reaction mixture samples were centrifuged (12,000 rpm, 20 min) followed by filtration through a 0.2 µm membrane filter, and appropriate dilution prior to injection into HPLC. For the experiments using free cells of *G. oxydans*, the concentration of cell mass (or growth profile of the microbial cells) was monitored by measuring absorbance at 660 nm with a UV–visible spectrophotometer (Model: LAMBDA 35; Make: Perkin Elmer).

6.2.8 Preparation of cell free extract and partial purification of enzymes

Initially, *G. oxydans* cells were grown in seed culture medium for 12 h. 5% v/v inoculum from the seed culture was transferred to the fermentation medium containing pure glycerol as substrate. This would trigger expression of enzyme glycerol dehydrogenase responsible for glycerol oxidation. For test experiments, the fermentation mixture was subjected to sonication (with 20% duty cycle) for 12 h at 31°C. For control experiments, another reaction flask containing the fermentation mixture was placed in incubator shaker (150 rpm, 31°C) for 12 h. After incubation, the broth was subjected to centrifugation at 12,000× g for 20 min at 4°C to separate the cells. The cell pellets were washed with phosphate buffer (50 mM, pH 6.0) twice and suspended in minimum volume of same buffer. These cells were disrupted using Constant Systems cell disrupter (Constant System Ltd., UK) at pressure of 20–25 kPa. The cell debris was removed by centrifugation at 12,000× g for 30 min. The cell–free extracts were brought to 30% saturation with $(NH_4)_2SO_4$ under constant stirring at 4°C for 3 h. The precipitate was removed by centrifugation (12,000× g, 20 min, 4°C), and the resultant supernatant was further saturated to 60% with addition of $(NH_4)_2SO_4$. The proteins were allowed to precipitate for 2 h, and were recovered by centrifugation (12,000× g, 20 min, 4°C). The protein pellets were suspended in minimum volume of 50 mM phosphate buffer (pH 6.0). Finally, the protein solution was subjected to dialysis using 12 kDa cutoff membrane against the same buffer for 12 h. Post dialysis, the intracellular proteins were analyzed for secondary structure using Circular Dichroism analysis.

6.2.9 Circular dichroism (CD) analysis

Far UV circular dichroism (CD) spectra of the intracellular proteins (containing the enzyme glycerol dehydrogenase) obtained from both native cells (i.e. grown with

mechanical shaking) and ultrasound–treated cells (grown with mechanical shaking and sonication) were recorded from the difference in absorption of left and right–circularly polarized light. The samples were placed in a suprasil quartz cuvette of 1 mm optical path length and analyzed using a Jasco J–815 spectro–polarimeter at temperature of 25 ± 1°C. Other parameters of CD analysis were as follows: spectral range = 240–190 nm, scan rate = 100 nm/min, bandwidth = 1 nm, 3 replicates. The CD spectra of intracellular proteins was expressed in terms of molar residual ellipticity (MRE, deg·cm^2·dmol^{-1}) and was plotted as a function of wavelength. Phosphate buffer solution was used as blank and the spectrum was subtracted from the average of three spectra to obtain corrected spectrum for each sample. The analysis of the CD spectra was done using the online server DICHROWEB to obtain the secondary structure (viz. percentage contents of α–helix, β–sheet, β–turn and random coil) of intracellular proteins (Sreerama and Woody, 2000; Whitmore and Wallace, 2004, 2008).

6.3 RESULTS AND DISCUSSION

6.3.1 Optimization of duty cycle of sonication

The results of flow cytometric analysis of native and ultrasound–treated cells of *G. oxydans* for the assessment of morphological changes induced by sonication (for 20% and 30% duty cycle) are shown in Figs. 6.4A–F. Figs. 6.4A, C & E depict the acquisition dot plots (FSC versus SSC) of the *G. oxydans* cells, while Figs. 6.4B, D & E show the histogram plots (counts versus FSC) for the microbial cells. SSC–H is a measure of cell surface topology.

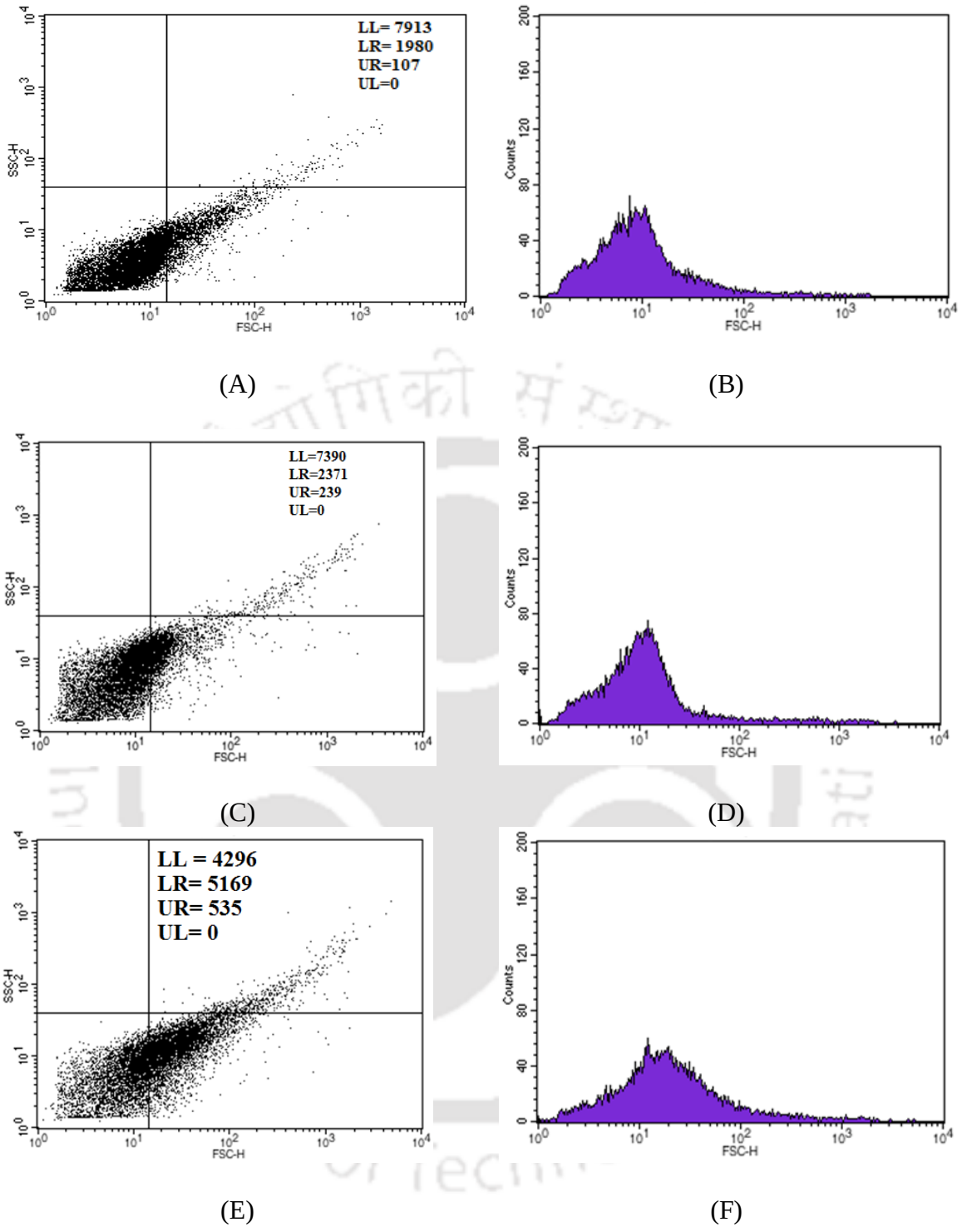

Figure 6.4. Results of flow cytometric analysis for assessment of morphological changes in *G. oxydans* cells prior and post sonication. (A),(C), and (E): Acquisition dot plots (FSC vs SSC) of *G. oxydans* cells in control (mechanical shaking), test 1 (sonication at 20% duty cycle + mechanical shaking), test 2 (sonication at 30% duty cycle + mechanical shaking) experiments, respectively. (B) ,(D), and (F): Histogram plots (counts vs FSC) of *G. oxydans* cells in control, test 1, and test 2 experiments, respectively.

As noted earlier, sonication induces strong micro–convection and shear stress in the medium. As a result, the surface of the microbial cells exposed to sonication is likely to become rough that results in increase of SSC–H. This may adversely affect the trans–membrane transport of nutrients and substrate in microbial cells, leading to reduction in efficacy of fermentation. The parameter of FSC is representative cell size and varies proportionately with it, i.e. the greater the FSC, the higher the cell size. Comparison of Figs. 6.4A & C does not reveal any significant change in FSC and SSC upon sonication as most of the cells, viz. native (79.13%) as well as ultrasound–treated (73.9%), are in the lower left quadrant. Also, histogram plots in Figs. 6.4B & D show similar pattern for both native and ultrasound–treated cells. These results essentially indicate no morphological changes in *G. oxydans* cells after exposure to sonication with 20% duty cycle. The results of flow cytometric analysis for ultrasound–treared cells at 30% duty cycle are shown in Fig. 6.4E & F. Acquisition dot plots (FSC versus SSC) of the ultrasound–treated cells at 30% duty cycle show significant change, as compared to native cells. In this case, a significant fraction of the cells falls in the lower right quadrant (51.69%) leaving only 42.96% cells in lower left quadrant. This essentially indicates that sonication at 30% duty cycle induces signficant changes in the morphology of the cells, which could adversely affect their viabiity. Sonication at 10% duty cycle also did not induce any change in cell morphology. However, the total fermentation period would be too long for such short duty cycle.

6.3.2 Fermentation experiments

The time profiles of glycerol fermentation (in both pure and crude form) by free cells of *G. oxydans* are shown Fig. 6.5. Figs. 6.5A and C show the time profiles of glycerol fermentation using mechanical shaking (or control experiment) for pure and crude versions

of glycerol as substrate, respectively. Figs. 6.5B and D show the time profiles of for test experiments that employed combination of sonication (20% duty cycle) and mechanical shaking for pure and crude versions of glycerol as substrate, respectively. The initial substrate concentration in these experiments was 20 g/L. Figs. 6.6A–D and Figs. 6.7A–D depict the corresponding fermentation profiles for glycerol fermentation with initial substrate concentration of 30 and 50 g/L, respectively. The fermentation profiles essentially include time histories of glycerol consumption, DHA production, and biomass growth. The results for immobilized cell experiments are depicted in Figs. 6.8A–E for various concentrations of pure and crude glycerol in the fermentation medium. The summary of final results of fermentation is given in Table 6.1A and B for free cells of *G. oxydans*, while Table 6.2A and B summarize the fermentation results for the immobilized cells of *G. oxydans*. Peculiar trends and facets of pure and crude glycerol fermentation by free and immobilized cells of *G. oxydans* with mechanical shaking and mechanical shaking coupled with sonication that can be deduced from Tables 6.1 and 6.2 can be summarized as follows:

(1) Application of sonication during fermentation of both pure and crude glycerol leads to substantial rise in both kinetics of substrate consumption and final DHA yield. The range of enhancement in DHA production with application of sonication is 60–84%. The pseudo–1st order kinetic constant of glycerol consumption also shows rise in the range of 1.4× to 2.9×. Relatively lower rise in the kinetic constant for test experiments with initial substrate concentration of 50 g/L is attributed to effect of substrate inhibition.

(2) For fermentation of pure glycerol, the net glycerol consumption shows marginal rise (~ 10%) after immobilization of the cells. However, the corresponding DHA yield is relatively smaller for free cells, as some portion of glycerol consumed by the free *G. oxydans* cells is bifurcated towards cell maintenance and growth.

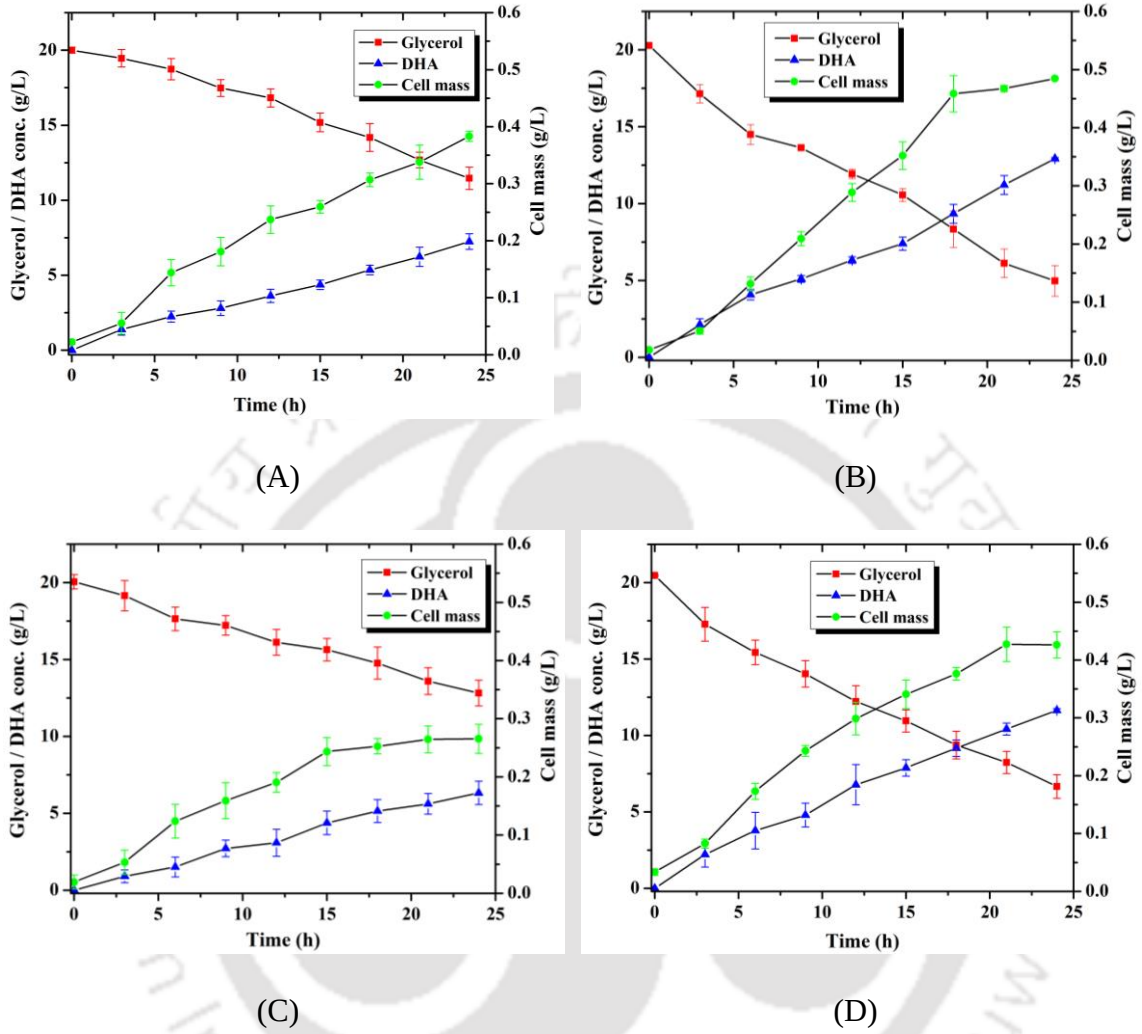

Figure 6.5. Time profiles of cell mass growth and glycerol bioconversion (initial conc. 20 g/L) to DHA by free cells of *G. oxydans* in control (mechanical shaking) and test (sonication + mechanical shaking) experiments. (A) pure glycerol (control expt); (B) pure glycerol (test expt); (C) crude glycerol (control expt); (D) crude glycerol (test expt).

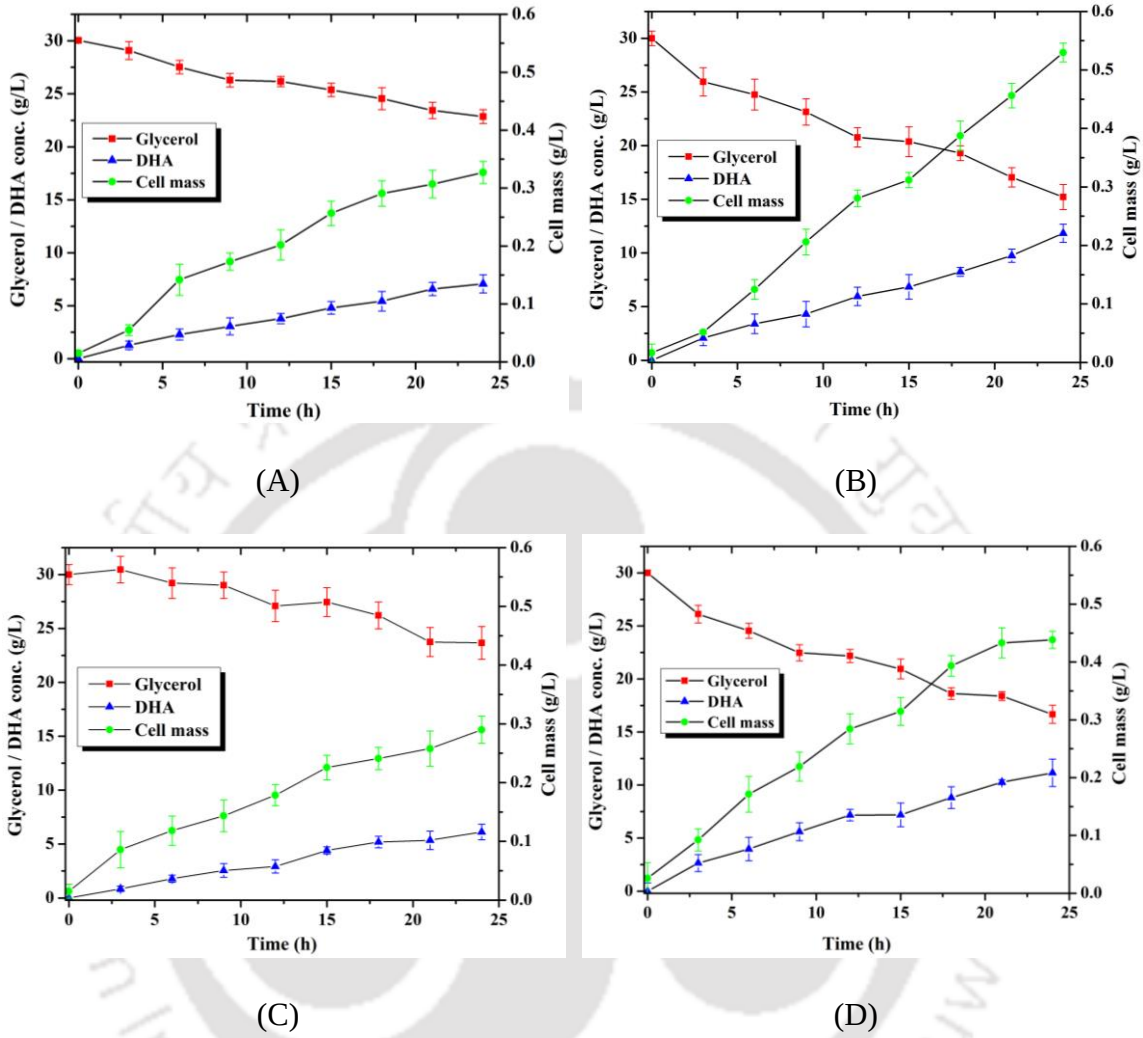

Figure 6.6. Time profiles of cell mass growth and glycerol bioconversion (initial conc. 30 g/L) to DHA by free cells of *G. oxydans* in control (mechanical shaking) and test (sonication + mechanical shaking) experiments. (A) pure glycerol (control expt); (B) pure glycerol (test expt); (C) crude glycerol (control expt); (D) crude glycerol (test expt).

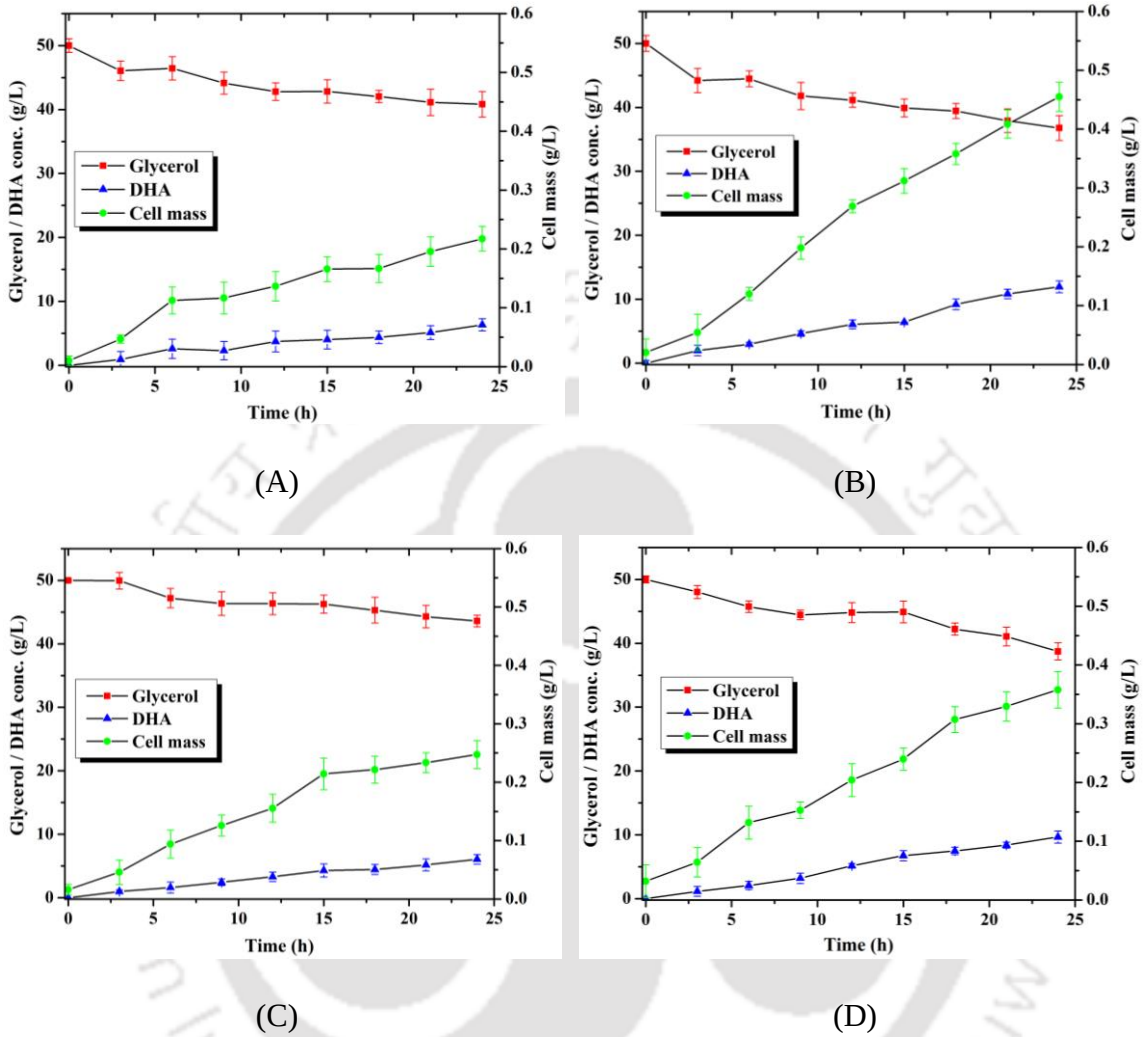

Figure 6.7. Time profiles of cell mass growth and glycerol bioconversion (initial conc. 50 g/L) to DHA by free cells of *G. oxydans* in control (mechanical shaking) and test (sonication + mechanical shaking) experiments. (A) pure glycerol (control expt); (B) pure glycerol (test expt); (C) crude glycerol (control expt); (D) crude glycerol (test expt).

Table 6.1(A). Summary of pure glycerol fermentation by free cells of *G. oxydans* for DHA production

	Initial pure glycerol concentration					
	20 g/L		30 g/L		50 g/L	
	MS + US	MS	MS + US	MS	MS + US	MS
Final DHA conc. (g/L)	12.93	7.25	11.84	7.07	11.95	6.34
Net glycerol consumption in 24 h (g/L)	15.03	8.53	14.79	7.15	13.21	9.17
Fermentation yield (wt%)	66.04	37.03	40.35	24.09	24.44	12.97
Enhancement in DHA production with sonication (%)	78.4	--	67.4	--	88.5	--
DHA productivity ($g \cdot L^{-1} \cdot h^{-1}$)	0.54	0.30	0.49	0.30	0.50	0.26
k_1 (h^{-1})	0.052	0.020	0.0274	0.011	0.0141	0.009

Table 6.1(B). Summary of crude glycerol fermentation by free cells of *G. oxydans* for DHA production

	Initial crude glycerol concentration					
	20 g/L		30 g/L		50 g/L	
	MS + US	MS	MS + US	MS	MS + US	MS
Final DHA conc. (g/L)	11.64	6.33	11.15	6.12	9.67	6.07
Net glycerol consumption in 24 h (g/L)	13.34	7.18	13.33	6.34	11.27	6.41
Fermentation yield (wt%)	59.51	32.36	38.00	20.86	19.78	12.41
Enhancement in DHA production with sonication (%)	84	--	82	--	59	--
DHA productivity ($g \cdot L^{-1} \cdot h^{-1}$)	0.49	0.26	0.47	0.26	0.40	0.25
k_1 (h^{-1})	0.043	0.018	0.025	0.009	0.010	0.006

Notation: MS+US = Mechanical shaking with sonication; MS = Mechanical shaking; k_1 = pseudo 1st order rate constant of fermentation

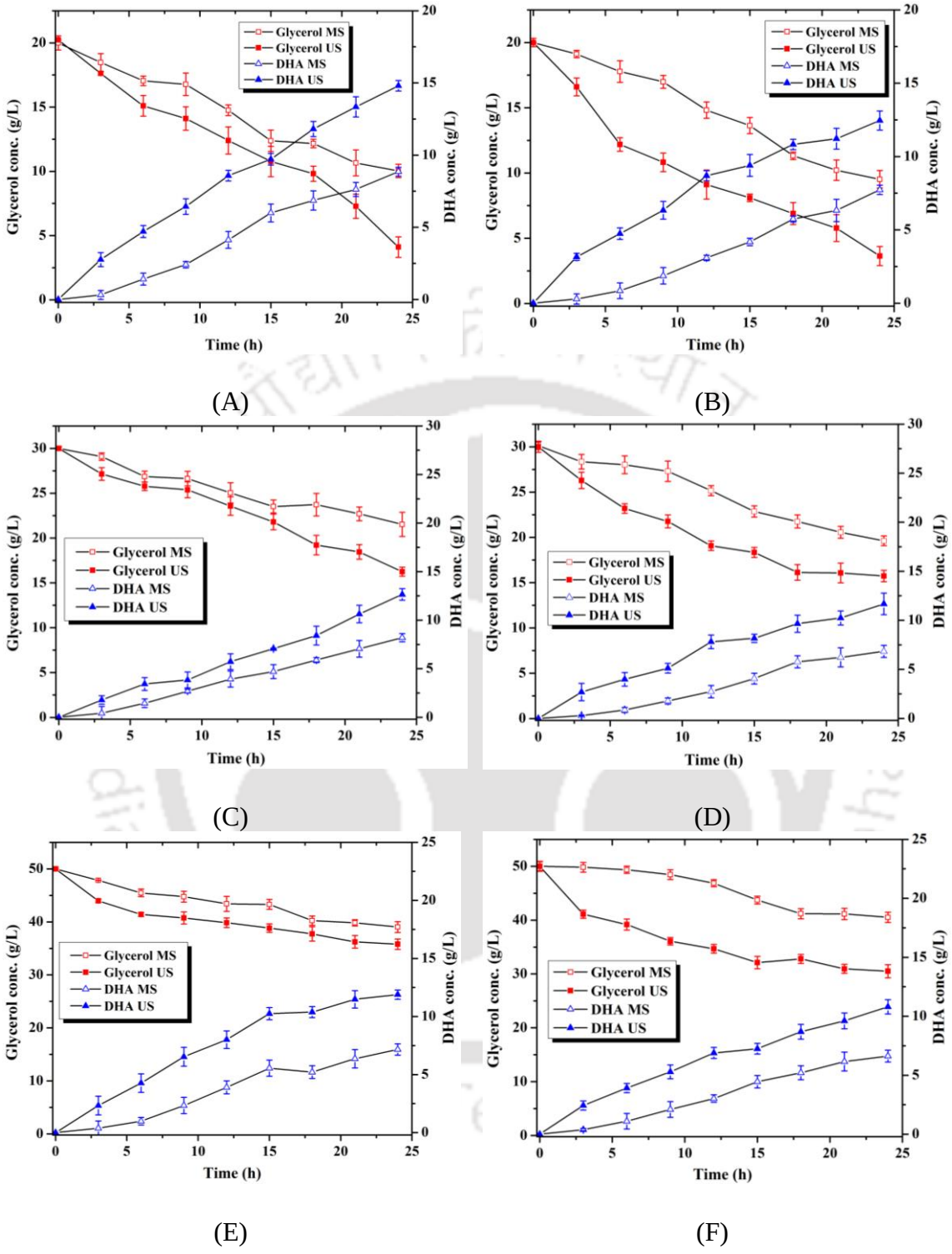

Figure 6.8. Time profiles of glycerol conversion and DHA formation in control (mechanical shaking, MS) and test experiments (sonication with mechanical shaking, US) for different initial concentrations of glycerol by immobilized cells of *G. oxydans*. (A) pure glycerol, 20 g/L. (B) crude glycerol, 20 g/L. (C) pure glycerol, 30 g/L. (D) crude glycerol, 30 g/L. (E) pure glycerol, 50 g/L. (F) crude glycerol, 50 g/L.

Table 6.2(A). Summary of pure glycerol fermentation by immobilized cells of *G. oxydans* for DHA production

	Initial pure glycerol concentration					
	20 g/L		30 g/L		50 g/L	
	MS + US	MS	MS + US	MS	MS + US	MS
Final DHA conc. (g/L)	14.81	8.85	12.65	8.19	11.89	7.16
Net glycerol consumption in 24 h (g/L)	15.9	9.97	13.75	8.48	14.21	11.97
Fermentation yield (wt%)	75.72	45.25	43.12	27.91	24.31	14.64
Enhancement in DHA production with sonication (%)	67.30	--	54.46	--	66.00	--
DHA productivity ($g \cdot L^{-1} \cdot h^{-1}$)	0.617	0.369	0.527	0.341	0.495	0.298
k_1 (h^{-1})	0.046	0.029	0.023	0.014	0.016	0.011

Table 6.2(B). Summary of crude glycerol fermentation by immobilized cells of *G. oxydans* for DHA production

	Initial crude glycerol concentration					
	20 g/L		30 g/L		50 g/L	
	MS + US	MS	MS + US	MS	MS + US	MS
Final DHA conc. (g/L)	12.46	7.74	11.68	6.84	10.80	6.63
Net glycerol consumption in 24 h (g/L)	16.36	10.48	14.27	10.37	19.48	9.48
Fermentation yield (wt%)	63.70	39.57	39.81	23.31	22.09	13.56
Enhancement in DHA production with sonication (%)	61.06	--	70.70	--	62.95	--
DHA productivity ($g \cdot L^{-1} \cdot h^{-1}$)	0.519	0.322	0.487	0.285	0.450	0.276
k_1 (h^{-1})	0.064	0.029	0.031	0.017	0.025	0.009

* Notation: MS+US = Mechanical shaking with sonication; MS = Mechanical shaking; k_1 = pseudo 1st order rate constant of fermentation

In case of crude glycerol fermentation, the net glycerol consumption shows significant (20–30%) rise as the *G. oxydans* cells are immobilized over PU foam. However, the corresponding DHA yield does not show proportionate rise. A plausible explanation for this result could be given as follows: crude glycerol contains alkali (Na^+) ions impurities due to traces of alkali catalyst left in glycerol after transesterification, which leads to formation of sodium glycerate during metabolism of glycerol by *G. oxydans* (Lidia and Stanislaw, 2012). As seen from Tables 6.2A and B, the DHA productivity of the immobilized cells is higher in fermentation of pure glycerol, although the net substrate consumption is higher in fermentation of crude glycerol. This discrepancy can also be explained along similar lines. Bifurcation of glycerol towards formation of sodium glycerate in the metabolism of *G. oxydans* results in lesser substrate utilization towards DHA production, and thus, reduced DHA productivity. Higher substrate consumption by the immobilized cells of *G. oxydans* in crude glycerol fermentation (in both control and test experiments) is a possible consequence of reduced viscosity of crude glycerol due to traces of methanol left in it (Liu et al., 2016). Due to lesser viscosity, crude glycerol can be easily transported across immobilization matrix, and thus, the access of substrate to microbial cells is enhanced resulting in greater consumption of substrate. As a consequence, the pseudo 1^{st} order kinetic constant of fermentation for the immobilized cells is also higher for crude glycerol as substrate. This result is consistent for fermentation with all three initial glycerol concentrations, viz. 20, 30 and 50 g/L.

(3) The net substrate consumption is practically same in fermentation with initial glycerol concentration of 20 and 30 g/L. This trend is consistent in both control and test experiments (with pure & crude glycerol and free & immobilized cells of *G. oxydans*) as seen from Tables 6.1A, 6.1B, 6.2A and 6.2B. Slight reduction in glycerol consumption for substrate concentration of 50 g/L is attributed to the substrate inhibition effect.

Consequently, the DHA productivity is also practically similar in glycerol fermentation with initial substrate concentrations of 20 and 30 g/L for both control and test experiments.

An explanation for these results of fermentation experiments can be given on the basis of analysis of circular dichroism spectra of intracellular proteins extracted from native and ultrasound–treated microbial cells of *G. oxydans* presented in the next section.

6.3.3 Results of circular dichroism analysis

A linear chain of α–amino acids linked together via amide (or peptide) bonds forms the primary structure of protein macromolecules, such as enzymes. However, the protein chain may get folded due to formation of H–bond between hydrogen in amide ($–NH_2$) group and oxygen in carboxyl (–COOH) group. This leads to formation of two types of secondary structures, viz. α–helix and β–conformations (i.e. β–sheet and β–turns). Exposure of enzyme protein to intense micro–convection generated by ultrasound and cavitation can induce conformational changes in these secondary structures, which in turn leads to augmentation of enzymatic activity. This phenomenon has been demonstrated in pervious literature including some of our own studies (Gulseren et al., 2007; Subhedar and Gogate, 2014; Wang et al., 2012).

A brief description of technique of circular dichroism spectroscopy for determination of secondary structures of proteins, polypeptides and peptides has been given in our previous paper (supplementary material of Agarwal et al., 2016). In the present study, the intracellular proteins obtained after dialysis of the lysate of the native and ultrasound–treated *G. oxydans* cells essentially contains the enzyme glycerol dehydrogenase, in addition to other proteins and chiral organic molecules. Determination of the secondary structure of these proteins has several practical difficulties such as unknown exact concentration of the proteins (or even the relative ratio of their concentrations) and the mean residue weight calculation. In the present study, the CD spectra of the native and

ultrasound–treated protein mixture have been analyzed using Dichroweb server. This software has capability of handling wide range of input formats, and pre–analysis processing and conversion programs including most popular algorithms such as CONTILL, VARSLC and SELCON3. The SELCON3 algorithm does not require input of exact concentrations of proteins nor the ratio of their concentrations. Analysis of CD spectra using SELCON3 can reveal overall percentage contributions of secondary structure components of α– helix, β–sheet, β–turn and other irregular or random coil structures) present in the intracellular proteins. In other words, the Dichroweb analysis with SELCON3 gives only a qualitative statement of changes induced in secondary structures of intracellular proteins extracted from native and ultrasound–treated *G. oxydans* cells – without their exact quantification. These results are sufficient for providing qualitative physical explanations to the experimental results of pure and crude glycerol fermentation obtained with free and immobilized cells of *G. oxydans* with mechanical shaking and sonication. Fig. 6.9 shows the collective CD spectra of the intracellular proteins obtained from native and ultrasound–treated *G. oxydans* cells. Table 6.3 depicts the Dichroweb analysis of the CD spectra of these intracellular proteins in terms of their secondary structures, viz. percentage contents of α–helix, β–sheet, β–turns and random coils. It could be inferred from results presented in Table 6.3 that α–helix and β–conformation content of the intracellular proteins including glycerol dehydrogenase enzyme shows significant reduction after ultrasound treatment. The random coil content of the enzymes shows more than 2.5–fold increment after ultrasound treatment. A brief description of structure of quinohemoprotein–dependent alcohol dehydrogenase enzymes (such as glycerol dehydrogenase) is given in the introduction section.

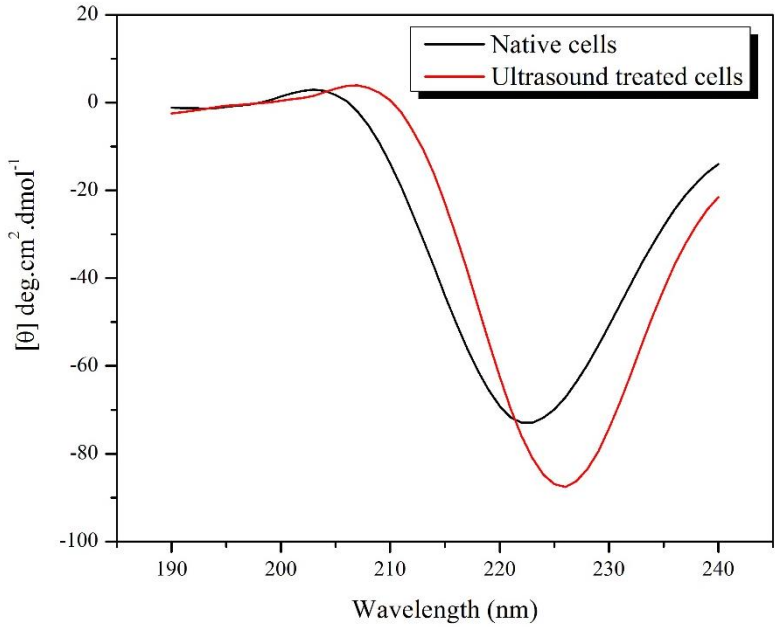

Figure 6.9. Circular dichroism spectra of intracellular protein extract from native (grown with mechcanical shaking) and ultrasound-treated (grown with sonication + mechanical shaking) cells of *G. oxydans*.

Table 6.3. Analysis of circular dichroism spectra using Dichroweb online server (Contents of secondary structure of intracellular proteins extracted from *G. oxydans* cells grown with mechanical shaking and with sonication)

Treatment	α – Helix (%)	β – sheet (%)	β – turns (%)	Random coils (%)
Native enzyme	20.45	25.09	19.67	34.69
Ultrasound treated enzyme	5.12	3.54	1.87	89.47

As described by Toyama et al. (2004), the active site of the alcohol dehydrogenase enzyme is located inside the cavity and the channel leading to the cavity is surrounded by hydrophobic wall comprising antiparallel β–sheets. Various amino acids residues like Phe, Val, Met etc. contribute to the hydrophobicity of the channel. The segment of about 100

amino acids (with low degree of sequence homology) located between the antiparallel β–sheets forms the site of substrate entry. As the substrate glycerol is a hydrophilic molecule, its entry could be retarded by the hydrophobic wall of the tunnel, which has hydrophobic amino acids. Reduction in the β–sheet content of the enzyme due to conformational changes induced by micro–convection generated by sonication can help in widening of the substrate entry segment. Moreover, the volume of the active site cavity may also enlarge due to pushing away of hydrophobic walls, thus, making substrate entry easier and faster. These effects essentially augment the substrate affinity of the enzyme leading to enhancement in reaction kinetics.

6.4 CONCLUSIONS

The present study addressed the issue of enhancement of glycerol fermentation to dihydroxyacetone with application of sonication. Fermentation using both free and immobilized cells of *G. oxydans* has been dealt with. The extent of glycerol consumption and DHA production by free and immobilized cells of *G. oxydans* shows marked rise with sonication. Sonication with duty cycle of 20% was not revealed to induce any morphological changes in the microbial cells. As compared to free cells, the substrate consumption by immobilized cells was higher.

As compared to pure glycerol, relatively smaller DHA yield from fermentation of crude glycerol (despite higher glycerol consumption) is attributed due to possible formation of sodium glycerate during metabolism of *G. oxydans*. A plausible explanation to the sonication–induced enhancement of glycerol fermentation was provided on the basis of circular dichroism analysis of the intracellular proteins obtained native and ultrasound treated *G. oxydans* cells. Intense micro convention generated by ultrasound and cavitation

was revealed to induce conformational changes in the secondary structure of the intracellular proteins in terms of reduction in α–helix and β–sheet content. These conformational changes could enhance the substrate affinity and activity of intracellular enzymes like glycerol dehydrogenase that resulted in faster metabolism of glycerol. In summary, the present study has not only demonstrated the potential of sonication in intensification of glycerol formation by *G. oxydans*, but has also attempted to gain biomechanistic insight into this process.

REFERENCES

Agarwal, M., Dikshit, P.K., Bhasarkar, J.B., Borah, A.J., Moholkar, V.S., 2016. Physical insight into ultrasound-assisted biodesulfurization using free and immobilized cells of *Rhodococcus rhodochrous* MTCC 3552. Chem. Eng. J., 295, 254-267.

Bar, R., 1988. Ultrasound enhanced bioprocesses: cholesterol oxidation by *Rhodococcus erythropolis*. Biotechnol. Bioeng. 32, 655–663.

Bhasarkar, J., Borah, A.J., Goswami, P., Moholkar, V.S., 2015a. Mechanistic analysis of ultrasound assisted enzymatic desulfurization of liquid fuels using horseradish peroxidase. Bioresour. Technol. 196, 88-98.

Bhasarkar, J.B., Dikshit, P.K., Moholkar, V.S., 2015b. Ultrasound assisted biodesulfurization of liquid fuel using free and immobilized cells of *Rhodococcus rhodochrous* MTCC 3552: A mechanistic investigation. Bioresour. Technol. 187, 369–378.

Chakma, S., Moholkar, V. S., 2013. Physical mechanism of sono-Fenton process. AIChE J. 59(11), 4303-4313.

Chakma, S., Moholkar, V.S., 2014. Investigations in synergism of hybrid advanced oxidation processes with combinations of sonolysis + Fenton process + UV for degradation of Bisphenol-A. Ind. Eng. Chem. Res., 53(16), 6855-6865.

Choudhury HA, Choudhary A, Sivakumar M, Moholkar VS. 2013. Mechanistic

investigation of the sonochemical synthesis of zinc ferrite. Ultrason Sonochem 20(1):294-302.

Claret, C., Salmon, J.M., Romieu, C., Bories, A., 1994. Physiology of *Gluconabacter oxydans* during dihydroxyacetone production from glycerol. Appl. Microbiol. Biotechnol. 41, 359 365.

Ertunc, S., Akay, B., Boyacioglu, H., Hapoglu, H., 2009. Self-tuning control of dissolved oxygen concentration in a batch bioreactor. Food Bioprod. Process. 87, 46–55.

Flickinger, C., Perlman, D., 1977. Application of oxygen–enriched aeration in the conversion of glycerol to dihydroxyacetone by *Gluconobacter oxydans* IFO 3293. Appl. Environ. Microb. 33, 706–712.

Gogate, P.R., Kabadi, A.M., 2009. A review of applications of cavitation in biochemical engineering/biotechnology. Biochem. Eng. J. 44, 60–72.

Gulseren, I., Guzzy, D., Bruce, B.D., Weiss, J., 2007. Structural and functional changes in ultrasonicated bovine serum albumin solutions. Ultrason. Sonochem. 14, 173–183.

Hekmat, D., Bauer, R., Neff, V., 2007. Optimization of the microbial synthesis of dihydroxyacetone in a semi–continuous repeated–fed–batch process by in situ immobilization of *Gluconobacter oxydans*. Process Biochem. 42, 71–76.

Hu, Z.–C., Zheng, Y.–G., 2011. Enhancement of 1,3-dihydroxyacetone production by a UV-induced mutant of *Gluconobacter oxydans* with DO control strategy. Appl. Biochem. Biotechnol. 165, 1152–1160.

Hu, Z.–C., Zheng, Y.–G., Shen, Y.–C., 2011. Use of glycerol for producing 1,3 dihydroxyacetone by *Gluconobacter oxydans* in an airlift bioreactor. Bioresour. Technol. 102, 7177–82.

Khanna, S., Jaiswal, S., Goyal, A., Moholkar, V.S., 2012. Ultrasound enhanced bioconversion of glycerol by *Clostridium pasteurianum*: A mechanistic investigation. Chem. Eng. J. 200, 416–425.

Kuppa, R., Moholkar, V.S., 2010. Physical features of ultrasound-enhanced heterogeneous permanganate oxidation. Ultrason. Sonochem. 17(1), 123-131.

Lidia, S. R., Stanisław, B., 2012. Production of dihydroxyacetone from an aqueous solution of glycerol in the reaction catalyzed by an immobilized cell preparation of acetic

acid bacteria *Gluconobacter oxydans* ATCC 621. Eur. Food Res. Technol. 235(6), 1125-1132.

Liu, Q., Yan, T., Jiang, Z., Fang, T., 2016. Sustainable utilization of crude glycerol from biodiesel production: Catalyst free monoacyglycerols production. J. Chem. Technol. Biotechnol. DOI: 10.1002/jctb.5181.

Malani, R.S., Patil, S., Roy, K., Chakma, S., Goyal, A., Moholkar, V.S., 2017. Mechanistic analysis of ultrasound-assisted biodiesel synthesis with Cu_2O catalyst and mixed oil feedstock using continuous (packed bed) and batch (slurry) reactors. Chem. Eng. Sci. DOI: http://dx.doi.org/10.1016/j.ces.2017.03.041.

Moholkar, V. S., Warmoeskerken, M. M. C. G., 2003. Integrated approach to optimization of an ultrasonic processor. AIChE J. 49, 2918–2932.

Morya, N.K., Iyer, P.K., Moholkar, V.S., 2008. A physical insight into sonochemical emulsion polymerization with cavitation bubble dynamics. Polymer 49(7), 1910-1925.

Siegell, S. D., Gaden, E. L., 1962. Automatic control of dissolved oxygen levels in fermentations. Biotechnol. Bioeng. 4(3), 345–356.

Singh, S., Sarma, S., Agarwal, M., Goyal, A., Moholkar, V.S., 2015. Ultrasound enhanced ethanol production from *Parthenium hysterophorus*: A mechanistic investigation. Bioresour. Technol. 188, 287–294.

Sivasankar, T., Paunikar, A.W., Moholkar, V.S., 2007. Mechanistic approach to enhancement of the yield of a sonochemical reaction. AIChE J. 53(5), 1132-1143.

Sreerama, N., Woody, R.W., 2000. Estimation of protein secondary structure from circular dichroism spectra: comparison of CONTIN, SELCON, and CDSSTR methods with an expanded reference set. Anal. Biochem. 287, 252–260.

Subhedar, P.B., Gogate, P.R., 2014. Enhancing the activity of cellulase enzyme using ultrasonic irradiations. J. Mol. Catal. B-Enzyme. 101, 108–114.

Sulaiman, A.Z., Ajit, A., Yunus, R.M., Chisti, Y., 2011. Ultrasound–assisted fermentation enhances bioethanol productivity. Biochem. Eng. J. 54, 141–150.

Toyama, H., Mathews, F.S., Adachi, O., Matsushita, K., 2004. Quinohemoprotein alcohol dehydrogenases: structure, function, and physiology. Arch. Biochem. Biophys. 428, 10–21.

Wang, Z., Lin, X., Li, P., Zhang, J., Wang, S., Ma, H., 2012. Effect of low intensity ultrasound on cellulase pretreatment. Bioresour. Technol. 117, 222–227.

Wei, S.H., Song, Q.X., Wei, D.Z., 2007. Repeated use of immobilized *Gluconobacter oxydans* cells for conversion of glycerol to dihydroxyacetone. Prep. Biochem. Biotechnol. 37, 67–76.

Whitmore, L., Wallace, B.A., 2004. DICHROWEB, an online server for protein secondary structure analyses from circular dichroism spectroscopic data. Nucleic Acid Res. (Web Server issue), 668–673.

Whitmore, L., Wallace, B.A., 2008. Protein secondary structure analyses from circular dichroism spectroscopy: Methods and reference databases. Biopolymers 89, 392–400.

You, Q., Xu, H., Yin, X., Zhu, H., Dai, X., 2013. Improvement of dihydroxyacetone production by *Gluconobater oxydans* NH–10 using a two–stage agitation speed operation strategy 11, 389–393.

Zabaneh, M., Bar, R., 1991. Ultrasound–enhanced bioprocess II. dehydrogenation of hydrocortisone by *Arthrobacter simplex*. Biotechnol. Bioeng. 37, 998–1003.

CHAPTER 7

OVERVIEW AND SUGGESTIONS FOR FUTURE WORK

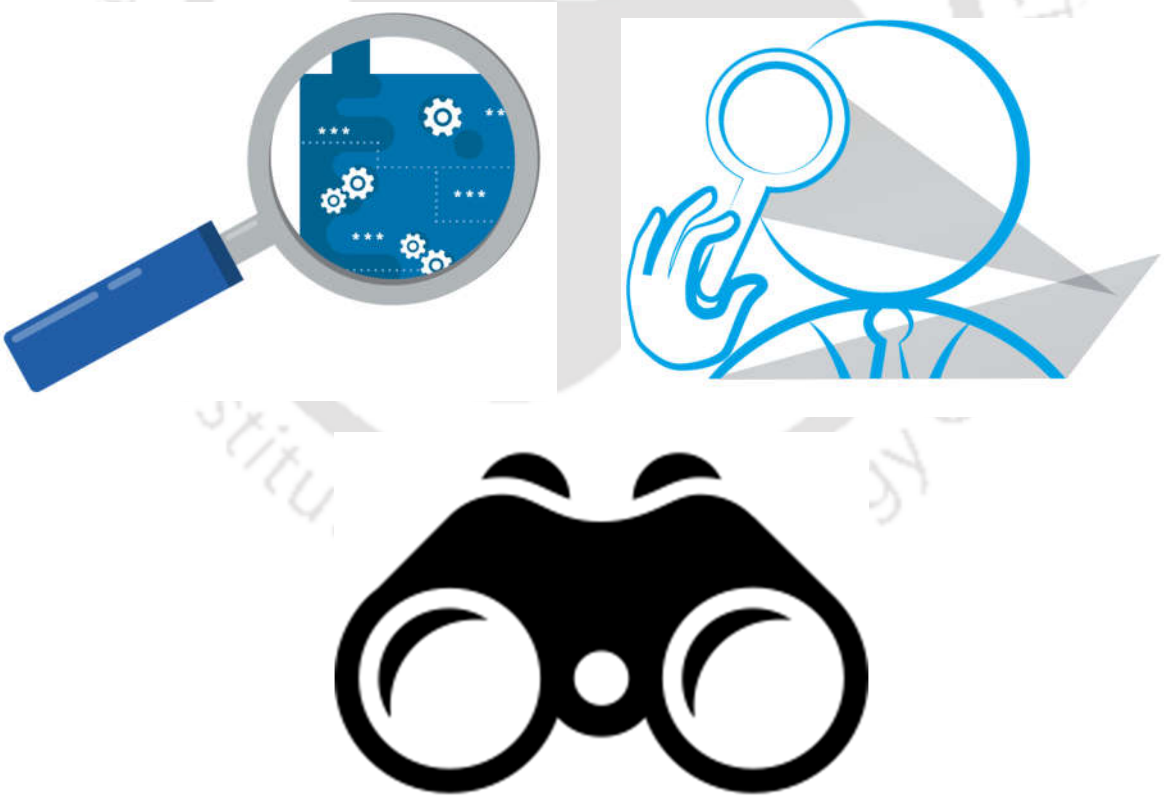

CHAPTER 7

OVERVIEW AND SUGGESTIONS FOR FUTURE WORKS

7.1 OVERVIEW

This thesis has addressed the issue of development, optimization and intensification of a potential bioprocess for conversion of waste glycerol into value–added product of dihydroxyacetone. The main theme or problem has been attacked in stepwise manner. Starting with kinetic analysis and substrate inhibition study with both free and immobilized cultures of *G. oxydans*. The optimization of the fermentation medium has been carried out in the second stage. Further optimization of process parameters has been dealt along with study of product inhibition effect. All of these studies have employed batch mode for glycerol fermentation. In the next phase, pure and crude glycerol fermentation has been carried out in fed–batch mode with different protocols of pulse–addition of glycerol. This methodology helped in avoiding the substrate inhibition and resulted in high DHA yield as compared to batch mode. Finally, the intensification of glycerol fermentation in pure and crude form has been carried out using sonication of the fermentation mixture.

In this final chapter, we present an overview of the main results of preceding chapters. These results, when viewed and analyzed at a glance, give an idea of potential of the bioprocess of glycerol conversion to DHA.

- Chapter 2, we presented the initial steps of process development such as selection of suitable carbon source in seed culture medium, and the selection of nitrogen source. This study has further extended for selection of amount of immobilization support and its reusability. Experiments were conducted in presence of varying initial substrate concentration (both pure and crude glycerol) and in presence free and immobilized *G. oxydans* cells to study the substrate inhibition kinetics. The experimental results were fitted to various substrate inhibition model in order to determine the kinetic parameters. Modified Haldane kinetics model, which gives fractional available of substrate inside immobilization matrix has also fitted to the experimental profile. Relative variations in the kinetic parameters reveal that immobilized *G. oxydans* cells (on PU foam substrate) with crude glycerol as substrate give higher order of inhibition and lower maximum reaction velocities. These results are essentially implications of substrate transport restrictions across immobilization matrix, which causes retention of substrate in the matrix and reduction in fractional available substrate for the cells. This causes reduction in both K_S (substrate concentration at $V_{max}/2$) and K_I (inhibition constant) as compared to free cells. For immobilized cells, substrate concentration (S_{max}) corresponding to V_{max} is practically same for both pure and crude glycerol as substrate.
- In Chapter 3, we have addressed the matter of optimization of production of the value added product, dihydroxyacetone, from crude glycerol using immobilized cells of *Gluconobacter oxydans*. Out of 6 medium components, 3 components viz. $MgSO_4 \cdot 7H_2O$, $(NH_4)_2SO_4$ and KH_2PO_4 revealed as the significant components, in addition to small concentration of yeast extract by Plackett–Burman design. These 3 components were further optimized using central composite design (CCD) method of optimization to find out their optimum values. These components augment the activity of glycerol dehydrogenase enzyme in metabolism and provide assimilable nitrogen and sulfur source for cell growth.

Yeast extract not only provides essential growth factors, but also accelerates production of alcohol dehydrogenase enzyme due to amino acids present. The DHA yield from crude glycerol (20 g/L) with optimized medium is 14.08 g/L, which is just 12% lower than the yield for pure glycerol. This study has thus established that proper optimization of fermentation medium reduces the adverse effect of impurities in crude glycerol on fermentation process and DHA yield.

- In Chapter 4, statistical optimization of process parameters for biodiesel–derived crude glycerol fermentation to DHA by immobilized *G. oxydans* cells over polyurethane foam was reported. Optimum concentrations of previously optimized medium components were selected for this study. The factors which were considered for optimization were pH, temperature and initial glycerol concentration. Optimum level of these factors were determined by Central composite design method of optimization. Effect of DHA (product) inhibition on crude glycerol fermentation was analyzed using conventional biokinetic models and new model that accounts for both substrate and product inhibition. Optimum values of fermentation parameters were: pH = 4.7, temperature = 31^{o}C, initial substrate concentration = 20 g/L. At optimum conditions, DHA yield was 89% (17.83 g/L). Effect of product inhibition on fermentation was trivial for DHA concentrations ≥ 30 g/L. At higher concentrations (≥ 50 g/L), kinetics and yield of fermentation showed marked reduction with sharp drop in V_{max} and K_S values. Inhibition effect was more pronounced for immobilized cells due to restricted transport of fermentation mixture across polyurethane foam. Retention of fermentation mixture in immobilized matrix resulted in higher localized DHA concentration that possibly enhanced inhibition effect.
- Chapter 5 presented batch and repeated–batch fermentation experiments with optimized medium and process parameters Fermentation of both pure and crude glycerol was carried out using free, immobilized, and whole/resting cells as catalyst. To overcome

the substrate inhibition effect, intermittent feeding of glycerol was employed to the fermentation broth to keep the substrate concentration < 5 g/L. The system behaves as batch fermentation in each cycle. Higher DHA yield productivity was achieved with feeding of 10 g/L of glycerol three times. Increase in duration of fermentation with increase in DHA concentration in the broth confirms the cells were partially inhibited at low concentration of product.

- Chapter 6 dealt with fermentation of crude glycerol by *G. oxydans* for production of DHA, and intensification of this process with sonication. Both free and immobilized cells of *G. oxydans* were used for fermentation. Application of sonication during fermentation was revealed to boost glycerol consumption rate by 60–84%. The kinetic constant of fermentation increased 1.4×–2.9×. DHA yield was higher for immobilized cells. Lesser DHA yield for crude glycerol (as compared to pure glycerol) was attributed to possible formation of sodium glycerate by *G. oxydans* due to alkali (Na+) impurities in crude glycerol. Slight reduction in DHA yield for initial substrate concentration of 50 g/L was attributed to substrate inhibition effect. Flow cytometric analysis of ultrasound–treated cells at 20% duty cycle did not reveal any morphological change. The circular dichroism analysis of intracellular proteins obtained from ultrasound–treated *G. oxydans* revealed significant reduction in α–helix and β–sheet content. These conformational changes in protein structure were possibly induced by strong micro–convection generated by sonication, and could lead to augmentation of activity and substrate affinity of the intracellular enzyme glycerol dehydrogenase. This phenomenon is essentially manifested in terms of enhanced kinetics of glycerol fermentation by *G. oxydans*.

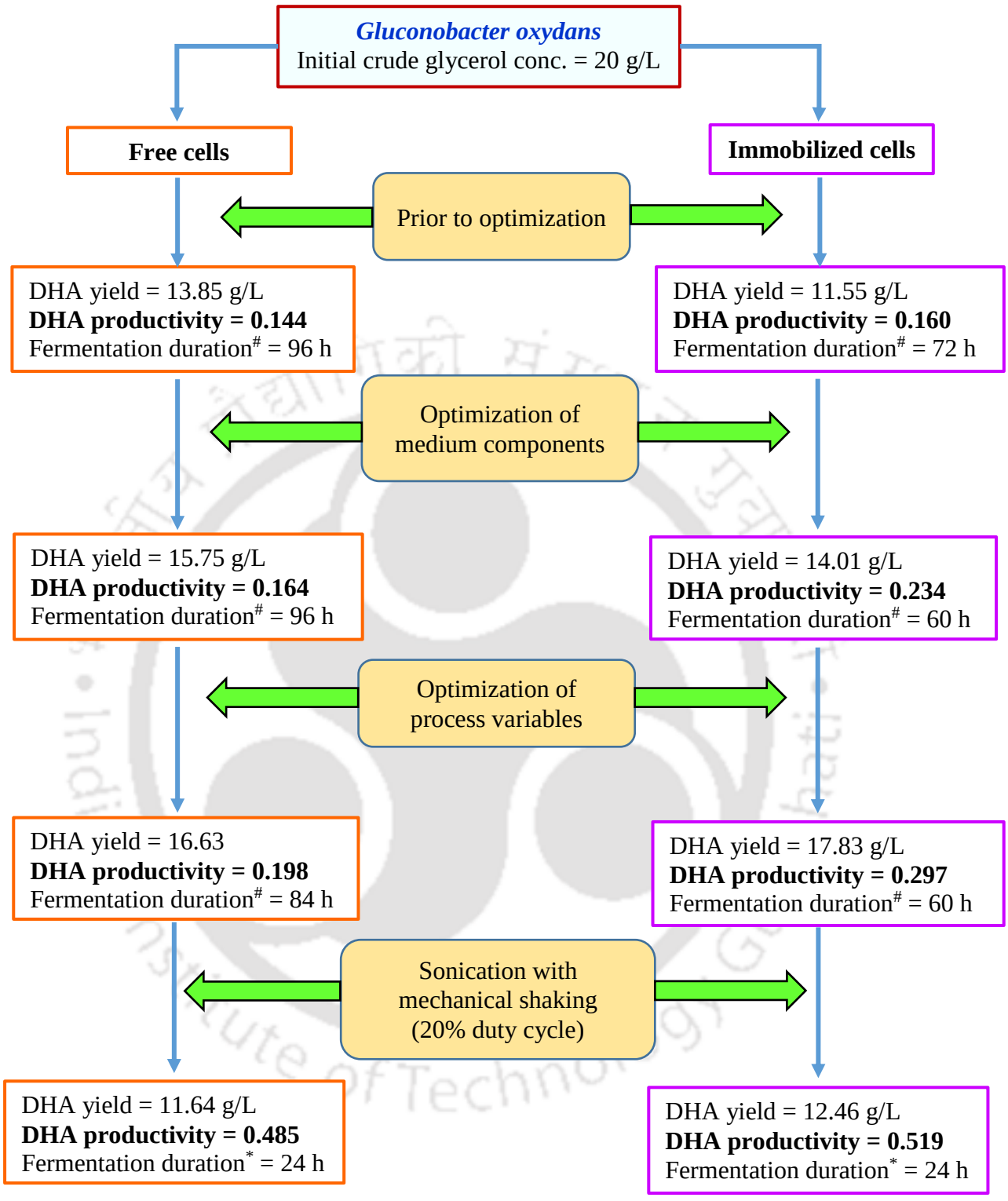

Figure 7.1. Schematic representation of the major results of the thesis.
Fermentation period was decided on the basis of complete glycerol consumption.
* Fermentation with sonication was carried out for a constant period of 24 h, in which the total glycerol in the fermentation mixture was not consumed.

7.2 SUGGESTIONS FOR FUTURE WORK

The present thesis aimed towards utilization of biodiesel derived crude glycerol for the production of dihydroxyacetone using immobilized *Gluconobacter oxydans* cells on laboratory scale. The results of this thesis can give more guidelines for development of a large/industrial scale process. Some suggestions to work further in this area can be given as follows:

1. All the experiments in this thesis were conducted in laboratory scale. These studies can be conducted in large-scale process.

2. Use of different reactor configurations: The process can be designed with other reactors like bubble column, fluidized bed. These reactors can be more efficient in terms of oxygen supply for achieving higher conversion.

3. The ultrasound enhanced processes need further optimization with higher frequencies. The ultrasound frequency for present study was kept constant (37 kHz), experiments with different frequencies will be able to ascertain individual contribution of ultrasound to the process.

4. The immobilization support can be replaced with better and low cost materials.

5. The extraction of enzyme glycerol dehydrogenase from *G. oxydans* cells, purification, and immobilization can be done for further experiments without immobilizing the whole cells.

6. The micro–organism (*G. oxydans*) used in present thesis is a commercial strain. This strain can be replaced with a genetically modified one for better yield and productivity.

7. The present study has revealed an interesting result that the secondary structure of the intracellular proteins of *G. oxydans* undergo significant alterations during sonication. This phenomenon needs to be studied in greater detail. The enzyme glycerol dehydrogenase needs to be isolated and purified from intracellular proteins, and the 3–D structure after

sonication needs to be established with standard procedure. The hypothesis of unfolding of enzyme proteins that makes substrate–binding site more accessible needs to be validated with proper in–depth studies involving SAXS, CD and X–ray crystallography techniques.

भारतीय प्रौद्योगिकी संस्थान गुवाहाटी
Indian Institute of Technology Guwahati

RESEARCH OUTPUTS

PUBLISHED IN PEER REVIEWED INTERNATIONAL JOURNALS

OUT OF THESIS

1. Pritam Kumar Dikshit, Vijayanand S. Moholkar. Kinetic analysis of dihydroxyacetone production from crude glycerol by immobilized cells of *Gluconobacter oxydans* MTCC 904. Bioresourse Technology 2016; 216:948–957.
2. Pritam Kumar Dikshit, Vijayanand S. Moholkar. Optimization of 1,3–dihydroxyacetone production from crude glycerol by immobilized *Gluconobacter oxydans* MTCC 904. Bioresourse Technology 2016; 216:1058–1065.
3. Pritam Kumar Dikshit, Susant Kumar Padhi, Vijayanand S. Moholkar. Process optimization and analysis of product inhibition kinetics of crude glycerol fermentation for 1,3–dihydroxyacetone production. Bioresourse Technology 2017; 244:362–370.

OTHER PUBLICATIONS

1. Sushobhan Pradhan, Pritam Kumar Dikshit, Arup Jyoti Borah, Maneesh Kumar Poddar, Lilendar Rohidas, Vijayanand S. Moholkar. Microbial production, ultrasound–assisted extraction and characterization of biopolymer polyhydroxybutyrate (PHB) from terrestrial (*P. hysterophorus*) and aquatic (*E. crassipes*) invasive weeds. Bioresourse Technology 2017; 242:304–310.
2. Pritam Kumar Dikshit, Mayank Agarwal, Jaykumar B. Bhasarkar, Arup Jyoti Borah, Vijayanand S. Moholkar. Physical insight into ultrasound–assisted biodesulfurization using free and immobilized cells of *Rhodococcus rhodochrous* MTCC 3552. Chemical Engineering Journal 2016; 295:254–267.
3. Sankar Chakma, Amrita Ranjan, Hanif A. Choudhury, Pritam Kumar Dikshit, Vijayanand S. Moholkar. Bioenergy from rice crop residues: role in developing economies. Clean Technologies and Environmental Policy 2015; 18:373–394.
4. Jaykumar B. Bhasarkar, Pritam Kumar Dikshit, Vijayananad S. Moholkar. Ultrasound assisted biodesulfurization of liquid fuel using free and immobilized cells of *Rhodococcus rhodochrous* MTCC 3552: A mechanistic investigation. Bioresource Technology 2015; 187: 369–378.

5. Shuchi Singh, Pritam Kumar Dikshit, Vijayananad S. Moholkar, Arun Goyal. Purification and characterization of acidic cellulase from *Bacillus amyloliquefaciens* SS35 for hydrolyzing *Parthenium hysterophorus* biomass. Environmental Progress and Sustainable Energy 2015; 34(3): 810–818.

CONFERENCE PRESENTATIONS

1. Poster Presentation: "Ultrasound enhanced bioconversion of crude glycerol to dihydroxyacetone by *Gluconobacter oxydans* MTCC 904" at 57th Annual Conference of Association of Microbiologist of India & International Symposium on "Microbes and Biosphere: What's New What's Next" organized by Gauhati University, Assam, India from 24–27 Nov., 2016 (International Conference).
2. Oral Presentation: "Statistical optimization of fermentation parameters for 1,3–dihydroxyacetone production from crude glycerol by immobilized *Gluconobacter oxydans* MTCC 904", in Recycle 2016: International Conference on Waste Management organized by Department of Civil Engineering, Indian Institute of Technology Guwahati, Guwahati, Assam, India from 1–2 April 2016 (International Conference).
3. Oral Presentation: "Mathematical model to study the inhibitory effect of crude/pure glycerol on free/immobilized cells of *Gluconobacter oxydans* MTCC 904 for the production of dihydroxyacetone", in CHEMCON 2015 organized by Indian Institute of Technology Guwahati, Guwahati, Assam, India from 27–30 Dec. 2015 (National Conference).
4. Poster Presentation: "Optimization of medium components using response surface methodology for the production of 1,3– dihydroxyacetone from crude glycerol by immobilized cells of *Gluconobacter oxydans* MTCC 904" at the New Horizons in Biotechnology Conference organized by NIIST, Trivandrum, India held from 22–25 Nov., 2015 (International conference).
5. Oral Presentation: "A design for utilization of crude glycerol for production of dihydroxyacetone by immobilized *Gluconobacter oxydans*" at 2nd International conference on bioenergy, environment and sustainable technologies organized by Arunai Engineering College, Tiruvannamalai, Tamilnadu held from 28th–31st Jan., 2015 (International Conference).

APPENDIX

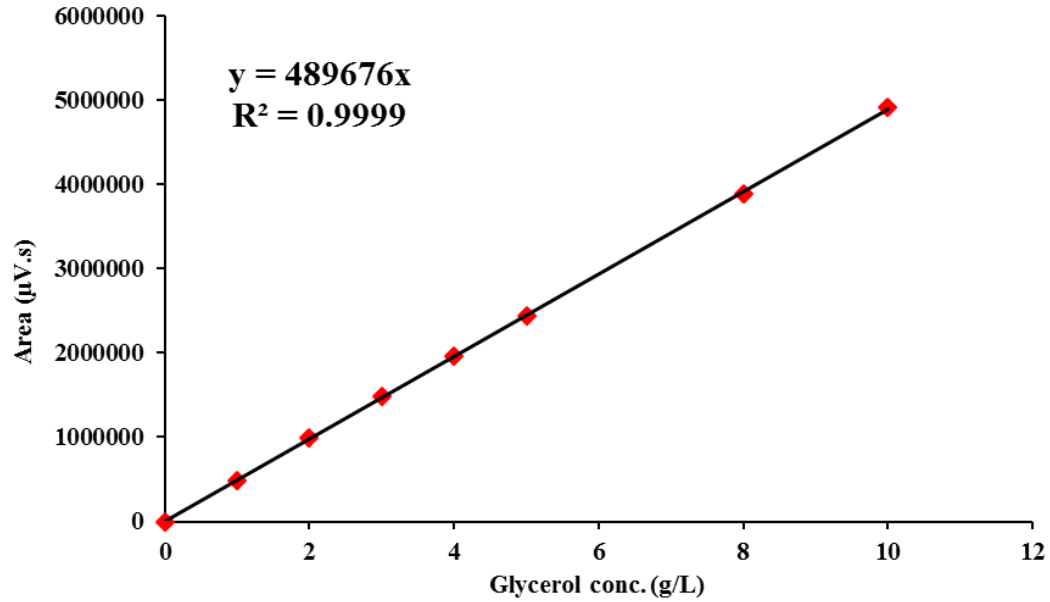

(A)

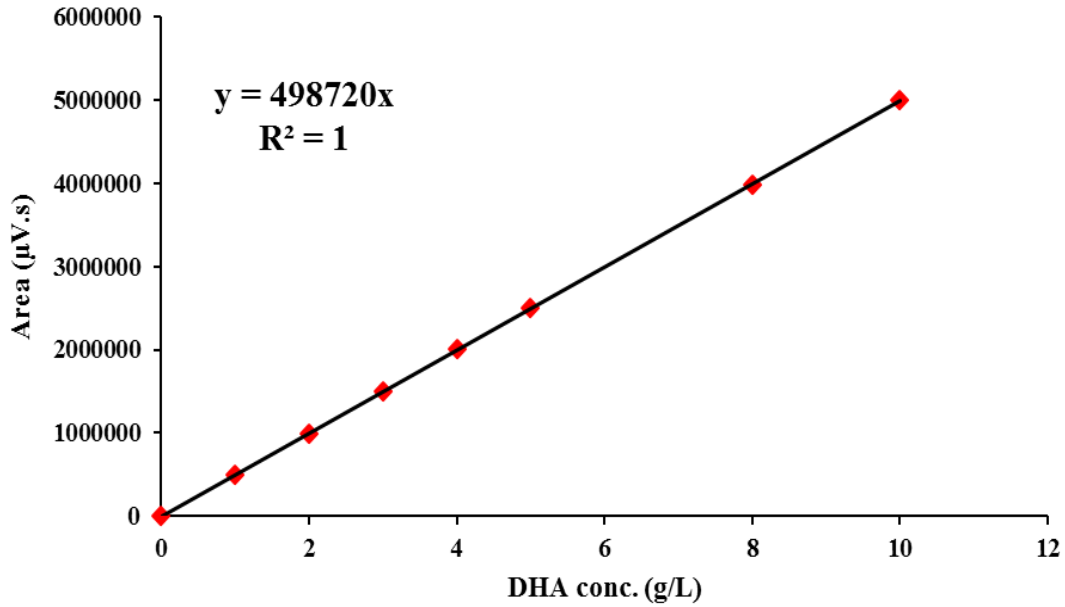

(B)

Figure A1. Standard calibration plots by HPLC analysis. (A) Plot for glycerol; (B) Plot for Dihydroxyacetone